

See discussions, stats, and author profiles for this publication at: <https://www.researchgate.net/publication/221881968>

# Carbon Nanomaterials: Carbon Nanomaterials for Advanced Energy Conversion and Storage (Small 8/2012)

ARTICLE *in* SMALL · APRIL 2012

Impact Factor: 8.37 · DOI: 10.1002/smll.201101594 · Source: PubMed

---

CITATIONS

280

READS

82

## 4 AUTHORS, INCLUDING:



Dong wook Chang

Pukyong National University

44 PUBLICATIONS 2,016 CITATIONS

[SEE PROFILE](#)



Jong-Beom Baek

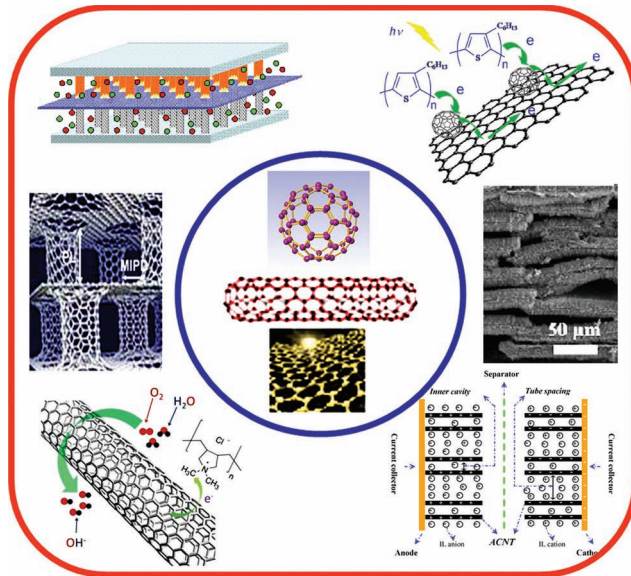
Ulsan National Institute of Science and Tec...

192 PUBLICATIONS 5,821 CITATIONS

[SEE PROFILE](#)

# Carbon Nanomaterials for Advanced Energy Conversion and Storage

Liming Dai,\* Dong Wook Chang, Jong-Beom Baek, and Wen Lu\*



## From the Contents

1. Introduction .....	1131
2. Carbon Nanomaterials .....	1131
3. Carbon Nanomaterials for Energy Conversion .....	1136
4. Carbon Nanotubes for Energy Storage .....	1150
5. Concluding Remarks .....	1159

**I**t is estimated that the world will need to double its energy supply by 2050. Nanotechnology has opened up new frontiers in materials science and engineering to meet this challenge by creating new materials, particularly carbon nanomaterials, for efficient energy conversion and storage. Comparing to conventional energy materials, carbon nanomaterials possess unique size-/surface-dependent (e.g., morphological, electrical, optical, and mechanical) properties useful for enhancing the energy-conversion and storage performances. During the past 25 years or so, therefore, considerable efforts have been made to utilize the unique properties of carbon nanomaterials, including fullerenes, carbon nanotubes, and graphene, as energy materials, and tremendous progress has been achieved in developing high-performance energy conversion (e.g., solar cells and fuel cells) and storage (e.g., supercapacitors and batteries) devices. This article reviews progress in the research and development of carbon nanomaterials during the past twenty years or so for advanced energy conversion and storage, along with some discussions on challenges and perspectives in this exciting field.

## 1. Introduction

The importance of developing new types of energy is evident from the fact that the global energy consumption has been accelerating at an alarming rate due to the rapid economic expansion worldwide, increase in world population, and ever-increasing human reliance on energy-based appliances. It was estimated that the world will need to double its energy supply by 2050.<sup>[1]</sup> To this end, advanced technologies for both energy conversion (e.g., solar cells and fuel cells) and storage (e.g., supercapacitors and batteries) are being extensively studied around the world. Nanotechnology has opened up new frontiers in materials science and engineering to meet this challenge.<sup>[2–4]</sup> In particular, carbon nanomaterials and nanotechnologies have been demonstrated to be an enabling technology for creating high-performance energy-conversion and storage devices.<sup>[5–7]</sup>

Like all other devices, performances of the energy-related devices depend strongly on the properties of the materials they employ. Recent development in materials science, particularly carbon nanomaterials, has facilitated the research and development of energy technologies. Comparing to conventional energy materials, carbon nanomaterials possess some unusual size-/surface-dependent (e.g., morphological, electrical, optical, and mechanical) properties useful in enhancing energy-conversion and storage performance.<sup>[8–11]</sup> Specifically, considerable efforts have been made to utilize the unique properties of fullerenes, carbon nanotubes (CNTs), and graphene as energy materials, and tremendous progress has been achieved in developing carbon nanomaterials for high-performance energy-conversion and storage devices. This article reviews progress in the research and development of carbon nanomaterials during the past twenty years or so for advanced energy conversion (i.e., solar cells and fuel cells) and storage (i.e., supercapacitors and batteries), along with some discussion on the challenges and perspectives in this exciting field.

## 2. Carbon Nanomaterials

Carbon has long been known to exist in three forms, namely, amorphous carbon, graphite, and diamond (Figure 1).<sup>[12]</sup> Depending on how the carbon atoms are arranged, their properties vary. For example, graphite is soft and black and the stable, common form of carbon with strong covalent bonding in the carbon plane and the much weaker van der Waals interactions in the transverse direction between the layers (Figure 1a). Diamond is hard and transparent with each carbon atom bound to four other carbon atoms in a regular lattice (Figure 1b).

It is the Nobel Prize-winning discovery of buckminsterfullerene C<sub>60</sub> (Figure 1c)<sup>[13]</sup> that has created an entirely new

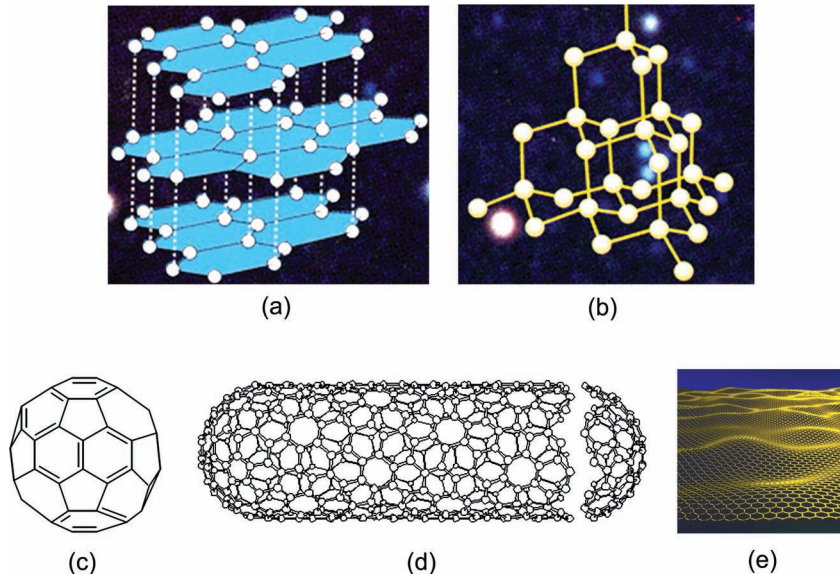


**Figure 1.** Carbon materials: a) graphite, b) diamond, c) buckminsterfullerene C<sub>60</sub>, d) single-walled carbon nanotube, and e) graphene.

branch of carbon chemistry.<sup>[14,15]</sup> The subsequent discovery of CNTs by Iijima<sup>[16]</sup> opened up a new era in materials science and nanotechnology.<sup>[5,17]</sup> These elongated nanotubes consist of carbon hexagons arranged in a concentric manner with both ends often capped by fullerene-like structures containing pentagons (Figure 1d). Graphene is the most recent addition to members of the carbon family (Figure 1e).<sup>[18]</sup> As the building blocks for CNTs and other carbon nanomaterials, graphene, the 2D single-atom-thick carbon nanosheets, has emerged as a new class of promising materials attractive for a wide range of potential applications,<sup>[8–11,19,20]</sup> including energy conversion and storage.

### 2.1. Fullerene C<sub>60</sub>, PC<sub>61</sub>BM, and PC<sub>71</sub>BM

In 1985, Kroto et al.<sup>[13]</sup> discovered that buckminsterfullerene C<sub>60</sub> has a soccer ball-like structure, with a diameter of

Prof. L. Dai  
Center of Advanced Science and  
Engineering for Carbon (Case4Carbon)  
Department of Macromolecular Science and Engineering  
Case Western Reserve University  
10900 Euclid Avenue, Cleveland, OH 44106, USA  
E-mail: liming.dai@case.edu

Dr. D. W. Chang, Prof. J.-B. Baek  
Interdisciplinary School of Green Energy  
Institute of Advanced Materials & Devices  
Ulsan National Institute of Science and Technology (UNIST)  
100 Banyeon, Ulsan, 689-798, South Korea

Dr. W. Lu  
EnerG2, Inc., 100 NE Northlake Way  
Suite 300, Seattle, WA 98105, USA  
E-mail: wlu@energ2.com

DOI: 10.1002/smll.201101594



7.1 Å and an approximately 10 Å centre-to-centre distance between neighbouring molecules in a single crystal,<sup>[21]</sup> consisting of 12 pentagons and 20 hexagons facing symmetrically (Figure 1c). This discovery opened up an entirely new branch of chemistry.<sup>[14,15,22,23]</sup> However, it was not until Kratschmer and Huffman<sup>[24]</sup> reported a simple way to produce macroscopic amounts of fullerenes in 1990 that scientists could finally study physicochemical properties of the C<sub>60</sub> carbon clusters with all of the conventional spectroscopic methods and use fullerenes as useful reagents in synthetic chemistry. Subsequently, other spherical fullerenes (collectively known as buckyballs) were synthesized with a different number of hexagonal faces. Due to their unusual molecular structures, fullerenes and their derivatives have been quickly shown to possess fascinating photonic, electronic, superconducting, magnetic, and biomedical properties.<sup>[21,25]</sup> Based on these findings, a wide range of applications have been proposed for fullerenes and their derivatives.<sup>[26,27]</sup>

In view of the scope defined in the introductory section, only the energy-related applications are discussed in this article. In this context, the photoinduced charge transfer of fullerenes discovered by Sariciftci et al.<sup>[28]</sup> in 1992 is of importance for the development of polymeric photovoltaic cells, which can be used to store light energy as electron relays for producing electricity. The photovoltaic effect involves the generation of electrons and holes in a semiconducting device under illumination, and subsequent charge collection at opposite electrodes. The first polymer solar cell was based on the photoinduced ultrafast electron transfer between a conjugated polymer, poly[2-(2'-ethylhexyloxy)-5-methoxy-1,4-phenylenevinylene] (MEH-PPV, **Figure 2a**) donor and C<sub>60</sub> acceptor in a double-layered structure.<sup>[28,29]</sup> Later, a soluble C<sub>60</sub> derivative, 6,6-phenyl-C<sub>61</sub>-butyric acid methyl ester (PC<sub>61</sub>BM, Figure 2b) or its C<sub>70</sub> counterpart (PC<sub>71</sub>BM, Figure 2c), was used to replace C<sub>60</sub> as the acceptor, which can be blended with conjugated polymer donors to form the so-called bulk-heterojunction polymer solar cells (*vide infra*).<sup>[30]</sup> Compared to PC<sub>61</sub>BM, PC<sub>71</sub>BM possesses a stronger visible absorption, useful for solar-cell applications.

## 2.2. Carbon Nanotubes

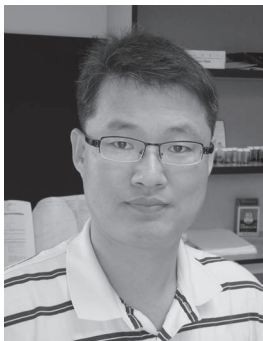
Using transmission electron microscope (TEM) to examine carbon samples generated by an arc-discharge method similar to that used for the fullerene synthesis, Iijima found the needlelike tubes now popularly known as carbon nanotubes.<sup>[16]</sup> The discovery of CNTs opened up a new era in material science and nanotechnology. Since Iijima's report on these microtubules of graphitic carbon in 1991, CNTs have attracted considerable attention as a new member of carbon family with novel electronic, optoelectronic, and electrochemical properties.

At the molecular level, CNTs can be viewed as a graphene sheet rolled up into a nanoscale tube form to produce a single-walled carbon nanotube (SWNT, **Figure 3**). There may be additional graphene coaxial tubes around the SWNT core to form a multiwalled carbon nanotube (MWNT).<sup>[5,6,16]</sup>



**Liming Dai** joined Case Western Reserve University (CWRU) in 2009 as the Kent Hale Smith Professor in the Department of Macromolecular Science and Engineering. He is also director of the Center of Advanced Science and Engineering for Carbon (CASE-4Carbon). Dr. Dai received a BSc from Zhejiang University in 1983 and a PhD from the Australian National University in 1991. He was a postdoctoral fellow at the Cavendish Laboratory at the University of Cambridge, and two years later a visiting fellow at the University of Illinois at Urbana-Champaign. He spent 10 years with CSIRO in Australia.

Before joining CWRU, he was an associate professor of polymer engineering at the University of Akron and the Wright Brothers Institute Endowed Chair Professor of Nanomaterials at the University of Dayton. Dr. Dai's expertise lies in the synthesis, chemical modification, and device fabrication of conjugated polymers and carbon nanomaterials for energy and biomedical applications.



**Jong-Beom Baek** is presently an associate professor and Director of Graphene Research Center in Ulsan National Institute of Science and Technology (UNIST, Korea). He obtained a PhD in Polymer Science from the University of Akron (USA). In 1999, he joined the Wright-Patterson Air Force Research Laboratory (AFRL) with a focus mainly on high-performance polymers. After approximately 4 years in AFRL, he returned to his home country as an assistant professor in Chonbuk National University (Korea) in 2003 and moved to UNIST in 2008. His current research focus is on the defect-selective functionalization of carbon-based nanomaterials via Friedel–Crafts acylation.



**Wen Lu** obtained his PhD at the University of Wollongong in Australia. Dr. Lu is currently a Senior Research Scientist and Group Leader of Electrochemistry and Device Development at EnerG2, Inc., in Washington. Previously, he has been a Senior Research Scientist and Energy Storage Program Manager at ADA Technologies, Inc., in Colorado, a Senior Scientist and Group Leader of Electronic and Electrochemical Devices Development at Santa Fe Science and Technology, Inc., in New Mexico, and a postdoctoral research fellow at Carleton University in Canada. His research activities have been

focused on the applications of electrochemistry and advanced materials (conducting polymers, carbon nanomaterials, and ionic liquid electrolytes) to the development of a range of electrochemical devices including energy-storage devices (batteries and ultracapacitors), energy-conversion devices (fuel and photoelectrochemical cells), electrochromic devices, electrochemical (bio)sensors, electromechanical actuators, and environmental remediation devices.

These elongated nanotubes usually have a diameter in the range from few angstroms to tens of nanometers and a length of several micrometers up to centimeters with both ends of the tubes often capped by fullerene-like structures containing pentagons.

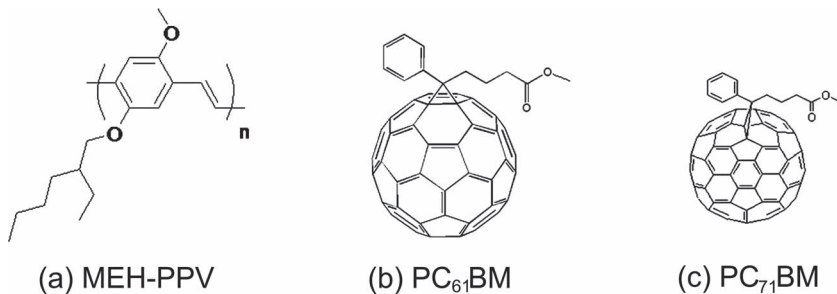


**Figure 2.** Molecular structures of a) MEH-PPV, b) PC<sub>61</sub>BM, and c) PC<sub>71</sub>BM.

Depending on their diameter and helicity of the arrangement of carbon atoms in the walls, CNTs can exhibit semiconducting or metallic behavior<sup>[5,6]</sup> with an electrical conductivity as high as 5000 S cm<sup>-1</sup>.<sup>[31]</sup> The highly conductive nature of the CNTs ensures their high charge transport capability. SWNTs have a higher theoretical specific surface area of 1315 m<sup>2</sup> g<sup>-1</sup> than that of MWNTs with the later being dependent on the diameter of the tubes and the number of the graphene walls.<sup>[32]</sup>

At the macroscopic level, CNTs can be produced, either in aligned and non-aligned forms.<sup>[33]</sup> They can be synthesized by a wide range of methods including, for example, carbon arc-discharge,<sup>[34]</sup> pyrolysis of hydrocarbons,<sup>[5,6,33]</sup> pulsed laser vaporization,<sup>[35,36]</sup> pyrolysis of carbon monoxide,<sup>[5,37]</sup> chemical vapor deposition (CVD),<sup>[5,6,38,39]</sup> and plasma-enhanced CVD.<sup>[40]</sup> Although unaligned CNTs are good enough for many materials applications, aligned or patterned CNTs are highly desirable for most device-related applications, including various energy-related devices to be described in this article.

Various growth and fabrication methods have been developed to produce vertically aligned MWNTs (VA-MWNTs), in a patterned or nonpatterned form, on a large variety of substrates.<sup>[41–49]</sup> **Figure 4a,b** show scanning electron microscope (SEM) images for some of the VA-MWNT micropatterns reported previously.<sup>[41,48]</sup> Although the formation of

aligned/micropatterned MWNTs has been known for some years, the syntheses of vertically aligned SWNTs (VA-SWNTs) have only recently been reported,<sup>[40,50–54]</sup> as exemplified in Figure 4c. Multicomponent micropatterns of VA-MWNTs interposed with nanoparticles, self-assembled unaligned CNTs, or VA-SWNTs have also been produced<sup>[55–58]</sup> (Figure 4d).<sup>[43]</sup>

For unaligned CNTs, a reasonably high surface area ( $\approx 400 \text{ m}^2 \text{ g}^{-1}$ ) has been obtained for a CNT “paper” electrode.<sup>[59]</sup>

Due to the entanglement of tubes, CNTs have a porosity in the mesopore range ( $\approx 2\text{--}50 \text{ nm}$ ).<sup>[59,60]</sup> The high surface area and unique mesoporosity of CNTs make them highly electrochemically accessible to the electrolyte. Apart from the good electrical conductivity and porosity, CNTs also possess a high thermal conductivity ( $6000 \text{ W mK}^{-1}$ ), high thermal stability (stable up to 2800 °C in vacuum), and good mechanical properties (tensile strength 45 billion Pascals).<sup>[61]</sup> These interesting properties make CNTs very attractive for a variety of potential applications in, for example, sensors,<sup>[62]</sup> hydrogen-storage systems,<sup>[63]</sup> piezoelectric and thermoelectric energy-harvesting devices,<sup>[64,65]</sup> organic photovoltaic cells,<sup>[66]</sup> fuel cells,<sup>[67,68]</sup> batteries,<sup>[69]</sup> and supercapacitors.<sup>[70]</sup> Furthermore, the aligned structure of VA-CNTs could offer opportunities to develop simple, but versatile, approaches for chemical modification of CNTs, even in an asymmetrical manner,<sup>[71,72]</sup> whilst largely retaining their structural integrity.<sup>[73]</sup>

### 2.3. Graphene

Graphene, the one-atom-thick planar sheets of sp<sup>2</sup>-bonded carbon atoms that are densely packed in a honeycomb crystal lattice, is a recent addition to the carbon family.<sup>[18]</sup> Graphene was first discovered in 2004 by Andre Geim and Konstantin Novoselov, who obtained graphene sheets by using cohesive

tape to repeatedly split graphite crystals into increasingly thinner pieces until individual atomic planes were reached.<sup>[18]</sup> This discovery was recognized by Nobel Prize in Physics for 2010 and led to an explosion of interest in graphene.<sup>[74–80]</sup>

As the mother of all graphitic forms, graphene is a building block for carbon materials of all other dimensionalities, such as 0D buckyballs, 1D nanotubes, and 3D graphite. Having many similarities to CNTs in structure and property, including its high aspect ratio (the ratio of lateral size to thickness), large surface area, rich electronic states, and good mechanical properties, graphene is an attractive candidate for potential uses in many areas where the CNTs have been exploited.<sup>[81]</sup> Superior to CNTs, however, the one atomically thick graphene sheets with a

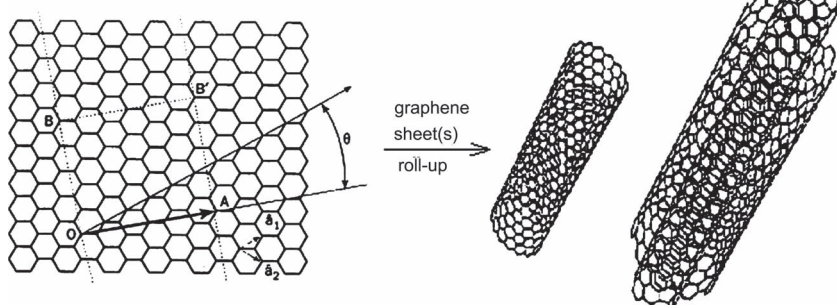


**Figure 3.** Schematic representation of the carbon nanotube formation by rolling up a 2D graphene sheet of lattice vectors  $a_1$  and  $a_2$ , the roll-up chiral vector  $C_h = n a_1 + m a_2$ , and the chiral angle  $\theta$  between  $C_h$  and  $a_1$ . When the graphene sheet is rolled up to form the cylindrical part of the nanotube, the chiral vector forms the circumference of nanotube's circular cross-section with its ends meeting each other. The chiral vector ( $n, m$ ) defines the tube helicity. If  $n-m \neq 3q$  ( $n, m$ , and  $q$  are integers), the SWNT is semiconducting; if  $n-m = 3q$ , the SWNT is metallic. Reproduced with permission.<sup>[38]</sup>

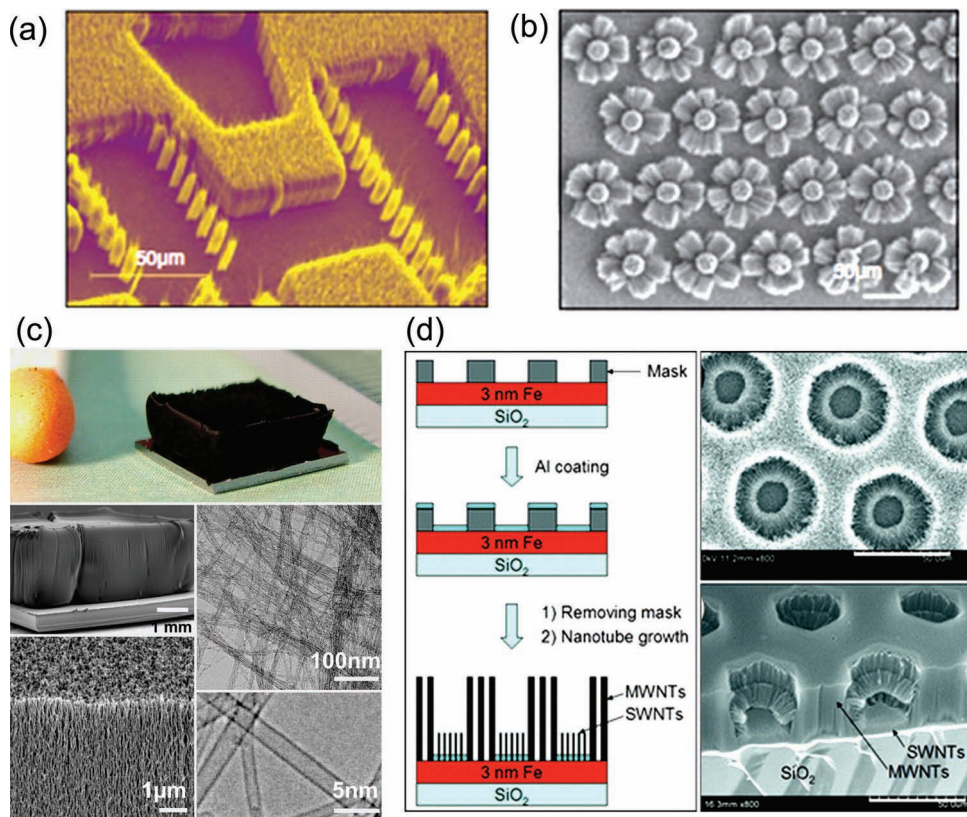


**Figure 4.** SEM images of VA–MWNT micropatterns prepared by a) pyrolysis of iron phthalocyanine onto a photopatterned substrate,<sup>[48]</sup> and b) simultaneous growth onto patterned silica surface with different tilt angles;<sup>[41]</sup> c) VA–SWNT forests prepared by the water-assisted growth method,<sup>[50]</sup> and d) (left panel) schematic representation of the growth procedure for an interposed VA–SWNT/VA–MWNT multicomponent pattern with its top view (right top, scale bar: 50 μm) and cross-sectional view (right bottom, scale bar: 50 μm).<sup>[40]</sup> Reproduced with permission.<sup>[43]</sup> Copyright 2008, Materials Research Society.

2D planar geometry will further facilitate electron transport, and hence the more effective electrode materials. **Table 1** lists some properties of graphene in comparison with those of CNTs. Owing to their superb properties as well as large surface area, graphene nanosheets (GNs) with a 2D carbon nanostructure have been studied as a new class of promising materials attractive for potential applications in sensors, actuators, solar cells, field-emission devices, field-effect transistors, supercapacitors, and batteries.<sup>[74–81]</sup>

Apart from the Scotch tape drawing method,<sup>[18]</sup> epitaxial growth of graphene on silicon carbide (SiC) has been

reported by heating SiC to high temperatures (>1100 °C) to reduce it into graphene.<sup>[83]</sup> Using standard lithographic techniques, researchers have produced hundreds of (high frequency) transistors on a single chip by patterning epitaxial graphene on SiC.<sup>[84]</sup> Another method of obtaining graphene is by CVD of hydrocarbons on a metal or metal-coated substrate.<sup>[85,86]</sup> Of particular interest, high-quality sheets of few layer graphene have been synthesized via CVD on thin Ni films, which can be transferred to various substrates for potential applications.<sup>[87–89]</sup> By replacing the Ni substrate with a Cu foil, it was found that the CVD growth process at a low pressure automatically stops after the formation of a single graphene layer,<sup>[88,90]</sup> though multilayer graphene may form in atmospheric pressure.<sup>[91]</sup> Recently, CVD methods have also been used to turn sucrose, among other substances such as Plexiglas, quickly and easily into graphene onto a Cu or Ni substrate at 800 °C under low pressure of argon and hydrogen gas for about 10 min only.<sup>[92]</sup> More recently, Choucair et al.<sup>[93]</sup> reported a process for producing gram quantities of graphene through the reduction of ethanol by sodium metal, followed by pyrolysis of the ethoxide product and washing with water to remove sodium salts. Large-scale production of graphene sheets has also been achieved by exfoliation of graphite via acid oxidation (e.g., nitric acid ( $pK_a = -1.5$ )/sulfuric acid ( $pK_a = -3.0$ ) mixture) into dispersible graphite oxide (GO),

**Table 1.** Some properties of graphene in comparison with those of CNTs.<sup>[5,6,82]</sup>

Properties	Graphene	CNTs
Fracture strength (GPa)	≈124 (Modulus: ≈1100 GPa)	45
Density (g cm <sup>-3</sup> )	>1	1.33
Thermal conductivity (W m <sup>-1</sup> K <sup>-1</sup> )	≈5000	3000
Electrical Conductivity (S cm <sup>-1</sup> )	10 <sup>6</sup>	5000
Charge mobility (cm <sup>2</sup> V <sup>-1</sup> s <sup>-1</sup> )	200 000	100 000
Specific surface area (m <sup>2</sup> g <sup>-1</sup> )	2630	400 (for nanotube “paper”)

followed by reduction of GO (e.g., by hydrazine,  $\text{NaBH}_4$ ) and annealing in argon/hydrogen to yield graphene sheets.<sup>[94,95]</sup>

Due to possible structural damages caused by solution chemical reactions, quality of graphene produced by graphite oxide reduction is lower compared to graphene produced by the Scotch tape drawing, epitaxial grown on SiC or CVD on metal substrates. However, solution methods have been used for the production of high-quality graphene ribbons through cutting to open nanotubes<sup>[96]</sup> in the presence of potassium permanganate and sulfuric acid.<sup>[97]</sup> In a similar but independent work, graphene nanoribbons were produced by plasma etching of nanotubes partly embedded in a polymer film.<sup>[98]</sup>

The availability of large-scale solution-processable graphene nanosheets allowed the formation of graphene-based functional films through various solution processing methods, including filtration,<sup>[99]</sup> solution-casting,<sup>[100]</sup> electrophoretic deposition,<sup>[101]</sup> and Langmuir–Blodgett deposition.<sup>[102]</sup>

## 2.4. Nitrogen-Doped Carbon Nanomaterials

### 2.4.1. Nitrogen-Doped Carbon Nanotubes

The introduction of surface heteroatoms (e.g., nitrogen) into carbon nanomaterials could cause electron modulation to provide desirable electronic structures for many potential applications of practical significance.<sup>[103]</sup> In particular, nitrogen-doping of CNTs has been studied for some years with attempts to modulate the nanotube electronic and other properties.<sup>[104,105]</sup> N-doped CNTs can be prepared either by in-situ doping during the nanocarbon synthesis or through post-treatment (i.e., post-doping) of preformed CNTs with nitrogen-containing precursors (e.g.,  $\text{NH}_3$ ).<sup>[106–110]</sup> Post-doping of carbon nanotubes often leads to surface functionalization only without altering their bulk properties.<sup>[107–110]</sup> In contrast, the in-situ doping can incorporate nitrogen atoms into the entire CNT structure homogeneously. Various N-doped CNTs have been synthesized by arc-discharge, laser

ablation, or CVD, either in aligned or nonaligned forms with or without template, via in-situ doping<sup>[111–114]</sup> in the presence of appropriate nitrogen containing precursors<sup>[115–119]</sup> for a wide range of applications,<sup>[118,120]</sup> including their use as metal-free catalysts for oxygen reduction reaction (ORR) at the cathode in fuel cells (see Section 3.2.2).<sup>[105,116,121]</sup>

### 2.4.2. Nitrogen-Doped Graphene

Although CNTs and their N-doped counterparts have been synthesized and studied for some years, the large-scale preparation of graphene sheets by CVD is only the recent development.<sup>[87,122]</sup> Attempts have recently been made to introduce heteroatoms (e.g., nitrogen) into nitrogen-doped graphene (N-graphene) sheets.<sup>[89,123]</sup> By a modified CVD process,<sup>[87]</sup> Qu and co-workers<sup>[89]</sup> have prepared N-graphene films using a nitrogen-containing reaction gas mixture ( $\text{NH}_3:\text{CH}_4:\text{H}_2:\text{Ar} = 10:50:65:200$  standard cubic centimeters per minute) and a Ni-coated  $\text{SiO}_2/\text{Si}$  substrate. The resultant N-graphene film can be readily etched off from the substrate by dissolving the residual Ni catalyst layer in an aqueous solution of  $\text{HCl}$ ,<sup>[89,122]</sup> allowing the freestanding N-graphene sheets to be transferred onto substrates suitable for subsequent investigation. Just like CVD-synthesized all-carbon graphene (C-graphene) films,<sup>[87]</sup> the N-graphene film thus produced is flexible and transparent, consisting of only one or a few layers of the graphitic sheets. The resultant N-graphene was demonstrated to act as a metal-free electrode with a much better electrocatalytic activity, long-term operation stability, and tolerance to crossover or CO-poisoning effect than platinum for oxygen reduction via a four-electron pathway in alkaline fuel cells (Section 3.2.2).

On the other hand, Baek and co-workers<sup>[124]</sup> have also developed a scalable synthetic method for producing high-quality N-graphene films via solution processing and subsequent heat-treatment of edge-selectively functionalized graphite (EFG, **Figure 5**). The desired EFG was prepared from the reaction between 4-aminobenzoic acid and the ‘pristine’ graphite (P-graphite) to afford 4-aminobenzoyl-functionalized graphite.<sup>[124]</sup> The EFG thus produced is

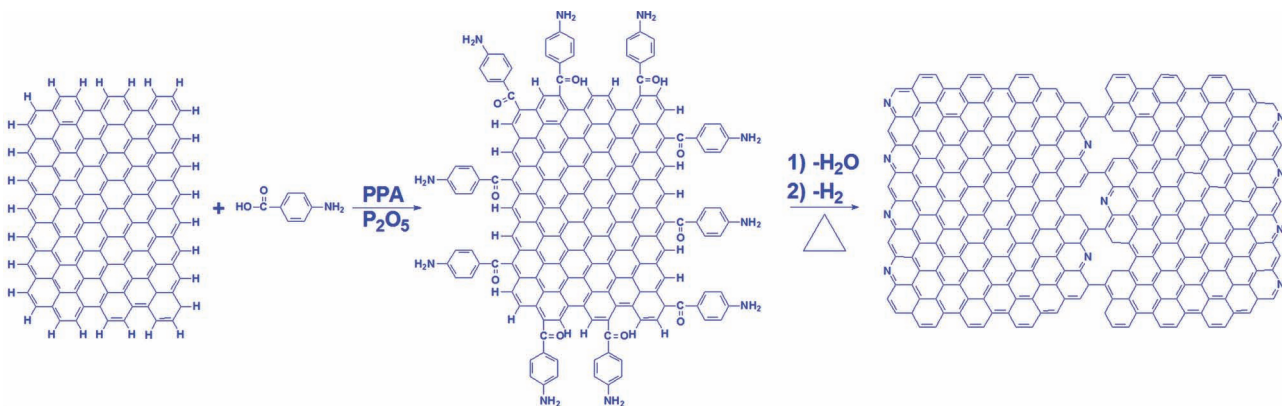


**Figure 5.** Functionalization of pristine graphite (P-graphite) with 4-aminobenzoic acid to produce edge-functionalized graphite (EFG) with 4-aminobenzoyl groups and subsequent heat treatment to prepare nitrogen-doped graphene (N-graphene). Reproduced with permission.<sup>[125]</sup> Copyright 2011, American Chemical Society.

readily dispersible in *N*-methyl-2-pyrrolidone (NMP). Solution-casting and subsequent heat-treatment can lead to the formation of large-area N-graphene film. The 4-aminobenzoyl moieties (4-H<sub>2</sub>N-Ph-CO-) at the edges of EFG can act as the in-situ feedstock for carbon and nitrogen sources for simultaneous ‘C-welding’ and ‘N-doping’ (Figure 5). The resultant N-graphene has been demonstrated to be attractive metal-free catalysts for ORR in fuel cells (*vide infra*).<sup>[125]</sup>

Edge-selective functionalization has many advantages over the commonly used nitric acid/sulfuric acid mixture for the synthesis of GO.<sup>[126,127]</sup> One of the salient features is that the reaction medium, polyphosphoric acid (PPA)/P<sub>2</sub>O<sub>5</sub>, does not oxidize graphite but selectively functionalize the sp<sup>2</sup> C–H defects at the edges of graphite (Figure 5),<sup>[124,125]</sup> leading to minimal carbon basal plane damage.

### 3. Carbon Nanomaterials for Energy Conversion

Carbon nanomaterials, including fullerenes, nanotubes and graphene as well as their N-doped derivatives, have been studied for a wide range of applications in energy conversion systems, such as solar cells and fuel cells. Here, we present an in-depth review of the broad scope of carbon nanomaterials and nanotechnology for cutting-age research and development in the field of energy conversion.

#### 3.1. Polymer Solar Cells

##### 3.1.1. Polymer Solar Cells Containing Fullerenes

The global energy consumption has been accelerating at an alarming rate. This, together with the limited supply of today’s main energy sources (i.e., oil, coal, uranium) and their detrimental long-term effects on the environment, has made it more important than ever to develop renewable energy sources. The sun does provide us with renewable energy sources, which neither run out nor have any significant harmful environmental effect. Ever since the French scientist Alexandre-Edmond Becquerel discovered the photovoltaic effect in 1839,<sup>[128]</sup> scientists and engineers have devoted considerable effort to realize the dream that human beings can one day convert the energy of sunlight directly into electricity by the photovoltaic effect to meet our daily energy needs.<sup>[129–131]</sup> After more than 170 years, however, this dream still has yet to be realized. Nevertheless, tremendous success has been made since the development of the first single-junction inorganic (Si) solar cell at Bell Laboratories in 1954.<sup>[132]</sup> Although a power-conversion efficiency up to 35% has now been achieved for inorganic (III–V semiconductor) multijunction solar cells in a lab scale,<sup>[133]</sup> the widespread use of the conventional silicon-based photovoltaic devices is still limited due to the difficulties in modifying the band gap of Si crystals and the high cost associated with the elaborate fabrication processes involving elevated temperature and high vacuum.<sup>[134,135]</sup> These inorganic solar cells are still too expensive to compete with conventional grid

electricity.<sup>[136]</sup> Thus, alternative approaches using organic materials, including organic dyes<sup>[137–140]</sup> and conjugated polymeric semiconductors,<sup>[66,141]</sup> have received considerable attention in the search for novel photovoltaic cells because of their potential benefits over the inorganic materials, including low cost, lightweight, flexibility, and versatility for fabrication (especially over a large area).<sup>[142]</sup> In this regard, the photoinduced charge transfer of fullerenes is of importance for the development of polymeric photovoltaic cells, which can be used to store light energy as electron relays for producing electricity.

The photovoltaic effect involves the generation of electrons and holes in a semiconducting device under illumination, and subsequent charge collection at opposite electrodes. Inorganic semiconductors, such as amorphous silicon, gallium arsenide, and sulfide salts, have been widely used in conventional photovoltaic cells, in which free electrons and holes were produced directly upon photon absorption.<sup>[143]</sup> Unlike their inorganic counterparts, however, photon absorption by conjugated polymers at room temperature often creates bound electron hole pairs (i.e., excitons). Charge collection, therefore, requires dissociation of the excitons, a process which is known to be favorable at the interface between semiconducting materials with different ionization potentials or electron affinities.<sup>[144]</sup>

The observation of photovoltaic effects arising from the photo-induced charge transfer at the interface between conjugated polymers as donors and C<sub>60</sub> film as an acceptor<sup>[28,29,145,146]</sup> suggests interesting opportunities for improving energy-conversion efficiencies of photovoltaic cells based on conjugated polymers.<sup>[147,148]</sup> Indeed, increased quantum yields have been obtained by the addition of C<sub>60</sub> to form heterojunctions with conjugated polymers, such as PPV, MEH-PPV,<sup>[29,145,149,150]</sup> poly(3-alkylthiophene) (P(3TA))<sup>[151]</sup> and platinum–polyyne.<sup>[152]</sup> In these conjugated polymer–C<sub>60</sub> systems, excitons generated in either layer diffuse towards the interface between the layers. Although the photoinduced charge transfer between the excited conducting polymer donor and a C<sub>60</sub> acceptor can occur very rapidly on a subpicosecond timescale,<sup>[153]</sup> with a quantum efficiency of close to unity for charge separation from donor to acceptor,<sup>[154]</sup> the conversion efficiency of a bilayer heterojunction device is still limited<sup>[29,145,154]</sup> by several other factors. Firstly, since the efficient charge separation occurs only at the heterojunction interface, the overall conversion efficiency is diminished by the limited effective interfacial area available in the layer structure. Secondly, because the exciton diffusion range is typically at least a factor of 10 smaller than the optical absorption depth,<sup>[144]</sup> the photoexcitations produced far from the interface recombine before diffusing to the heterojunction. Miscibility between the electron acceptor and donor at the interface, either caused by a cosolvent effect or post-fabrication diffusion, also creates problems in a bilayer device. Finally, the conversion efficiency is also limited by the carrier collection efficiency.

In order to overcome the above-mentioned deficiencies associated with polymer solar cells based on a bilayer heterojunction, interpenetrating networks consisting of two

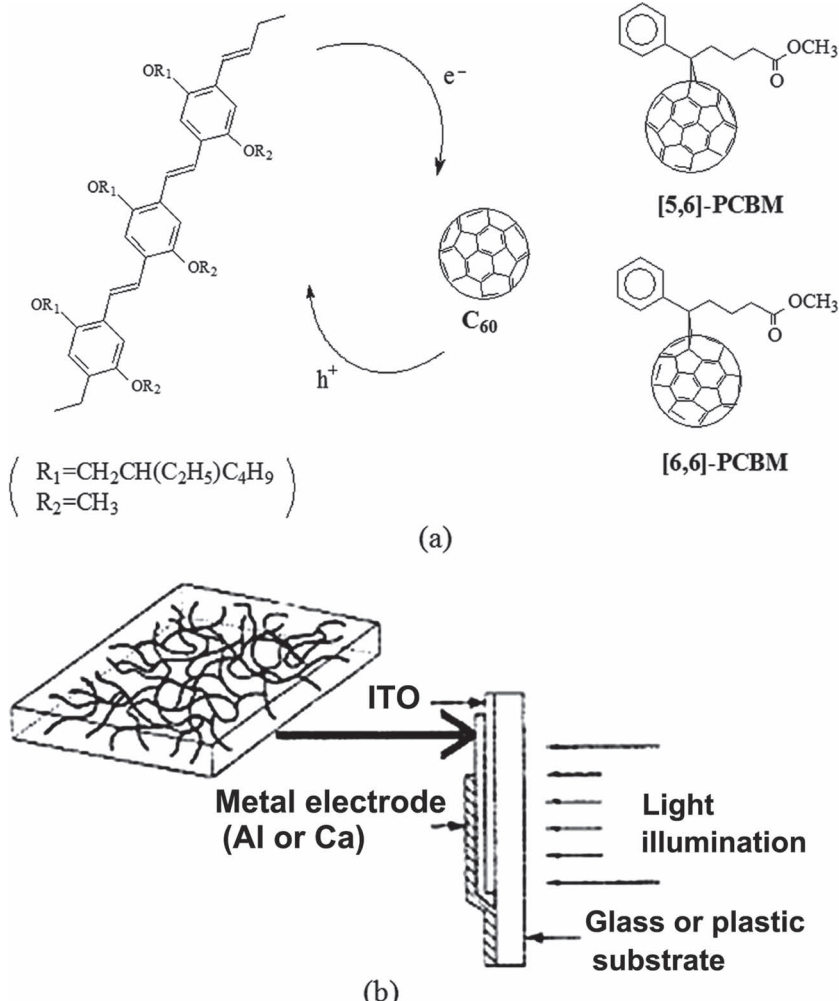


**Figure 6.** Schematic illustrations of a) charge transfer between C<sub>60</sub> derivatives and MEH-PPV; b) the interpenetrating conjugated polymer-C<sub>60</sub> (donor-acceptor) network and the photovoltaic cell. Reproduced with permission.<sup>[30]</sup> Copyright 1995, American Association for the Advancement of Science.

semiconducting polymers have been developed as ideal photovoltaic materials for a high-efficiency photovoltaic conversion (**Figure 6**).<sup>[30,142]</sup> The interpenetrating network structure provides the spatially distributed interfaces necessary for both an efficient photogeneration and a facile collection of the electrons and holes.<sup>[30,154,155]</sup> As a consequence, significantly improved conversion efficiencies up to ca. 8% have been reported recently for photovoltaic cells based on interpenetrating network composites consisting of conjugated polymer and C<sub>60</sub> derivatives.<sup>[30,156]</sup> The efficiency of polymer solar cells can be further improved by thermal annealing.<sup>[156–159]</sup> Although [6,6]-phenyl-C<sub>61</sub>-butyric acid methyl ester (PC<sub>61</sub>BM) has been widely used as the acceptor in polymer solar cells, other fullerene derivatives, including PC<sub>71</sub>BM or PC<sub>84</sub>BM with a broader visible absorption and PCBM bisadducts or multiadducts with a higher lowest unoccupied molecular orbital (LUMO) energy level and better solubility, were used occasionally to further improve the power-conversion efficiency of polymer solar cells.<sup>[160]</sup>

### 3.1.2. Polymer Solar Cells Containing Carbon Nanotubes

Tremendous progress has been achieved with materials and device fabrication methods for preparing the dispersed heterojunction organic solar cells during the past decade or so. Recently, more advanced nanoarchitecturing of the blends have been studied to further improve the performance of the dispersed heterojunction organic photovoltaic devices. To this end, considerable attention has been paid to disperse heterojunctions fabricated from polymer/CNT composite systems.

In a dispersed heterojunction organic solar cell, free charges usually percolate through the device as drift and diffusion currents. As an extended form of C<sub>60</sub>, CNT is expected to provide higher electron mobility with a lower percolation threshold. In fact, certain CNTs are known as an extremely electron-conductive semiconductor as field-effect electron mobility up to 77000 cm<sup>2</sup> V<sup>-1</sup> s<sup>-1</sup> has been reported.<sup>[161]</sup> In contrast, electron mobilities of PCBM, calculated from time-of-flight experiments and the analyses of field-effect transistors, ranged between 10<sup>-6</sup> and 10<sup>-1</sup> cm<sup>2</sup> V<sup>-1</sup> s<sup>-1</sup>.<sup>[162,163]</sup> The higher carrier mobility allows thicker devices to harvest more photons without sacrificing internal quantum efficiency. Typical thickness of the organic solar cell is in the order of 100 nm, which is limited by optical absorption and diffusion current at a given carrier mobility.<sup>[141,164]</sup>

On the other hand, recombination becomes competitive if the device becomes too thick. A simplified model demon-

strated that composites with better transport properties (higher carrier mobilities) allowed making thicker devices to absorb more photons while the charge recombination loss can be minimized through the fast charge diffusion/collection.<sup>[141]</sup> Thus, replacing PCBM with electron affinity materials of a higher-electron mobility, like CNTs, is considered to be promising route to improve the organic solar-cell performance.

The first rectifying heterojunction between MWNTs and a commercially available soluble derivative of PPV was reported by Romero et al.<sup>[165]</sup> in 1996. The junction was made by filtering a solution of MEH-PPV onto a mat of CNTs. Their results showed that the nonlinear current injection was enhanced by a local field created at the interface between the two materials upon exposure of the junction to light. Curran et al.<sup>[166]</sup> have also prepared a composite junction by mixing poly(*m*-phenylenevinylene-*co*-2,5-dioxy-*p*-phenylenevinylene) and MWNTs in toluene, followed by solution casting. It was found that the good wetting between the surface of MWNTs and polymer improved the photoconductivity, photoluminescence, and electroluminescence.<sup>[167,168]</sup>

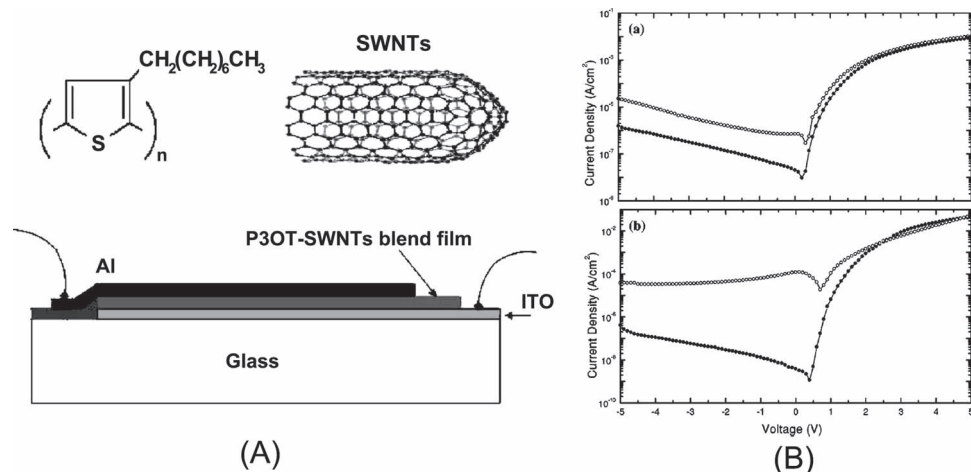


**Figure 7.** A) A typical device architecture of the P3HT/SWNT photovoltaic cell. B) a)  $I$ - $V$  characteristics of an ITO/P3OT/Al device in dark (lower curve) and under illumination (upper curve); b) the same data for an ITO/P3OT-SWNT/Al device. Reproduced with permission.<sup>[169]</sup> Copyright 2002, American Institute of Physics.

The above work was quickly followed by other reports on the PV effect from polymer/CNT heterojunctions.<sup>[168,169]</sup> In particular, Kymakis and Amaratunga<sup>[169]</sup> have spin-cast composite films of poly(3-octylthiophene) (P3OT) and SWNTs on indium tin oxide (ITO)-coated quartz substrates. They found that diodes with the Al/P3OT-SWNT/ITO structure (**Figure 7A**) showed photovoltaic behavior with an open circuit voltage of 0.7–0.9 V even at a low nanotube concentration (<1%). As shown in Figure 7B, the short-circuit current is increased by two orders of magnitude compared with the pristine polymer device, with an increased fill factor from 0.3 to 0.4 for the nanotube–polymer cell. The improved device performance has been attributed to the good electronic properties of CNTs and their large surface areas. CNTs can also provide good mechanical stability and high thermal conductivity. The addition of the dye molecules into polymer–CNT solar cells could further improve light absorption in the UV and red region, leading to an increase in the short-circuit current ( $I_{sc}$ ) by more than five times.

The bulk heterojunction concept has been widely used for polymer photovoltaic cells. Due to its high interfacial contact area between the donor and acceptor, the bulk heterojunction is more effective compared with a bilayer device structure. As mentioned earlier, the overall energy conversion efficiency of a bilayer device is diminished by the limited effective interfacial area available in the layer structure, and the photo-excitations produced far from the interface recombine before diffusing to the bilayer heterojunction. However, a bilayered device structure could be more favorable with respect to the bulk heterojunction for efficient charge transport since the separated charge carriers can easily transport to the opposite electrodes with a minimized recombination possibility.<sup>[170–172]</sup> In this regard, Wang et al.<sup>[172]</sup> reported that a poly(3-hexylthiophene)(P3HT)/PCBM bilayer polymer solar cell with a concentration gradient showed an enhanced photocurrent density and power-conversion efficiency compared to those of the bulk heterojunction photovoltaic cells under the same condition. On the other hand, the  $C_{60}$  layer in bilayer devices

could provide an additional protection to the polymer layer from possible degradation caused by oxygen and humidity, thus improving the device stability.<sup>[173]</sup> More importantly, the bilayer structure allows the  $C_{60}$  layer to prevent the polymer layer from direct contact with the cathode, reducing the recombination loss and eliminating any possible short circuit problem for polymer hybrid solar cells containing conducting additives (e.g., CNTs).

Using a bilayer photovoltaic device, Kuila et al.<sup>[174]</sup> have recently investigated the charge transfer at the polymer–CNT interface by grafting  $CH_2OH$ -terminated regioregular P3HT onto carboxylic groups of acid-oxidized CNTs via esterification reaction. The P3HT-attached CNTs (P3CNTs) are soluble in common organic solvents, facilitating an intimate mixing with free P3HT chains for strong electronic interactions. The optical and electrochemical properties of the resultant nanocomposite were found to be different from the conventional composite, in which the pristine CNT and P3HT were physically mixed together (P3HT/CNT). Electrochemical measurements on the onset oxidation and reduction potentials of the P3CNT showed positive shifts by 0.06 and 0.1 eV, respectively, with respect to the corresponding values of pure P3HT, indicating that P3CNT has lower highest occupied molecular orbital (HOMO) and LUMO energy levels than those of pure P3HT. Bilayer photovoltaic devices with a thin film of pure P3CNT as the electron-donor and  $C_{60}$  as the electron-acceptor layer showed an increase in the power-conversion efficiency by about 40% with respect to their counterpart based on pure P3HT.

Although CNTs have been used in both bilayer and bulk heterojunction polymer photovoltaic devices for enhanced charge separation and transport,<sup>[175–179]</sup> significant improvement in the overall device performance has not been achieved for such photovoltaic cells. Instead of randomly mixing a polymer with nonaligned CNTs in a solution to cast into a film, an ideal device structure for polymer/CNT dispersed heterojunction solar cell can be made by coating a polymer on a VA–CNT array.<sup>[66]</sup> In this case, VA–CNTs could provide a

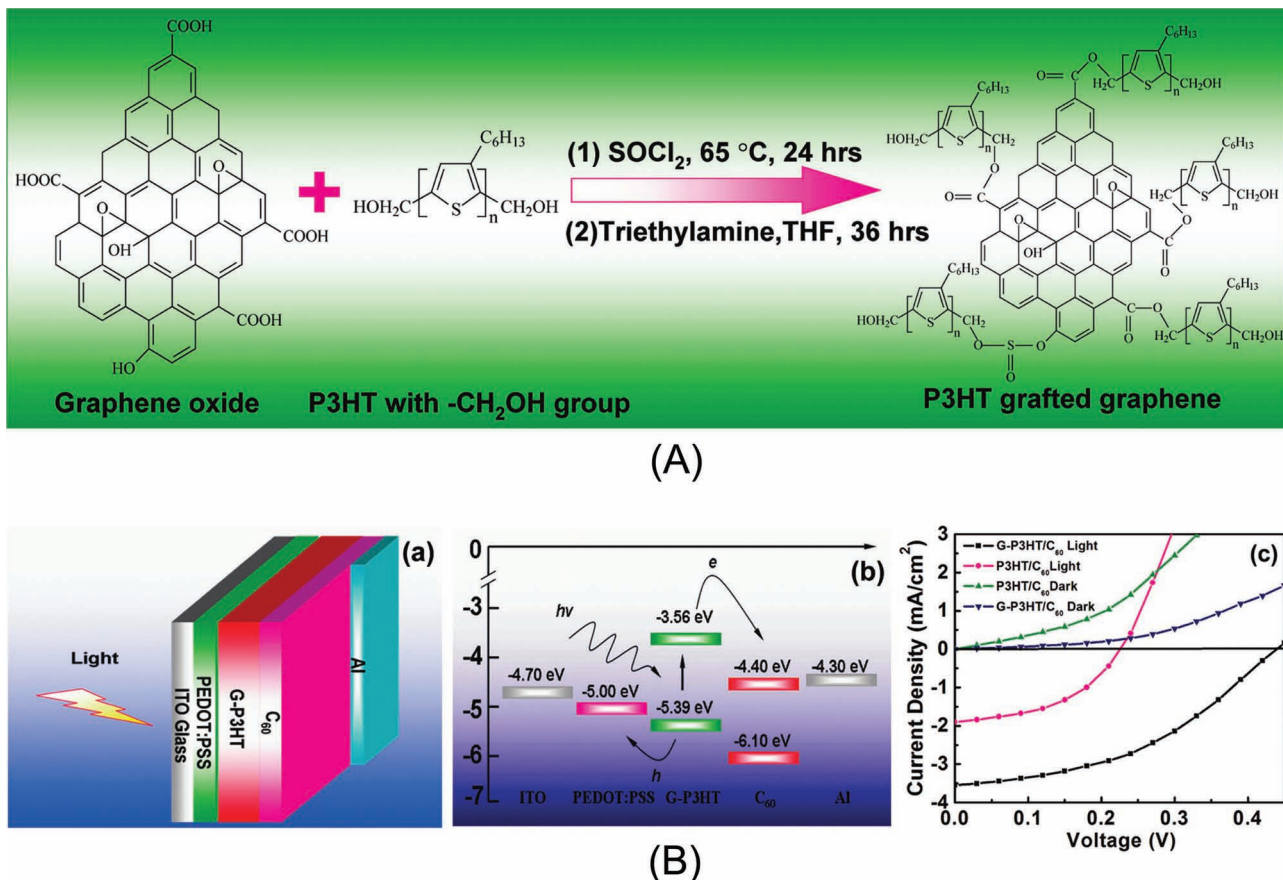


**Figure 8.** A) Synthetic procedure for chemical grafting of CH<sub>2</sub>OH-terminated P3HT chains onto graphene oxide, which involves the SOCl<sub>2</sub> treatment of GO (Step 1) and the esterification reaction between acyl chloride-functionalized GO and MeOH-terminated P3HT (Step 2). B) a) Schematic and b) energy-level diagram of an ITO/PEDOT:PSS/G-P3HT/C<sub>60</sub>/Al photovoltaic device. c) Current (*I*)–voltage (*V*) characteristics of the photovoltaic devices using P3HT/C<sub>60</sub> or G-P3HT/C<sub>60</sub> as the active layer. Reproduced with permission.<sup>[184]</sup> Copyright 2010, American Chemical Society.

facile route for charge collection while the well-defined large nanotube surface should allow for efficient light harvesting and charge separation. Spacing between VA–CNTs needs to be controlled within the exciton diffusion length to minimize charge recombination after the exciton dissociation<sup>[180]</sup> at interfaces between the polymer and the VA–CNTs. The vertical alignment also allows the constituent nanotube photovoltaic cells to be collectively addressed through a common substrate/electrode. We anticipate considerable technical challenges ahead but also believe much more developments will be made in a few years to advance the performance of organic solar cells based on VA–CNTs.

### 3.1.3. Polymer Solar Cells Containing Graphenes

Compared with CNTs, the one-atom thickness and 2D carbon network of graphene lead to a much higher specific surface area (hence, a larger interface in a polymer matrix) and a reduced possibility for the short circuit through the photovoltaic active layer even in a bulk heterojunction device.<sup>[181–185]</sup> Along with the 0D fullerenes and 1D CNTs, the 2D graphene nanosheets have also been explored as a new class of transport materials and/or acceptors in polymer solar cells (PSCs).<sup>[181–185]</sup> Of particular interest, Yu et al.<sup>[184]</sup> have

chemically grafted CH<sub>2</sub>OH-terminated regioregular P3HT onto carboxylic groups of graphene oxide (GO) via esterification reaction (Figure 8A). The resultant P3HT-grafted GO sheets (G-P3HT) were found to be soluble in common organic solvents, facilitating the structure/property characterization and device fabrication by solution processing. The covalent linkage and strong electronic interaction between the P3HT and graphene moieties in G-P3HT were confirmed by spectroscopic/electrochemical measurements, which played an important role in enhancing the device performance by improving the charge transport. A bilayer photovoltaic device based on the solution-cast G-P3HT/C<sub>60</sub> heterostructures showed a 200% increase of the power-conversion efficiency ( $\eta = 0.61\%$ ) with respect to the P3HT/C<sub>60</sub> counterpart under AM 1.5 illumination (100 mW cm<sup>-2</sup>) (Figure 8B). While the significantly improved device performance can be attributed to the strong electronic interaction and good bandgap matching (Figure 8Bb) between the chemically bonded P3HT and graphene, this work indicates that graphene can also be used as an efficient hole transporting material in polymer solar cells.

In a separate study, Yu et al.<sup>[186]</sup> have also developed a simple lithiation reaction to covalently attach monosubstituted C<sub>60</sub> onto graphene nanosheets (Figure 9A). The

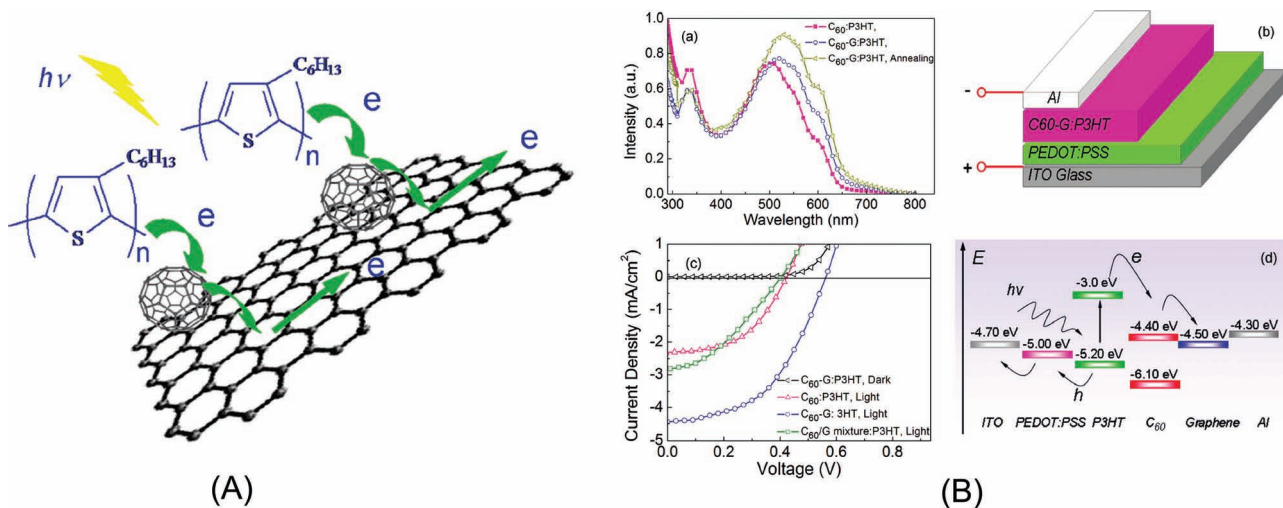


**Figure 9.** A) Schematic representation of C<sub>60</sub>-grafted graphene for facilitating the electron transfer and transport in a polymer solar cell. B) a) Absorption spectra of the C<sub>60</sub>-G:P3HT (1:1 wt/wt) film before and after annealing (130 °C, 10 min) and the C<sub>60</sub>:P3HT (1:1 wt/wt) film spin-coated onto quartz plates. B) Schematic of a hybrid photovoltaic device with the C<sub>60</sub>-G:P3HT composite as the active layer. c) J-V curves of the photovoltaic devices with the C<sub>60</sub>-G:P3HT (1:1 wt/wt), the C<sub>60</sub>:P3HT (1:1 wt/wt), or the C<sub>60</sub>/G mixture (10 wt% G):P3HT (1:1 wt/wt) as the active layers after annealing treatment (130 °C, 10 min). d) Energy-level diagram for the proposed photovoltaic device using the C<sub>60</sub>-G:P3HT composite as the active layer. Reproduced with permission.<sup>[186]</sup> Copyright 2011, American Chemical Society.

resultant C<sub>60</sub>-grafted graphene (C<sub>60</sub>-graphene or C<sub>60</sub>-G) nanosheets were used as electron acceptors in P3HT-based bulk heterojunction solar cells to significantly improve the electron transport, and hence the overall device performance (Figure 9B).

On the other hand, Chen and co-workers<sup>[181,182]</sup> reported that the efficiency of P3HT/P3OT-based photovoltaic cells was strongly enhanced after incorporation of functionalized graphene as an acceptor, indicating an efficient charge transfer from the polymer donor to graphene acceptor. However, the device performance depended strongly on several other factors, including the concentration of graphene, annealing time, and annealing temperature.

### 3.1.4. Graphene Quantum Dot Solar Cells

Recently, solar cells based on quantum dots (QD solar cells) have attracted a great deal of interest because of their potential in exceeding the Shockley–Queissar limit of 32% power-conversion efficiency for Si solar cells and achieving size-tunable optical absorption and efficient multiple carrier generation.<sup>[187,188]</sup> One of the major challenges in developing high-performance QD solar cells is to effectively separate photogenerated electron–hole pairs and to facilitate the electron transfer to the electrode.

Carbon nanomaterials of suitable band energies, such as fullerenes and SWNTs, have been used in QD solar cells as efficient electron acceptors.<sup>[6,189–195]</sup> However, even the highest incident photon-to-charge carrier generation efficiency (IPCE = 5% under light illumination of 100 mW cm<sup>-2</sup>) reported for most carbon-based QD solar cells,<sup>[6,189–195]</sup> is still too low to meet the requirement for their commercialization. Recent development in nanomaterials and nanotechnology has opened up new frontiers in materials science and device

engineering to create novel carbon nanomaterials with tailored bandgaps and new devices with desirable structures for enhancing the solar cell performance.<sup>[6,189–197]</sup>

In this regard, Guo et al.<sup>[198]</sup> have recently reported a significant advance in the development of layered graphene/quantum dots for highly efficient solar cells. Instead of using 1D, cylindrical CNTs to construct CdS QD solar cells<sup>[192,193]</sup> with an inhomogeneous CdS distribution, these authors used the 2D, single-atom-thick graphene sheets to support CdS QDs.<sup>[190,198]</sup> Compared with CNTs for this particular application, graphene sheets offer many competitive advantages, including their versatility for solution-based large-scale fabrication, good transparency, high charge mobility, large specific surface area, and low cost.<sup>[76,199]</sup> By creating a novel layered nanofilm of graphene/CdS QDs as the electrode (**Figure 10Aa**) from all aqueous solutions through sequential electrophoretic and chemical deposition, Guo et al.<sup>[198]</sup> successfully increased the IPCEs of the QD solar cell by more than a 3-fold up to 16% (Figure 10Ab).

As demonstrated by Guo et al.<sup>[198]</sup> graphene showed a relatively good band energy match with CdS QD in respect to SWNTs (Figure 10Ac) for an effective charge separation, and allowed for a uniform distribution of the QD nanoparticles (vide infra) to maximize the solar absorption and charge collection.<sup>[188]</sup> Indeed, Figure 10Ba clearly shows a conformal graphene layer on the ITO glass produced by the electrophoretic deposition. Subsequent chemical reduction of Cd<sup>2+</sup> from CdCl<sub>2</sub> in an aqueous solution of Na<sub>2</sub>S led to the formation of crystalline CdS QDs of ≈5 nm in diameter, which are uniformly distributed over the predeposited graphene film (Figure 10Bb,c). The resulting ITO/graphene/CdS QD bilayer photovoltaic device exhibited an IPCE of 5%, a value which is much higher than the highest IPCE = 0.45% reported for its ITO/SWNT/CdS QD counterpart.<sup>[192,193]</sup>

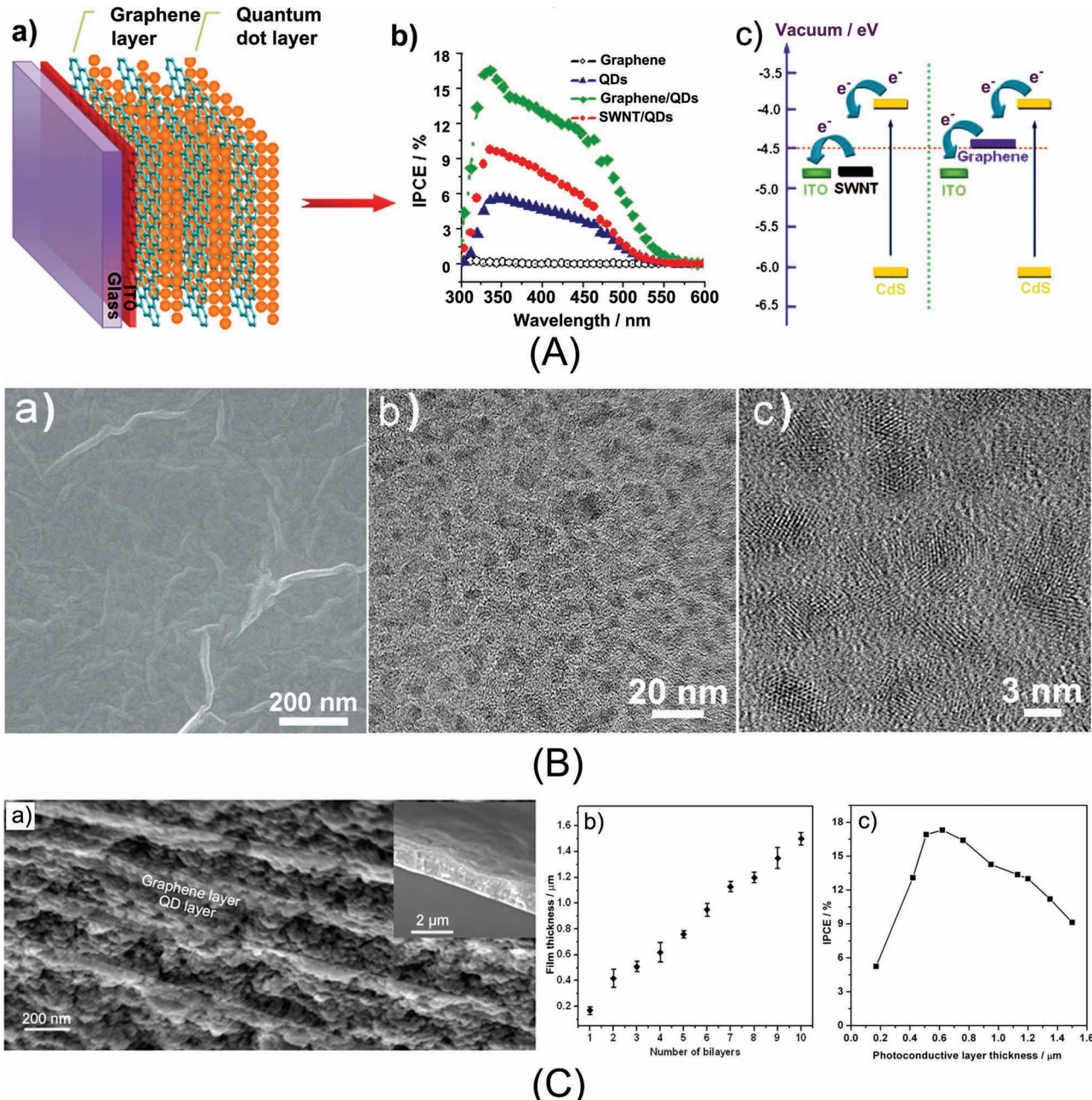


**Figure 10.** A) a) Schematic representation of the layered nanofilm of graphene/CdS QDs on an ITO glass electrode. b) The IPCEs for different photoelectrodes. c) Energy-level diagrams. B) a) SEM image of the graphene layer electrophoretically deposited on an ITO-coated glass. b,c) TEM images of CdS QDs on the graphene layer under different magnifications. C) a) Cross-section SEM image of a layered film of (graphene/CdS QD)<sub>n</sub> and the inset shows its thickness. b) The plot of the film thickness ( $\mu\text{m}$ ) against the number of (graphene/CdS QD) bilayers. c) IPCEs (recorded at 400 nm) for the layered ITO/(graphene/CdS QD)<sub>n</sub> against the photovoltaic active layer thickness ( $\mu\text{m}$ ). Reproduced with permission.<sup>[198]</sup>

To further improve the device performance, Guo et al.<sup>[198]</sup> prepared a multilayer (graphene/CdS QD)<sub>n</sub> nanoassembly while largely retaining the intimate contact and large interface between each of the adjacent graphene and CdS QD layers (Figure 10Ca) by sequentially depositing the graphene and CdS QD layer on each other through the electrophoretic and chemical deposition, respectively.

The aforementioned innovative approach has not only significantly increased the solar-absorption efficiency by increasing the total film thickness in a controllable fashion

(Figure 10Cb),<sup>[134,196]</sup> but has also offered potential for minimizing the recombination loss of charge carriers by independently tuning the thickness and morphology for each of the constituent layers. As a consequence, IPCEs up to 16% (Figure 10Cc), 3-fold higher than the value (5%) of ITO/graphene/CdS QD bilayer, was obtained in this study<sup>[198]</sup> and even higher efficiencies could be achievable. The IPCEs of the multilayer graphene/CdS QD nanoassembly are much superior to that of other carbon based QD solar cells reported so far, for example, 0.45% for SWNT/CdS QD solar cell,<sup>[192,193]</sup>

4.5% for fullerene/CdSe QD composite,<sup>[190]</sup> 5% for stacked carbon nanocup/CdSe QD solar cell,<sup>[190]</sup> and 1.2% for SWNT/pyrene/CdTe.<sup>[195]</sup>

On the other hand, several researchers have used graphene film and graphene quantum dots (GQDs) for various parts of QDs-based solar cells, including electron acceptors<sup>[198]</sup> and active light absorbers.<sup>[200]</sup> The conversion of two dimensional graphene sheets into zero dimensional GQDs seems to be a promising approach due to efficient fabrication of nanodevice and fine tuning of band gap of graphene. In particular, Li et al.<sup>[201]</sup> reported the application of electrochemically synthesized GQDs with a uniform size of  $\approx 3\text{--}5\text{ nm}$  as electron acceptors in P3HT-based solar cells. The power-conversion efficiency of P3HT devices using newly developed GQDs as acceptors was greatly improved due to the effective charge separation and transport. Continued research in this important area could overcome some of the major hurdles that solar cells are facing in the race to the technological marketplace.

### 3.1.5. Dye-Sensitized Solar Cells Containing Carbon Nanotubes

Dye-sensitized solar cells (DSSCs) are a relatively new class of low-cost solar cells of great promise.<sup>[202]</sup> They are based on a semiconductor formed between a photosensitized anode and an electrolyte, a *photoelectrochemical* system. In a typical Grätzel DSSC,<sup>[129]</sup> a fluorine-doped tin oxide coated glass plate (FTO glass) was used as the transparent anode, on which a highly porous thin layer of titanium dioxide ( $\text{TiO}_2$ ) was deposited. After soaking the plate in a mixture of a photosensitive ruthenium-polypyridine dye and a solvent, a thin layer of the dye was deposited onto the  $\text{TiO}_2$  surface. A conductive sheet (typically, Pt metal) covered with a thin layer of the iodide electrolyte was then used as the counter electrode and sealed together with the anode to prevent the electrolyte from leaking (Figure 11).<sup>[203]</sup> In operation, sunlight enters the cell through the transparent FTO glass to create an excited state of the dye on the surface of the  $\text{TiO}_2$  for injecting an electron directly into the conduction band of the  $\text{TiO}_2$  (Figure 11). The injected electron then moves by a chemical diffusion gradient to the clear anode. Meanwhile, the dye molecule strips one electron from iodide in electrolyte by oxidizing it into triiodide. This reaction occurs quite quickly compared to the time that it takes for the injected

electron to recombine with the oxidized dye molecule, minimizing the recombination loss. The triiodide then recovers its missing electron from the external circuit by diffusing to the counter electrode.

In terms of the quantum efficiency, DSSCs are extremely efficient. This is because the large surface area and “depth” nanostructure of the highly porous thin layer of  $\text{TiO}_2$  allow a photon to be efficiently absorbed, and the dyes are very effective at converting them to electrons. Most of the small losses that do exist in DSSC's include the conduction losses from the  $\text{TiO}_2$  to the clear electrode, and the optical losses in the front electrode. As mentioned earlier, the rate for the injected electron to recombine back into the dye is quite slow compared to the rate that the dye regains an electron from the surrounding electrolyte. Recombination directly from the  $\text{TiO}_2$  to the electrolyte is not possible, due to differences in energy levels. Therefore, the simple electron–hole recombination that affects the efficiency of traditional solar cells does not apply to DSSCs. These features (low losses and lack of recombination), together with the low production cost, make DSSCs extremely attractive as a replacement for other existing solar cell technologies in “low density” applications like rooftop solar collectors. Unlike most traditional solar cells, DSSCs are also able to work under cloudy skies and even in indoor environments to collect energy for small devices from the lights in the house. However, the currently achievable power-conversion efficiency of about 12% for DSSCs<sup>[204]</sup> is still much lower than that of silicon solar cells.

To further increase the DSSC power-conversion efficiency, it is essential to enhance the dye absorbance for efficient solar absorption and to reduce the series resistance to facilitate the charge transport from the  $\text{TiO}_2$  to anode. Since the dye molecules are quite small, in order to capture a reasonable amount of the incoming light the layer of dye molecules needs to be made fairly thick. Further improvements in the performance of these solar cells are envisioned by using quantum dots for conversion of higher-energy (higher frequency) light into multiple electrons, dye molecules with much wider frequency response in the visible, red and IR regions, solid-state polymeric electrolytes and a methanofullerene blends, and doped  $\text{TiO}_2$  to better match it with the electrolyte.<sup>[205,206]</sup>

**DSSCs with VA-CNTs, Graphene and/or Graphene Quantum Dots as Photovoltaic Active Materials:** As mentioned above, nanostructured  $\text{TiO}_2$  films have been widely used in DSSCs as photoanode materials due to their relatively low cost, easy fabrication and efficient electron-transport properties. So far, the device performance can be reached to ca. 12% by using  $\text{TiO}_2$ ,<sup>[203]</sup> further improvement is still required.<sup>[207,208]</sup> The charge loss during the transport of photogenerated electrons in photoanodes is a major problem of  $\text{TiO}_2$  film. To suppress this undesirable charge loss, several approaches were examined by considering the charge transport properties.<sup>[209,210]</sup> The incorporation of carbon-based nanomaterials, such as CNTs and graphene, in the anode seems to be a very promising but challenging approach to improve device performance. However, the enhancement of device performance using the carbon nanotubes incorporated  $\text{TiO}_2$  film as a photoelectrode is limited, due to the insufficient contact between  $\text{TiO}_2$  nanoparticles and rodlike

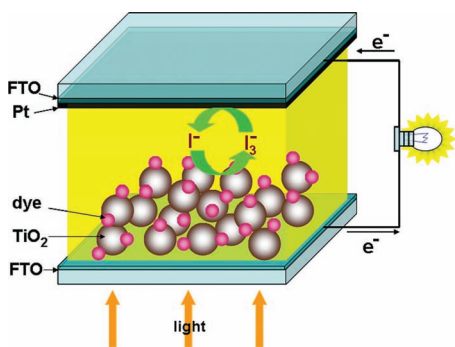
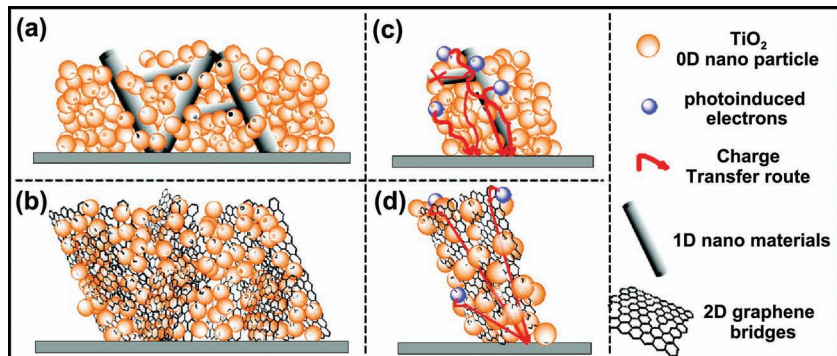


Figure 11. Schematic representation of the working principle for a DSSC.



**Figure 12.** a,c) 1D and b,d) 2D nanomaterial composite electrodes. In 2D nanomaterials composite electrodes (graphene), the  $\text{TiO}_2$  particles can anchor in the graphene better, and photoinduced electrons can be captured and transferred by the graphene. With the 1D nanomaterials compositing, however, there are less intermolecular forces and connection between  $\text{TiO}_2$  and the 1D nanomaterials; therefore, the transfer barrier is larger and the recombination is much easier to happen. Reproduced with permission.<sup>[185]</sup> Copyright 2010, American Chemical Society.

1D carbon nanotubes. On the other hand, graphene, the 2D layered carbon structure, could have more advantages than CNTs because of its good electrical conductivity and better contact with  $\text{TiO}_2$  nanoparticles. In this context, graphene composites with nanostructured  $\text{TiO}_2$  have been used as photoanode materials in DSSCs.<sup>[185,211]</sup> For instance, Yang et al.<sup>[185]</sup> obtained the drastic enhancement of the power-conversion efficiency ( $\approx 40\%$  enhancement compared with standard  $\text{TiO}_2$  electrode) and the short-circuit current density ( $\approx 45\%$ ) by using graphene oxide modified  $\text{TiO}_2$  electrode. A lower recombination, a faster electron transport and a higher light scattering are the main reasons for this improvement. The expected differences between CNT and graphene modified  $\text{TiO}_2$  electrodes are shown in **Figure 12**.

Sun et al.<sup>[211]</sup> also reported similar enhancement of the power-conversion efficiency by using a composite photoanode with nafion-modified graphene and  $\text{TiO}_2$ . The longer electron lifetime and efficient dye adsorption in the graphene-modified electrode resulted in this sharp improvement ( $\approx 59\%$  higher than the  $\text{TiO}_2$  electrode). Recent studies,<sup>[212,213]</sup> including our own,<sup>[212]</sup> have demonstrated a very fast and strong photocurrent generation by  $\text{TiO}_2$ -coated VA-CNT arrays, indicating the possible use of the  $\text{TiO}_2$ -coated VA-CNT arrays as the electrode in DSSCs. The use of the  $\text{TiO}_2$ -coated nanotube array electrode could offer significant advantages. Using electrophoresis for  $\text{TiO}_2$  coating and photoexcited electrons for metal nanoparticle deposition, for example, Yang et al.<sup>[212]</sup> have developed a facile yet versatile and effective method for the development of aligned coaxial nanowires of CNTs sheathed with  $\text{TiO}_2$ . These vertically aligned CNT- $\text{TiO}_2$  coaxial nanowires showed very fast photocurrent responses to a pulsed light beam ( $\lambda = 254 \text{ nm}$ , 4 W) with a good repeatability. They should also be useful in DSSCs because the use of metallic VA-MWNTs as the scaffold can serve double-duty to not only provide a 3D matrix for the dye adsorption but also effectively reduce the series resistance for the aligned CNT DSSCs via a direct electron-transfer path from the dye-coated  $\text{TiO}_2$  to aligned CNTs.

In view of possibilities for further improvements in the performance of DSSCs by using quantum dots for conversion of higher-energy (higher frequency) light into multiple electrons and dye molecules with much wider frequency response in the visible, red and IR regions (vide supra), Pan et al.<sup>[200]</sup> synthesized solution-processable, black GQDs with uniform size through general solution chemistry and used them as sensitizers in DSSCs. As mentioned earlier, Li et al.<sup>[201]</sup> have also developed a facile electrochemical approach for large scale preparation of functional graphene quantum dots with unexpected luminescence and electron-accepting properties. The unique features of those GQDs, including good solubility, well-defined structure, wide absorption spectrum and larger molar extinction coefficient, make them ideal to be used as sensitizers. Although the efficiency of DSSCs using GQDs as a sensitizer is still low due to low adsorption of GQDs on  $\text{TiO}_2$  electrode and the consequent poor charge injection, this approach opens new opportunities to synthesize GQDs with controlled optical and electrical properties for photovoltaic devices.

**DSSCs with Graphene Sheets as Transparent (Flexible) Electrodes:** In DSSCs, there are two electrodes called as a window electrode (anode) in which either ITO or fluorine tin oxide (FTO) is generally used and counter electrode (cathode) in which gold, platinum and FTO are commonly used (Figure 11). Due to the above-mentioned advantages of graphene (e.g., high transparency, high conductivity), several researchers have published work about the replacement of those electrodes with graphene based materials.<sup>[76,99,214–216]</sup> In particular, Wang et al.<sup>[76]</sup> investigated a graphene film prepared by reduced graphene oxide as a transparent electrode for DSSCs. Although this graphene film showed high transmittance over 80% and good conductivity around  $727 \text{ S cm}^{-1}$ , the overall power-conversion efficiency of cells is still lower than that of FTO-based cell (0.26% for graphene film vs. 0.84% for FTO). Large-area graphene films form solution-casting of certain edge-functionalized graphite (EFG), followed by subsequent heat treatment, have also been demonstrated to show a sheet resistance as low as  $60 \Omega \text{ sq}^{-1}$ , potentially useful as transparent electrodes.<sup>[125]</sup> In addition to window electrode, the utilization of graphene-based materials as a counter electrode, which is an indispensable component in DSSCs and involved the reduction of  $\text{I}_2$  to  $\text{I}^-$  after electron injection, has also been investigated, because the most commonly used platinum catalytic materials for counter electrode is very expensive. Shi et al.<sup>[99,214]</sup> reported the utilization of graphene-modified FTO and polymer-graphene composite film as a counter electrode. Both graphene-coated FTO and the graphene-composite film showed better efficiency in DSSCs compared with the bare FTO and conducting polymer electrodes. However, the overall efficiencies of cells using graphene containing cells were still lower than that of the standard cells using Pt-coated FTO and Pt as

**Table 2.** Classification of fuel cells.<sup>[217]</sup>

Fuel cell type	Electrolyte used	Operating temperature	Electrode reactions
Polymer electrolyte	Polymer Membrane	60 – 140 °C	Anode: $\text{H}_2 = 2\text{H}^+ + 2\text{e}^-$ Cathode: $\frac{1}{2}\text{O}_2 + 2\text{H}^+ + 2\text{e}^- = \text{H}_2\text{O}$
Direct Methanol	Polymer Membrane	30 – 80 °C	Anode: $\text{CH}_3\text{OH} + \text{H}_2\text{O} = \text{CO}_2 + 6\text{H}^+ + 6\text{e}^-$ Cathode: $\frac{3}{2}\text{O}_2 + 6\text{H}^+ + 6\text{e}^- = 3\text{H}_2\text{O}$
Akaline	Potassium Hydroxide	150 – 200 °C	Anode: $\text{H}_2 + 2\text{OH}^- = \text{H}_2\text{O} + 2\text{e}^-$ Cathode: $\frac{1}{2}\text{O}_2 + \text{H}_2\text{O} + 2\text{e}^- = 2\text{OH}^-$
Phosphoric Acid	Phosphoric Acid	180 – 200 °C	Anode: $\text{H}_2 = 2\text{H}^+ + 2\text{e}^-$ Cathode: $\frac{1}{2}\text{O}_2 + 2\text{H}^+ + 2\text{e}^- = \text{H}_2\text{O}$
Molten Carbonate	Lithium/Potassium Carbonate	650 °C	Anode: $\text{H}_2 + \text{CO}_3^{2-} = \text{H}_2\text{O} + \text{CO}_2 + 2\text{e}^-$ Cathode: $\frac{1}{2}\text{O}_2 + \text{CO}_2 + 2\text{e}^- = \text{CO}_3^{2-}$
Solid Oxide	Yittria Stabilized Zirconia	1000 °C	Anode: $\text{H}_2 + \text{O}^{2-} = \text{H}_2\text{O} + 2\text{e}^-$ Cathode: $\frac{1}{2}\text{O}_2 + 2\text{e}^- = \text{O}^{2-}$

electrodes. Recently, Lin et al.<sup>[215]</sup> synthesized boron-doped graphene and applied it in quantum dot DSSCs as a counter electrode. The boron-doped graphene electrode shows the highest efficiency among the reduced graphene oxide and pristine graphene electrodes. This enhancement was caused by the higher electrical conductivity and high work function of the boron-doped graphene electrode.

### 3.2. Fuel Cells

Instead of burning fuel to create heat, fuel cells convert chemical energy directly into electricity. Although many different types can be constructed depending on the nature of the electrolyte materials used (**Table 2**),<sup>[217]</sup> they all work in the same principle. They all in principle are an electrochemical cell consisting of the anode, the electrolyte, and the cathode. By pumping, for example, hydrogen gas onto one electrode (the anode), hydrogen is split into its constituent electrons and protons (Figure 13).<sup>[218]</sup> While the protons diffuse through the cell toward a second electrode (the cathode), the

electrons flow out of the anode to provide electrical power. Electrons and protons both end up at the cathode to combine with oxygen to form water (Figure 13).

The oxygen reduction reaction (ORR) at cathode can proceed either through a four-electron process to directly combine oxygen with electrons and protons into water as the end product or a less efficient two-step, two-electron pathway involving the formation of hydrogen peroxide ions as an intermediate.<sup>[121]</sup> The reduction would naturally happen very slowly without catalyst on the cathode to speed up the ORR, leading to insignificant production of electricity. Platinum nanoparticles have long been regarded as the best catalyst for the ORR, though the Pt-based electrode suffers from its susceptibility to time-dependent drift and CO deactivation.<sup>[121]</sup> Moreover, the high cost of the platinum catalysts has been shown to be the major “showstopper” to mass market fuel cells for commercial applications. Indeed, the large-scale practical application of fuel cells has not been realized, though alkaline fuel cells with platinum as an ORR electrocatalyst were developed for the Apollo lunar mission as early as the 1960s.

On the other hand, considerable research has been performed to improve the performances of proton exchange membrane fuel cells (PEMFCs) since the invention of the first PEMFC in the early 1960s by Willard Thomas Grubb and Lee Niedrach of General Electric.<sup>[219]</sup> Hydrogen and methanol are two frequently employed fuels in the so-called direct hydrogen PEMFCs and direct methanol PEMFCs (i.e., DMFCs), respectively. For hydrogen PEMFCs, the total catalyst loading required for both the anode and cathode is about  $0.8 \text{ mg/cm}^2$ .<sup>[220]</sup> DOE estimates that this loading needs to be reduced by four times in order for hydrogen PEMFCs to be an alternative to internal combustion engines.<sup>[221]</sup> Along this line, Pt-alloys have been used in catalyzing methanol oxidation in DMFCs.<sup>[222]</sup> Specifically, Pt–Ru alloy is the most active binary anode catalyst able to eliminate CO poisoning problem for DMFCs. However, a high catalyst loading ( $2\text{--}8 \text{ mg cm}^{-2}$ ) is required in order to achieve acceptable fuel cell performance. It has been suggested that, to make DMFCs commercially viable, the anode catalyst loadings must be

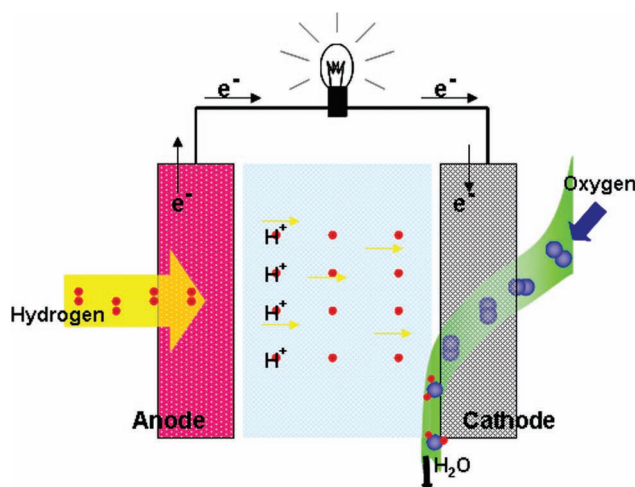


**Figure 13.** Schematic representation of the working principle for a fuel cell.

dropped to a level of <1.0 mg cm<sup>-2</sup>.<sup>[222]</sup> Therefore, in order to reduce the precious-metal loading for PEMFC electrodes, catalytic activity of the catalysts needs to be enhanced. Moreover, in order to prolong the lifetimes for PEMFCs, durability of the catalyst electrodes needs to be improved too. All of these require the improved properties for the catalysts and the supporting materials of the catalysts.

### 3.2.1. Fuel Cells with Carbon Nanomaterials as the Catalyst Support

While carbon nanomaterials have been studied as new electron-acceptors for improving the energy conversion efficiency of organic solar cells (Section 3.1), their initial use in fuel cells are mainly as catalyst supports for lowering the load of precious metals and enhancing the catalyst activity with prolonged catalyst durability. For instance, carbon blacks (e.g., Vulcan XC-72, Acetylene Black, Ketjen Black, etc.) are commonly used support materials for PEMFC catalysts. Properties of these carbon supports, including their specific surface area, pore structure, electrical conductivity, mechanical strength, and corrosion resistance, determine the performances of the catalysts and thus the performance of PEMFCs. To develop high-performance PEMFCs, carbon supports of a large specific surface area is needed to ensure a high activity for the supported catalysts.<sup>[223]</sup> Vulcan XC-72, having a relatively high surface area (237 m<sup>2</sup> g<sup>-1</sup>) among all carbon black materials,<sup>[222]</sup> is the widely used catalyst support in current PEMFCs. In this regard, further performance improvement requires carbon supports with an even larger specific surface area. Besides, pore structures of the carbon support affect the catalytic activity of the catalysts.<sup>[224]</sup> According to the IUPAC classification (Section 4.1.1),<sup>[225,226]</sup> there are three classes of pore sizes, i.e., micropores (<2 nm), mesopores ( $\approx$ 2–50 nm), and macropores ( $>$ 50 nm). Upon the catalyst deposition, some catalyst nanoparticles may be sunk into the micropores of Vulcan XC-72. The catalysts inside the micropores have less or no electrochemical activity due to the poor reactant accessibility and the insufficient formation of triple-phase boundaries (gas–electrode–electrolyte). This explains why Vulcan XC-72, having a large ratio of micropores (up to 47%),<sup>[225]</sup> suffers from a low catalytic activity.<sup>[226]</sup> Consequently, relatively larger and more accessible pores (i.e., mesopores) are desirable for a good carbon support. Furthermore, carbon supports of a high electrical conductivity are needed to ensure a high catalytic activity for the supported catalysts. The relatively high electrical conductivity (4.0 S cm<sup>-1</sup>) of Vulcan XC-72 among all carbon black materials has, once again, made it a predominant catalyst support material.<sup>[227]</sup> Finally, mechanical property and corrosion behavior of the carbon supports also affect the durability of the catalysts.<sup>[228]</sup> Carbon black is known to undergo electrochemical oxidation to produce surface oxides, and eventually to CO<sub>2</sub> at the cathode of a fuel cell.<sup>[229]</sup> As carbon is corroded away, precious metal nanoparticles will be lost from the electrode or aggregated to larger particles, resulting in the activity degradation of the catalysts. Therefore, mechanically strong and corrosion-resistant carbon supports are needed to improve the durability of the catalysts. In order to develop

high-performance catalyst electrodes with low precious metal loading, high catalytic activity and long durability for advanced PEMFCs, therefore, there is a need for new support materials with superior properties over the currently used carbon blacks. The high specific surface area, high mesoporosity, high electrical conductivity, high mechanical strength, and high corrosion-resistance of CNTs make them a class of very promising catalyst support materials for PEMFCs (both hydrogen PEMFCs and DMFCs).<sup>[65]</sup> Compared to carbon blacks, the higher surface area of CNTs enables a highly dispersed and uniformly distributed deposition of catalyst nanoparticles while their higher mesoporosity prevents the catalyst deposition from sinking into micropores (as encountered with carbon blacks)<sup>[226]</sup> and facilitates the formation of triple-phase-boundaries.<sup>[230]</sup> These superior properties, along with their higher electrical conductivity, allow CNTs for significantly improving the catalytic activity and electrochemical utilization for the CNT-supported catalysts.

For hydrogen PEMFCs, it has been demonstrated that a CNT supported Pt catalyst with 12 wt% Pt loading could give a 10% higher fuel cell voltage and twice power density than a carbon black supported catalyst with 29 wt% Pt loading.<sup>[231]</sup> Li et al.<sup>[232]</sup> reported that MWNT supported catalysts exhibited better performance in DMFCs with respect to those supported by carbon black (XC-72) both in half cell and full cell testing. Their results showed a mass activity of 14.7 mA mg<sup>-1</sup> (Pt) for a Pt/MWNT catalyst at 0.7 V vs. the dynamic hydrogen electrode (DHE), much higher than that of 2.2 mA mg<sup>-1</sup> (Pt) for a Pt/XC-72 catalyst. SWNT supported Pt electrodes were also reported to exhibit higher catalytic activities for both methanol oxidation and ORR than the unsupported Pt electrode.<sup>[233]</sup> The onset potential of methanol oxidation on the nanotube electrode was 200 mV lower than that of the unsupported Pt electrode (400 mV vs. the standard calomel electrode, SCE). The higher catalytic activity was thereby attributed to the larger surface area of CNT architecture and the lower overpotential for methanol oxidation.

Furthermore, the high mechanical strength and superb corrosion-resistance of CNTs provide an excellent durability for the nanotube electrode. Wang et al.<sup>[234]</sup> compared the electrochemical surface oxidation of Vulcan XC-72 against MWNTs following potentiostatic treatments up to 168 hours under conditions simulating PEMFC cathode environment. Compared to Vulcan XC-72, MWNTs were found to be electrochemically more stable with less surface oxide formation and 30% lower corrosion current. As a result of high corrosion resistance, CNTs showed lower loss in Pt surface area and ORR activity. After 168 h oxidation treatment, the size distribution of Pt nanoparticle on Vulcan XC-72 became broader and the average particle size became larger (Figure 14a,b). In contrast, Pt particles on MWNTs barely showed any increase in size (Figure 14c,d). The negligible aggregation of Pt nanoparticles on MWNTs indicates a high corrosion resistance and excellent mechanical strength for the CNT support. Thus, CNTs have been investigated as promising support materials to improve the catalyst durability for PEMFCs.

Comparing with the randomly oriented CNTs, aligned CNTs with a well-defined high surface area as well as good electrical and mechanical properties provide additional

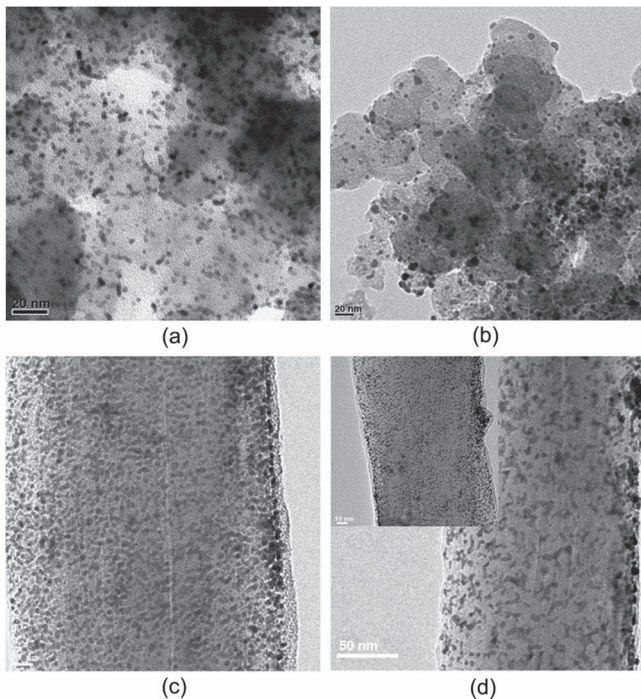


**Figure 14.** TEM images of a) Pt/Vulcan XC-72 before durability test, b) 30 wt% Pt/Vulcan XC-72 after durability test for 168 h, c) Pt/MWNTs before durability test, and d) 30 wt% Pt/MWNTs after durability test for 168 h. Inset of (d) shows a typical region. Reproduced with permission.<sup>[234]</sup> Copyright 2006, Elsevier.

benefits for them to be used as supporting electrodes in fuel cells. Specifically, both Pt<sup>[234]</sup> and Pt-alloy<sup>[235]</sup> catalysts have been deposited on VA-CNTs for hydrogen PEMFC<sup>[236]</sup> and DMFC<sup>[237]</sup> applications. Li et al.<sup>[238]</sup> developed a filtration method to prepare partially oriented CNT films via self-assembly of CNTs precoated with Pt nanoparticles and used the resultant oriented Pt/CNT electrode ( $0.20 \text{ mg cm}^{-2}$  Pt, no PTFE) to test direct hydrogen PEMFCs. Higher fuel cell performance of this oriented Pt/CNT electrode than a non-oriented Pt/CNT electrode ( $0.20 \text{ mg cm}^{-2}$  Pt, no PTFE) and a commercial Pt/carbon black electrode ( $0.25 \text{ mg cm}^{-2}$  Pt, 30% PTFE) was achieved, attributable to the improved Pt utilization and mass transport raised from the oriented CNT structures. Tang et al.<sup>[236]</sup> observed increased catalytic activity (decreased overpotential and increased current by 1.2 times) for methanol oxidation when comparing a Pt-aligned CNT catalyst with a Pt-random CNT catalyst. In order to solve the CO poisoning problem for DMFCs, Ahn et al.<sup>[235]</sup> deposited Pt-Ru binary catalysts on a 3D CNT array electrode prepared by an anodic aluminum oxide template (Section 2.2). With the presence of Ru in the catalyst, the Pt-Ru/CNT array electrode efficiently eliminated the CO poisoning. Comparing to a Pt-Ru thin-film electrode, the Pt-Ru/CNT array electrode showed a 10-fold increase in current for methanol oxidation, indicating the improved catalytic activity induced by the aligned structures of the VA-CNTs. Rajesh et al.<sup>[237]</sup> studied Pt, Pt-Ru, Pt-WO<sub>3</sub> catalysts on VA-CNTs and achieved improved catalytic activity for these VA-CNT-supported catalysts than those supported on Vulcan XC-72.

The Pt-WO<sub>3</sub>/CNT showed the highest activity and stability with a better CO tolerance than that of the Pt-WO<sub>3</sub> catalyst.

Surface chemistry of the support materials can also greatly affect the performance of the resultant catalysts as the interaction between the support and the catalyst can modify the electronic structure of catalyst metals, which in turn changes the catalytic activity<sup>[239]</sup> and durability of the catalysts.<sup>[234,240]</sup> Doping of carbon can effectively change the nanotube surface chemistry, and hence the conductivity and catalytic activity. For PEMFC applications, in particular, nitrogen-doped CNTs (NCNTs) have demonstrated promising potential either as the catalyst support materials or directly as the so-called metal-free catalysts (Section 3.2.2).<sup>[105]</sup>

As new support materials, NCNTs improve the dispersion of catalyst nanoparticles on the CNT surface, resulting in an enhanced catalytic activity for the catalysts. N-doping can also strengthen the binding between the catalyst and the CNT surface to enhance durability for the catalysts. These have been demonstrated for both methanol oxidation and oxygen reduction. Vijayaraghavan et al.<sup>[241]</sup> obtained a high ORR catalytic activity with their Pt/NCNT catalysts, showing a mass-transport limited current density and mass activity of  $2.3 \text{ mA cm}^{-2}$  and  $0.05 \text{ mA g}^{-1}$ , respectively. Viswanathan<sup>[242]</sup> also studied Pt-alloy catalysts (Pt-Ru, Pt-WO<sub>3</sub>) on NCNTs and achieved better activity and stability for methanol oxidation than those on conventional CNTs. These authors suggested that the anchoring sites (namely the hetero atoms) of NCNTs disperse the catalyst nanoparticles and prevent them from agglomeration, improving the activity and stability for the catalysts.

Like conventional CNTs, aligned structures are also preferred for NCNTs for fuel cell applications. For example, Maiyalagan et al.<sup>[118]</sup> reported the use of Pt nanoparticles supported by aligned NCNTs for methanol oxidation. They observed an enhanced catalytic activity and stability toward methanol oxidation on Pt/NCNTs as compared with commercial E-TEK Pt/Vulcan by measuring the onset potential for methanol oxidation (0.22 V vs. 0.45 V, Ag/AgCl) and the forward peak current density in cyclic voltammogram ( $13.3 \text{ mA cm}^{-2}$  vs.  $1.3 \text{ mA cm}^{-2}$ ). These authors believed that NCNTs highly dispersed Pt nanoparticles and the nitrogen functional groups on the CNT surface intensified the electron withdrawing effect against Pt. This resulted in decreased electron density of Pt so as to facilitate the oxidation of methanol.

### 3.2.2. Fuel Cells with Carbon Nanomaterials as Metal-Free Catalysts

Apart from the use of CNTs and NCNTs as catalyst supports described above, the research on exploring the use of carbon nanomaterials as metal-free catalysts in fuel cells is growing rapidly. Comparing to conventional CNTs, nitrogen-doped carbon nanomaterials have a unique property being able to catalyze ORR in the absence of any metal catalyst.<sup>[68,169]</sup> The N-doped CNFs showed an over 100-fold increase in catalytic activity for H<sub>2</sub>O<sub>2</sub> decomposition in both neutral and alkaline conditions,<sup>[243]</sup> but still less electroactive than the platinum catalyst. Maldonado and Stevenson<sup>[244]</sup> demonstrated that N-doped carbon nanofiber (CNF) electrodes, prepared

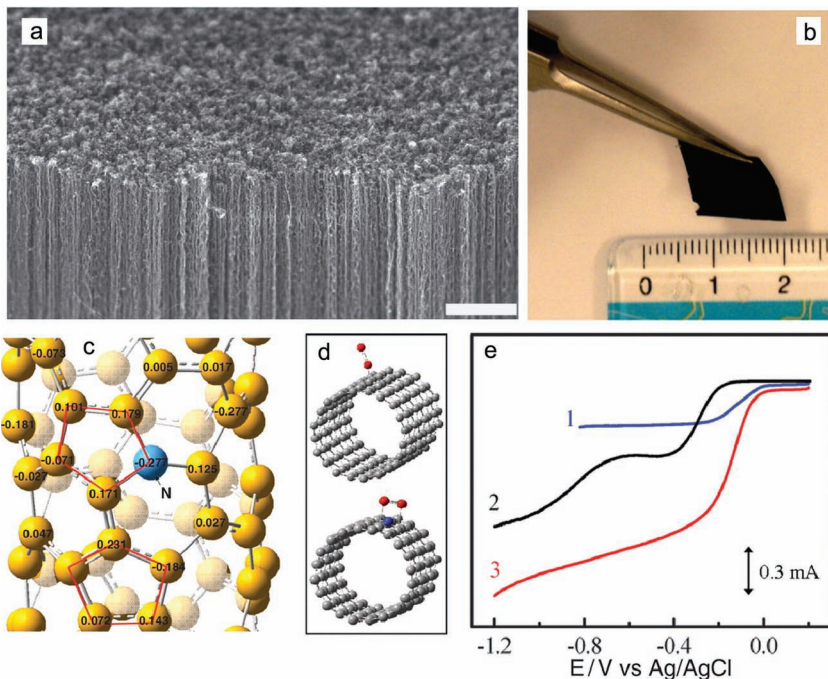


**Figure 15.** a) SEM image of the *as-synthesized* VA-NCNTs prepared by pyrolysis of iron phthalocyanine (FePc) on a quartz substrate (Scale bars, 2  $\mu\text{m}$ ). b) Digital photograph of the VA-NCNT array after having been transferred onto a polystyrene–nonaligned CNT conductive nanocomposite film. c) Calculated charge density distribution for the NCNTs. (d) Schematic representations of possible adsorption modes of an oxygen molecule at the CCNTs (top) and NCNTs (bottom). e) The steady-state voltammograms for oxygen reduction in air saturated 0.1 M KOH at the Pt–C (curve 1), VA–CCNT (curve 2), and VA–NCNT (curve 3) electrodes. Reproduced with permission.<sup>[121]</sup> Copyright 2009, American Association for the Advancement of Science.

by a floating catalyst CVD of ferrocene and either xylene or pyridine, exhibited electrocatalytic activities for ORR via a two-step two-electron pathway, and that the N-doped CNFs showed an over 100-fold increase in catalytic activity for  $\text{H}_2\text{O}_2$  decomposition in both neutral and alkaline conditions, albeit still less electroactive than the platinum catalyst. A strong correlation between the ORR peak potential and the nitrogen doping level was also observed.<sup>[244]</sup> ORR peaks shifting about +30 mV per 1 atom% nitrogen incorporated. VA–CNTs formed by CVD of certain metal heterocyclic molecules (e.g., ferrocene/ $\text{NH}_3$ ) have also been shown to exhibit some ORR catalytic activities, which was attributed to the presence of  $\text{FeN}_2\text{-C}$  and/or  $\text{FeN}_4\text{-C}$  active sites in the nanotube structure.<sup>[245]</sup> Along with the recent intensive research efforts in reducing or replacing Pt-based electrode in fuel cells, Gong et al.<sup>[121]</sup> have recently found that VA–NCNTs (**Figure 15a,b**) could act as extremely effective metal-free ORR electrocatalysts even after a complete removal of the residual Fe catalyst by electrochemical purification, demonstrating that the ORR activity of VA–NCNTs is solely due to the nitrogen doping.

Quantum mechanics calculations indicate that carbon atoms adjacent to nitrogen dopants of the VA–NCNTs possess a substantially high positive charge density to counterbalance the strong electron affinity of the nitrogen atom (**Figure 15c**).<sup>[121]</sup> The nitrogen-induced charge delocalization could change the electrochemical potential for ORR and the

chemisorption mode of  $\text{O}_2$  from the usual end-on adsorption (Pauling model) at the conventional CNT surface to a side-on adsorption (Yeager model) at the NCNT surface (**Figure 15d**).<sup>[121,246]</sup> The parallel diatomic adsorption could effectively weaken the O–O bonding to facilitate ORR at the NCNT electrodes. As such, doping CNT with nitrogen heteroatoms can efficiently create the metal-free active sites for electrochemical reduction of  $\text{O}_2$ . In alkaline electrolytes, these metal-free VA–NCNTs were shown to catalyze a four-electron ORR process with a much higher catalytic activity (4.1 mA  $\text{cm}^{-2}$  vs. 1.1 mA  $\text{cm}^{-2}$ , **Figure 15e**), lower overpotential, smaller crossover effect, and better long-term operation stability comparing to commercially available Pt/carbon black catalysts (C2-20, 20% platinum on VulcanXC-72R; E-TEK).<sup>[121,244,247]</sup>

The crossover test demonstrated that VA–NCNTs are highly tolerant to various commonly used fuel molecules, including hydrogen gas, glucose, methanol, and formaldehyde.<sup>[121,244]</sup> Such high tolerance to fuel crossover effect of VA–NCNTs has been attributed to their much lower ORR potential than that required for oxidation of the fuel molecules.<sup>[121,244,248,249]</sup> Moreover, being nonmetallic, the VA–NCNTs were insensitive to CO poisoning.<sup>[121,244]</sup>

These results indicate the excellent effectiveness of VA–NCNTs as practically useful metal-free cathodic catalysts for ORR in fuel cells.

As a building block for carbon nanotubes, graphene is an attractive candidate for potential uses as the metal-free ORR catalyst. Indeed, N-graphene films produced by CVD in the presence of ammonia have recently been demonstrated to show a superb ORR performance similar to that of VA–NCNTs with the same nitrogen content in alkaline medium.<sup>[89]</sup> The ease with which graphene materials and their N-doped derivatives can be produced by various low-cost large-scale methods, including the chemical vapor deposition,<sup>[87–92]</sup> chemical reduction of graphite oxide,<sup>[94,95,250]</sup> exfoliation of graphite,<sup>[18,251]</sup> microwave plasma reaction,<sup>[252]</sup> and atmospheric pressure graphitization of silicon carbide,<sup>[253]</sup> suggests considerable room for cost effective preparation of metal-free efficient graphene-based catalysts for oxygen reduction.

As the CVD processes for producing the VA–NCNTs and N-graphene films used in the aforementioned studies involve metal catalysts (e.g., Fe, Ni),<sup>[89,121]</sup> considerable care has been taken during the electrode preparation to completely remove the catalyst residue. In particular, the VA–NCNT electrode was purified by electrochemical oxidation in a phosphate buffered solution (pH 6.8) at a potential of 1.7 V (vs. Ag/AgCl) for 300 s at room temperature (25 °C), followed by potential sweeping from 0.0 V to 1.4 V in 0.5 M  $\text{H}_2\text{SO}_4$  until a stable voltammogram free from any Fe redox signal was obtained. X-ray photoelectron spectroscopic (XPS)

measurements on the electrochemically purified VA-NCNTs confirmed the removal of residual iron catalyst particles.<sup>[121]</sup> In view of the detection limitation intrinsically associated with the electrochemical and XPS measurements, however, possible effects of metal contaminants on the observed superb ORR performance could still be a matter of controversy unless nitrogen-doped carbon nanomaterials with excellent ORR electrocatalytic activities can be produced by a metal-

free preparation procedure. In this regard, it is important to note that Liu et al.<sup>[254]</sup> have reported the ORR electrocatalytic performance better than platinum for nitrogen-doped ordered mesoporous graphitic arrays (NOMGAs) prepared by a metal-free nanocasting technology using a nitrogen-containing aromatic dyestuff, *N,N'*-bis(2,6-diisopropylphenyl)-3,4,9,10-perylenetetracarboxylic diimide (PDI), as the carbon precursor (**Figure 16a**). Owing to the metal-free preparation

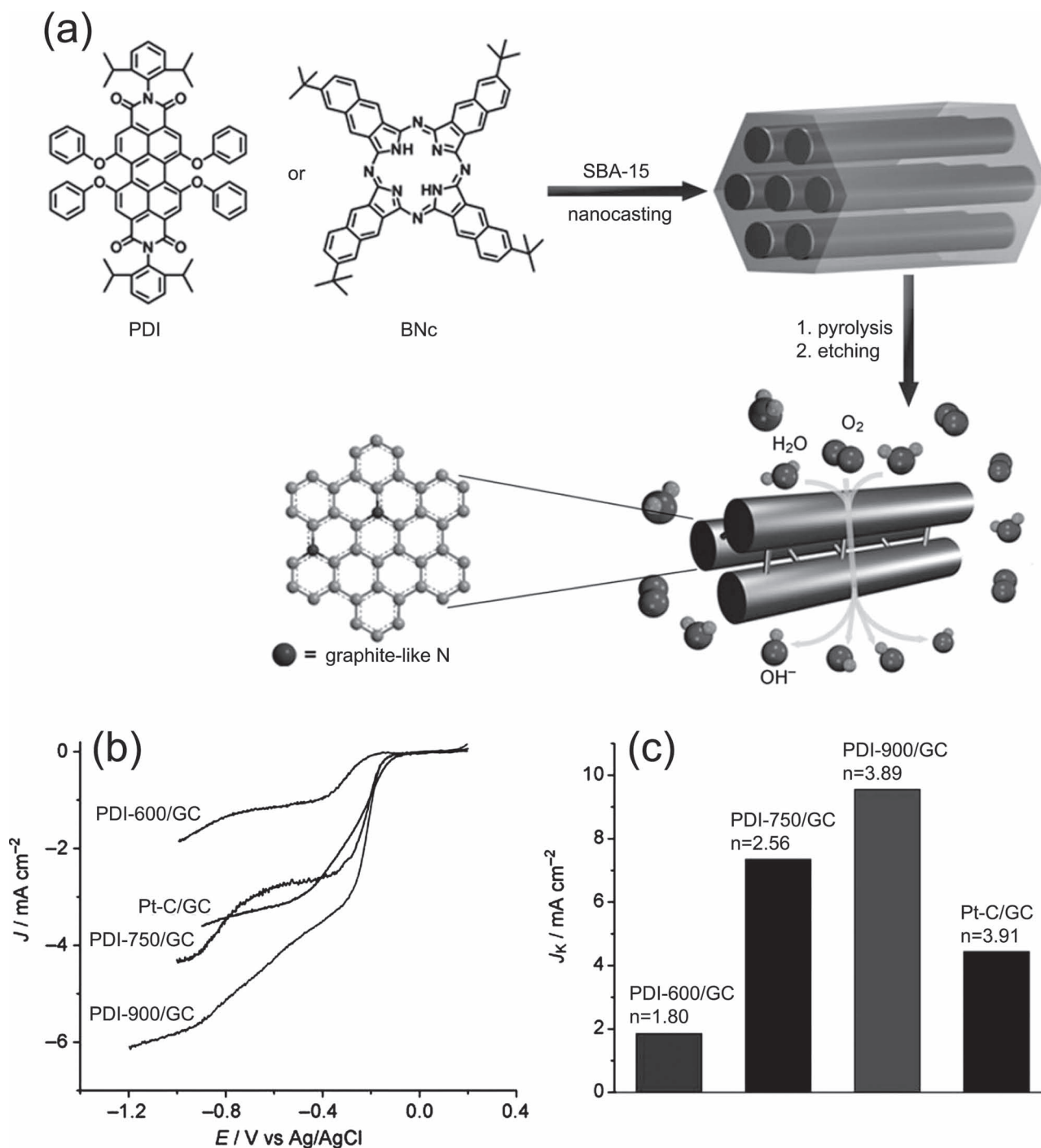


**Figure 16.** a) Preparation of NOMGAs as metal-free catalysts for the ORR. b) RDE voltammograms of the series of PDI-NOGMAs and Pt-C supported on GC electrodes at a rotation rate of 1600 rpm. c) Electrochemical activity given as the kinetic-limiting current density ( $J_K$ ) at 0.35 V for the PDI-NOGMAs supported on GC electrodes in comparison with that of a commercial Pt-C electrode. Reproduced with permission.<sup>[254]</sup>

procedure, the reported electrocatalytic activity can be attributed exclusively to the incorporation of nitrogen in PDI-NOMGAs (Figure 16).<sup>[254]</sup>

Metal-free N-doped MWCNTs or ordered mesoporous carbons (OMCS) have also been produced through carbonization of a MWCNT-supported polyaniline (PANI) coating<sup>[255]</sup> or via NH<sub>3</sub> activation.<sup>[256]</sup> These metal-free N-doped nanocarbons have also been demonstrated to exhibit high ORR activities even in acidic electrolytes. Good ORR activities in the acidic media have also been observed for NCNTs produced by both metal catalyzed and metal-free nanotube growth processes.<sup>[257,258]</sup>

Although most recent studies on the N-doped carbon nanostructures focused on the ORR reaction in alkaline electrolytes, fuel cells that operate with acidic electrolytes, particularly PEMFC, could have a more significant economic impact. Recently, Kundu et al.<sup>[259]</sup> have found that NCNTs prepared by pyrolysis of acetonitrile could show a considerably higher

and more stable ORR activity in 0.5 M H<sub>2</sub>SO<sub>4</sub> compared with their undoped counterparts. They pointed out that the incorporation of nitrogen functional groups within the carbon structure improved the oxidative stability of the NCNTs under ORR conditions even in the acidic medium. More recently, Wang et al.<sup>[256]</sup> demonstrated that nitrogen-doped OMCS via NH<sub>3</sub> activation can also act as alternative metal-free catalysts with a high ORR activity and better stability than Pt-based electrocatalysts in 0.05 M H<sub>2</sub>SO<sub>4</sub>. On the other hand, Ozaki et al.<sup>[260]</sup> reported the ORR activity in 0.5 M H<sub>2</sub>SO<sub>4</sub> from the shell-like nanocarbons produced by carbonization of furan resin in the presence of acetylacetones and metal phthalocyanines. These authors found that the high ORR activity was not resulted from metal species on the surface, which have been removed by acid washing. However, the catalytic performance of these reported N-doped carbon nanomaterials in acidic medium still needs to be further improved to meet the requirement for practical applications.

Since nitrogen plays an essential role in the active sites for the nanocarbon ORR catalysts and at least three different forms (i.e., pyrrolic, pyridinic, and graphitic) of the surface nitrogen atoms have been observed, it is important to understand the influence of the nitrogen content and its chemical nature on the ORR performance. The proposed structural models for the bonding configuration of nitrogen doping in CNTs are shown in **Figure 17**. There are three primary candidates: pyridine-like (Figure 17a), pyrrolelike (Figure 17b), and graphitic where N replaces a graphitic carbon atom (Figure 17c). Other nitrogen-vacancy complexes containing pyridinic two-fold coordinated nitrogen atoms neighboring a carbon vacancy (V), such as NV, N<sub>2</sub>V, and N<sub>3</sub>V,<sup>[116]</sup> as shown in Figure 17f,g, as well as nitrile –C≡N (Figure 17d), primary amine (Figure 17e) and ‘interstitial’ divalent nitrogen atoms (Figure 17h)<sup>[261]</sup> are also possible.

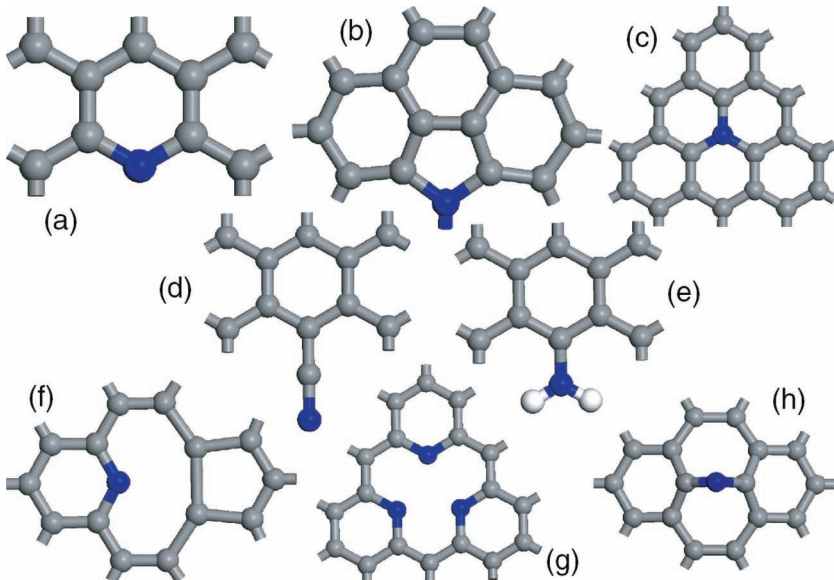


**Figure 17.** The bonding configurations for N in CNTs, a) pyridinelike N, b) pyrrole-type nitrogen, c) graphite like, d) Nitrile –C≡N, e) –NH<sub>2</sub>, f) pyridinic N-vacancy complex, g) pyridinic N<sub>3</sub>-vacancy, h) interstitial N. Reproduced with permission.<sup>[116]</sup> Copyright 2004, American Chemical Society.

Using ethylenediamine (EDA-NCNT) and pyridine as different precursors, Chen et al.<sup>[262]</sup> produced NCNTs with varying nitrogen contents through a single-step CVD process. These authors found that NCNTs with higher nitrogen content and more defects exhibited better ORR performance in acidic electrolytes.<sup>[262]</sup> On the other hand, Kundu et al.<sup>[259]</sup> prepared NCNTs via pyrolysis of acetonitrile over cobalt catalysts at different temperatures. The NCNTs prepared at 550 °C was found to possess a higher amount of pyridinic groups and a higher ORR electrocatalytic activity than its counterpart prepared at 750 °C. However, recent studies suggest that more graphitic nitrogen atoms rather than the pyridinic ones are important for the ORR.<sup>[89,254]</sup> Therefore, the exact catalytic role for each of the nitrogen forms in nanocarbon ORR catalysts is still a matter of controversy.<sup>[89,254,259,262]</sup> In addition, it is a challenge to determine the exact locations of nitrogen atoms in the nanocarbon structures, chemical nature of the catalytic sites, and electrochemical kinetics of the N-doped nanocarbon electrodes. A combined experimental and theoretical approach would be essential. Computer simulation and calculation have proved to be a powerful technique in searching novel electrocatalysts and study the basic science behind the electrocatalysis. Thus, theoretical calculations should be employed in studying the N-doped nanocarbon catalysts.

In addition to the *intramolecular* charge-transfer that impart ORR electrocatalytic activities to NCNTs and N-graphene discussed above, Wang et al.<sup>[263,264]</sup> have recently demonstrated that certain polyelectrolyte (e.g., PDDA) functionalized nitrogen-free CNTs, either in an aligned or nonaligned form, could also act as metal-free electrocatalysts for ORR through the *intermolecular* charge-transfer from the all-carbon CNTs to the adsorbed PDDA (**Figure 18a**). It is notable that the PDDA adsorbed vertically aligned CNT

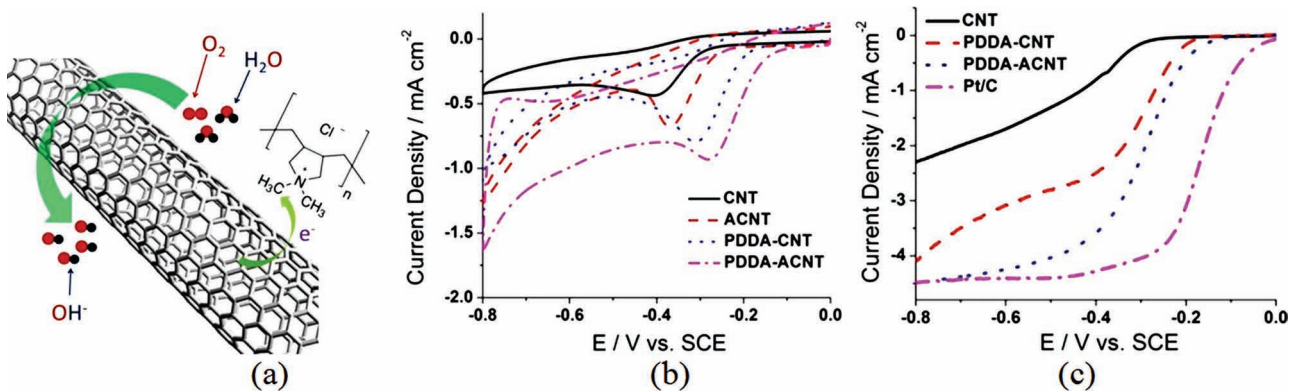


**Figure 18.** a) Illustration of charge transfer process and oxygen reduction reaction on PDDA–CNT. b) The cyclic voltammetry curves for oxygen reduction in the O<sub>2</sub>-saturated 0.1 M KOH solution. c) Linear sweep voltammetry curves of ORR in an O<sub>2</sub>-saturated 0.1 M KOH solution at a scan rate of 10 mV s<sup>-1</sup>. The rotation rate is 1600 rpm. Reproduced with permission.<sup>[263]</sup> Copyright 2011, American Chemical Society.

electrode possesses remarkable electrocatalytic properties for ORR; similar to that of commercially available Pt/C electrode (Figure 18b,c).

This work clearly indicates that the important role of intermolecular charge-transfer to ORR for nitrogen-free CNTs can be applied to other carbon nanomaterials for the development of various other metal-free efficient ORR catalysts, including PDDA-adsorbed CNTs<sup>[263]</sup> and graphene,<sup>[264]</sup> for fuel cell applications, even new catalytic materials for applications beyond fuel cells (e.g., metal-air batteries). The recent progresses discussed above proved to have a large impact on not only the commercialization of the fuel cell technology but also many other catalytic processes beyond fuel cells, and their repercussions are continuing. However, further study on the catalytic mechanism and kinetics is still needed in order to design and develop carbon-based catalysts with a desirable activity and durability. The performance evaluation of these nanocarbon catalysts in actual fuel cells should also be performed.

### 3.2.3. Fuel Cells with Carbon Nanomaterials as Electrolytes/Membranes

In recent years, apart from their major applications in the electrode (i.e., as catalyst supports and catalyst materials), CNTs have also been utilized to design new electrolyte materials for fuel cells. Specifically, Kannan et al.<sup>[265]</sup> incorporated SWNTs pre-functionalized with sulfonic acid groups (S-SWCNTs) into a Nafion matrix. The acid content of the CNT connects the hydrophobic regions of the membrane, thus providing a network with enhanced proton mobility and improved mechanical stability for Nafion membranes in H<sub>2</sub>/O<sub>2</sub> fuel cells. By extension, Kannan et al.<sup>[266]</sup> have used sulfonic acid-functionalized MWNTs to manipulate the hydrophilic domain size of Nafion to enhance the proton conductivity of Nafion membranes. The nanotube-tailored Nafion membranes ameliorate the performance of H<sub>2</sub>/O<sub>2</sub> fuel cells as confirmed by a maximum power density of 380 mW cm<sup>-2</sup>, higher than those of Nafion 115 (250 mW cm<sup>-2</sup>) and recast Nafion (230 mW cm<sup>-2</sup>) membranes. Thus, the use of CNTs either as an anchoring backbone for –SO<sub>3</sub>H groups to enhance proton

conductivity or as a blending agent to improve the mechanical characteristics of the Nafion phase could be able to alleviate many critical problems associated with the use of commercial Nafion membranes.

## 4. Carbon Nanotubes for Energy Storage

Supercapacitors and batteries are two important electrochemical energy storage devices that have been extensively developed for many applications. Improved energy storage capability, power delivery capability, and cycle life are highly desired for these devices to better satisfy the increasing performance demands. CNTs and graphene have been explored as both electrode materials and electrode additives for developing high-performance supercapacitors and batteries.

### 4.1. Supercapacitors

Supercapacitors (a.k.a., electrochemical capacitors or ultracapacitors) are electrochemical energy storage devices that combine the high energy-storage capability of conventional batteries with the high power-delivery capability of conventional capacitors.<sup>[267,268]</sup> The supercapacitor concept was first described in a patent filed by Becker in 1957 and the first supercapacitor products were commercialized by Panasonic (Matsushita) in 1978 and NEC (Tokin) in 1980.<sup>[269]</sup> Being able to achieve higher power and longer cycle life than batteries, supercapacitors have been developed to provide power pulses for a wide range of applications. In advanced electric transportation technologies, for example, supercapacitors are used as power assists for hybrid electric vehicles and plug-in hybrids, where the supercapacitor is operated to provide peak power during acceleration and hill-climbing, and it can be recharged during regenerative braking.<sup>[270]</sup>

Supercapacitors have been realized with three principal types of electrode materials, namely high-surface-area activated carbons,<sup>[271]</sup> transition metal oxides,<sup>[272]</sup> and electroactive conjugated polymers.<sup>[273]</sup> Properties of electrode materials play an important role in determining the performances of

the supercapacitors. Charge storage capability of these materials is usually evaluated by their capacitance. The maximum energy ( $E_{\max}$ ) and maximum power ( $P_{\max}$ ) of a supercapacitor are given by:

$$E_{\max} = (CU^2)/2 \quad (1)$$

$$P_{\max} = U^2 / (4R) \quad (2)$$

where  $C$  is capacitance,  $U$  is cell voltage, and  $R$  is total equivalent series resistance (ESR) of the capacitor.<sup>[268]</sup> Overall performance of the supercapacitor is determined by the physical properties of both the electrode and the electrolyte materials. Having the advantages of relatively low cost, commercial availability, and well-established electrode production technologies, high-surface-area activated carbons (specific surface area:  $\approx 1000$ – $2000 \text{ m}^2 \text{ g}^{-1}$ ) have been the major electrode materials for commercial supercapacitors.<sup>[274]</sup> Charge storage capability of these materials is usually evaluated by their capacitance, which is associated with the electrode/solution interface that varies with the type of carbon and its conditions of preparation (typically,  $\approx 20$ – $50 \mu\text{F cm}^{-2}$ ).<sup>[268]</sup> Taking a specific surface area of  $1000 \text{ m}^2 \text{ g}^{-1}$  for carbon as an example, its ideal attainable capacitance would be  $\approx 200$ – $500 \text{ F g}^{-1}$ . However, the practically obtained values are of only a few tens of  $\text{F g}^{-1}$ . Poor accessibility of carbon surface to electrolyte (i.e., electrolyte accessibility) has been confirmed to be the most important reason for the absence of proportionality between specific capacitance and surface area of these materials.

#### 4.1.1. Supercapacitors with Activated Carbon Electrodes

As mentioned earlier, according to the IUPAC classification, there are three classes of pore sizes: micropores ( $< 2 \text{ nm}$ ), mesopores ( $\approx 2$ – $50 \text{ nm}$ ), and macropores ( $> 50 \text{ nm}$ ).<sup>[268]</sup> It is known that most of the surface area of activated carbons resides in the scale of micropores.<sup>[275]</sup> Pores of this scale are generally considered to be poorly or not at all accessible for electrolyte ions (especially for organic electrolytes) and thus are incapable of supporting an electrical double layer. In contrast, mesopores contribute the most to the capacitance in an electrical double-layer capacitor.<sup>[276,278]</sup> However, recent experimental and theoretical studies have demonstrated that charge storage in pores of  $0.5$ – $2 \text{ nm}$  in size (smaller than the size of solvated electrolyte ions) increased with decreasing pore size due to the closer approach of the ion center to the electrode surface in the smaller pores.<sup>[279</sup>–<sup>282</sup>] Pores less than  $0.5 \text{ nm}$  wide are too small for double layer formation.<sup>[282]</sup> Currently available activated carbon materials have high surface area but unfortunately low mesoporosity, resulting in their low electrolyte accessibility and thus limited capacitance.<sup>[275]</sup> This translates to the limited energy density of the resultant supercapacitors. Moreover, along with their poor electrical conductivity, the low electrolyte accessibility of activated carbons produces a high internal resistance and hence a poor power density for the capacitors.<sup>[280]</sup> Consequently, currently available supercapacitors based on these activated carbon electrodes possess a limited energy density ( $4$ – $5 \text{ Wh kg}^{-1}$ ) and a limited power density ( $1$ – $2 \text{ kW kg}^{-1}$ ).<sup>[274]</sup> Therefore, new materials are needed to overcome the drawbacks of activated

carbon electrode materials in order to improve the performances for supercapacitors.

#### 4.1.2. Supercapacitors with Carbon Nanotube Electrodes

Owing to their high electrical conductivity, high charge transport capability, high mesoporosity, and high electrolyte accessibility, CNTs are attractive electrode materials for developing high-performance supercapacitors.<sup>[60,70]</sup> Research has been performed to develop different types of CNT electrode materials and combine them with various electrolytes to improve the performance, safety, and lifetimes for supercapacitors.

Randomly entangled CNTs are the first type of CNT materials that were studied for supercapacitor applications. Comparing with high-surface-area activated carbons, CNTs possess a moderate specific surface area. Nevertheless, higher capacitance has been reported for CNTs (e.g.,  $102 \text{ F g}^{-1}$  for MWNTs<sup>[59]</sup> and  $180 \text{ F g}^{-1}$  for SWNTs<sup>[283]</sup>) in contrast to that of only tens of  $\text{F g}^{-1}$  for activated carbons. Based on the commonly realizable charge densities of  $20$ – $50 \mu\text{F cm}^{-2}$  for electrical double-layer capacitors,<sup>[268]</sup> An et al.<sup>[275]</sup> estimated the theoretical capacitance for their CNTs (specific surface area:  $357 \text{ m}^2 \text{ g}^{-1}$ ) to be  $71$ – $178 \text{ F g}^{-1}$ , in good agreement with the observed values ( $180 \text{ F g}^{-1}$ ) in the upper bound, indicating a perfect electrolyte accessibility for the CNTs. The unique mesoporosity induced by the tube entanglement is responsible for the high electrolyte accessibility, and hence high capacitances observed for the CNT electrodes.<sup>[59,271,275]</sup>

Indeed, an supercapacitor fabricated from SWNT electrodes and KOH electrolyte showed a promising power density of  $20 \text{ kW kg}^{-1}$  with a maximum energy density of  $\approx 10 \text{ Wh kg}^{-1}$  (performance based on the mass of SWNTs).<sup>[275]</sup> A power density of  $> 8 \text{ kW kg}^{-1}$  (with a maximum energy density of  $\approx 1 \text{ Wh kg}^{-1}$ ) has been realized for a packaged supercapacitor fabricated from MWNT electrodes and  $\text{H}_2\text{SO}_4$  electrolyte.<sup>[59]</sup> These power densities are higher than those attainable by activated carbon-based commercial capacitors,<sup>[274]</sup> but the energy densities still need to be improved. The equivalent series resistance (ESR), consisting of the resistance of the electrode itself, the resistance of the electrolyte within the porous layer of the electrode, and the contact resistance between the electrode and the current collector of the capacitor, was all very small. This, coupled with the excellent electrical conductivity, high mesoporosity, and high electrolyte accessibility of CNTs, led to the fast delivery of the stored charge and thus a very high power density for the capacitors.

In recent years, VA-CNTs have been demonstrated to be advantageous over their randomly entangled counterparts for supercapacitor applications. First, VA-CNTs are better-structured materials for supercapacitors. Unlike the irregular pore structures of random CNTs, the vertically aligned structures and the well-defined tube spacing in a VA-CNT array (**Figure 19a–c**) provide a more electrolyte-accessible surface.<sup>[70,283]</sup> The aligned structures should also provide improved charge storage/delivery properties as each of the constituent aligned tubes can be connected directly onto a common electrode to allow them to effectively participate

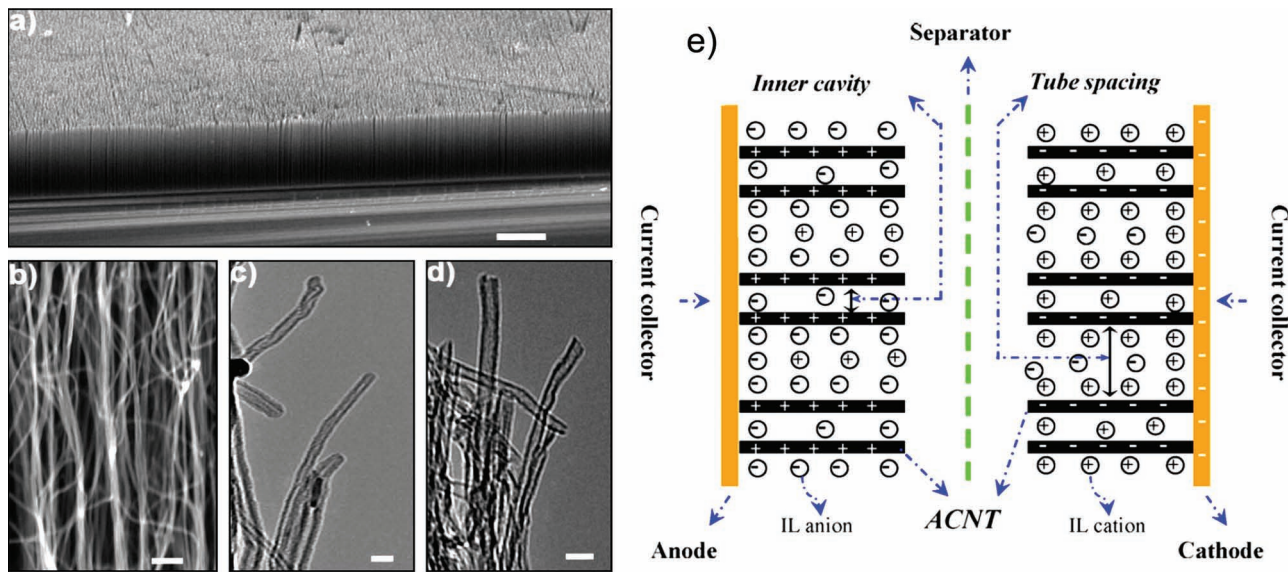


**Figure 19.** a) SEM image of a plasma-etched, VA-CNT electrode (scale bar: 100  $\mu\text{m}$ ). b) Higher magnification view of the electrode (scale bar: 100 nm). TEM images of the CNTs before (c) and after (d) plasma etching (scale bar: 20 nm). The multiwalled CNT array is highly aligned with the tube length of  $\approx 150 \mu\text{m}$  and outer and inner diameters of approximately 10 and 5 nm, respectively. e) Schematic representation of a supercapacitor based on plasma-etched VA-MWNT electrodes and ionic liquid electrolyte. Reproduced with permission.<sup>[70]</sup> Copyright 2009, Elsevier.

in the charge/discharge process. This indicates a combined charge capacity from all individual tubes of the VA-CNT electrode, and thus enhanced energy density for the capacitor. In turn, the stored energy can be delivered rapidly through each tube of the electrode, and hence an excellent power density for the capacitor. Second, VA-CNTs possess a well-defined surface area for each of the constituent tubes to be accessible to the electrolyte ions. Moreover, the top end-caps of VA-CNTs can be properly opened (Figure 19d) under appropriate conditions (e.g., by plasma etching).<sup>[284]</sup> The end-cap-opening then allows the electrolyte access to the inner cavity of the VA-CNTs, resulting in an enhanced overall surface area (from both internal and external walls of tubes) for charge storage on the VA-CNTs (Figure 19e).<sup>[70,285]</sup> Consequently, recent research has demonstrated the improved rate capability for VA-CNTs over random CNTs.<sup>[286–290]</sup> Specifically, a high capacitance has been obtained in 1 M H<sub>2</sub>SO<sub>4</sub> for a VA-CNT array electrode (365 F g<sup>-1</sup>) prepared by template-assisted CVD<sup>[291]</sup> and in ionic liquid electrolytes<sup>[292]</sup> and for an VA-CNT electrode (440 F g<sup>-1</sup>) prepared by a template-free CVD approach.<sup>[70,293]</sup>

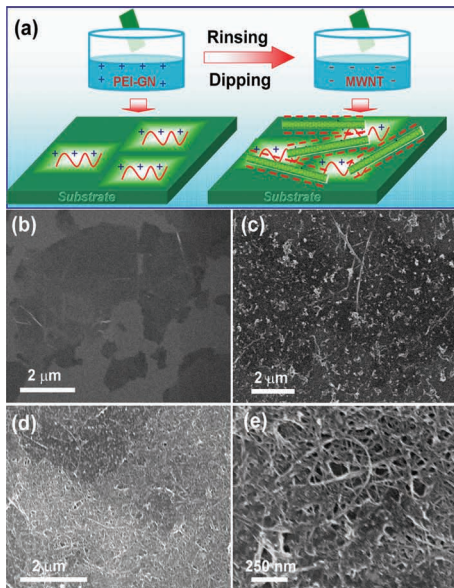
#### 4.1.3. Supercapacitors with Graphene Electrodes

Although CNTs have been used for supercapacitance since the end of 1990's,<sup>[59,294]</sup> CNT-based capacitors do not exhibit satisfactory capacitance for the expected device performance. This is because of the high contact resistance between CNT-based electrode and current collector, inefficient interaction between CNT-based electrode and electrolyte, and the instability of double-layer. Due to its large surface area, high carrier transport mobility and excellent thermal/mechanical stability, graphene has recently been studied as an alternative carbon based electrode in supercapacitors.<sup>[295]</sup> Theo-

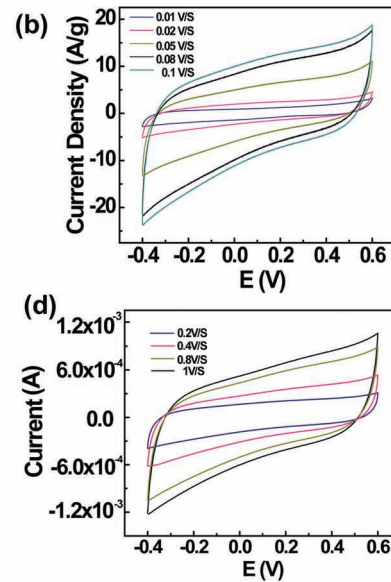
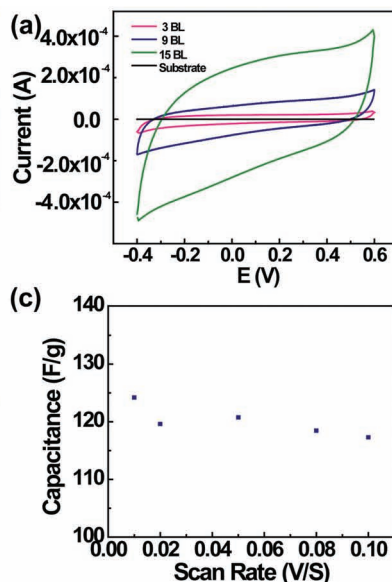
retically, the double-layer capacitance value of a graphene electrode can reach up to 550 F g<sup>-1</sup>, the highest value of intrinsic capacitance among all carbon-based electrode.<sup>[296,297]</sup> Using chemically modified graphene oxide electrode, Stoller et al.<sup>[298]</sup> obtained the specific capacitance of 135 and 99 F g<sup>-1</sup> in aqueous and organic electrolytes, respectively. By using simple microwave heating and propylene carbonate solution methods for exfoliation and reduction of graphene oxide, the same group has also obtained the capacitance values of 191 and 120 F g<sup>-1</sup>, respectively, for the reduced graphene oxides.<sup>[299,300]</sup> In addition to reduced graphene oxide, various graphene based materials, such as graphene oxide-metal oxide nanocomposites,<sup>[301]</sup> graphene–CNT hybrid films,<sup>[302]</sup> graphene–carbon black composites<sup>[303]</sup> and graphene–polymer nanocomposites,<sup>[304]</sup> have been used as electrodes in supercapacitors with high capacitances.

#### 4.1.4. Supercapacitors with Carbon Nanotubes and/or Graphene Hybrid Electrodes

As can be seen from the above discussion, graphene nanosheets have emerged as a new class of promising materials attractive for potential applications in supercapacitors due to their unique electrical and mechanical properties as well as large surface area. Due to their strong pi-pi stacking, however, a large portion of the surface area associated with the individual graphene sheets in the graphene electrode is unaccessible. A particularly attractive option is to design and develop hybrid films based on graphene sheets as electrodes.<sup>[305,306]</sup> In this context, it is critical to tailor properties of the hybrid films by controlling their composition and architecture at nano-/micrometer scale. Therefore, it is highly desirable to use 1D CNTs to physically separate 2D graphene nanosheets to preserve graphene's high surface area.



(A)



(B)

**Figure 20.** A) a) Illustration of positively charged PEI–GN and negatively charged MWNT film deposition process on an appropriate substrate (e.g., silicon wafer, ITO glass). SEM images of b) the first layer PEI–GN and c) the first bilayer  $[PEI-GN/MWNT-COOH]_1$  film deposited on a silicon substrate. d,e) SEM images of the  $[PEI-GN/MWNT-COOH]_9$  film after the 9th deposition cycle under different magnifications. B) a) Cyclic voltammograms (CV) at the scan rate of  $0.05\text{ V s}^{-1}$  in  $1.0\text{ M H}_2\text{SO}_4$  at room temperature obtained from heat-treated  $[PEI-GN/MWNT-COOH]_n$  films with bilayer number  $n = 3, 9, 15$ . b,c) CV and specific capacitance at the scan rates of  $0.01, 0.02, 0.05, 0.08$  and  $0.1\text{ V s}^{-1}$  from  $[PEI-GN/MWNT-COOH]_9$  film in  $1.0\text{ M H}_2\text{SO}_4$  at room temperature (specific capacitance is derived at the potential of  $0.1\text{ V}$ ). (d) CV from  $[PEI-GN/MWNT-COOH]_9$  film at higher scan rate of  $0.2, 0.4, 0.8, 1\text{ V s}^{-1}$  in  $1.0\text{ M H}_2\text{SO}_4$  at room temperature. Reproduced with permission.<sup>[302]</sup> Copyright 2010, American Chemical Society.

The availability of solution-processable graphene oxides allowed the formation of graphene nanosheet (GN)-based functional films through various solution processing methods.<sup>[99–102,199,258,307]</sup> In this regard, Yu and Dai<sup>[302]</sup> prepared stable aqueous dispersions of polymer-modified graphene sheets via in-situ reduction of exfoliated graphite oxides in the presence of cationic poly(ethyleneimine) (PEI). The resultant water-soluble PEI-modified graphene nanosheets (PEI–GN) with abundant  $-\text{NH}_2$  groups could be protonated ( $-\text{NH}_3^+$ ) over a certain pH range (pH = 2–9) after dissolving the PEI–GN into deionized (DI) water,<sup>[107]</sup> which was then used for layer-by-layer sequential assembly with the negatively charged MWNT prepared by acid oxidation (i.e., MWNT–COOH)<sup>[308]</sup> to form hybrid carbon films (**Figure 20A**). As can be seen in Figure 20A, the self-assembly process has successfully led to the fabrication of a reasonably uniform film with well-interconnected carbon-based hybrid materials. Thereafter, the substrate-supported self-assembled hybrid film was heated at  $150\text{ }^\circ\text{C}$  for 12 h in a vacuum oven, resulting in the formation of amide bonds between the PEI-modified graphene and carboxylic acids on the acid-oxidized MWNT surface.<sup>[309]</sup> The SEM images of the  $[PEI-GN/MWNT-COOH]_9$  multilayer films after the 9th deposition cycle in Figure 20Ad,e reveal a relatively dense and uniform network carbon nanostructure with well-defined nanoscale pores. It is anticipated that an extended conjugated network can be formed with nanotubes bridging between graphene sheets. Since both graphene and CNTs could have intrinsically high electrical conductivity and large surface area, the resultant network structures with well-defined porous could

serve as fast electronic and ionic conducting channels, providing ideal electrodes for energy storage devices, particularly supercapacitors.

Figure 20B shows cyclic voltammograms (CVs) of the heat-treated  $[PEI-GN/MWNT-COOH]_9$  films on ITO glasses in  $1.0\text{ M H}_2\text{SO}_4$  solution at room temperature as a function of the bilayer number (Figure 20B).<sup>[302]</sup> The coated ITO glass was used as the working electrode, an Ag/AgCl (3 M KCl filled) electrode as the reference electrode, and a platinum wire as the counter electrode. CV studies were performed within the potential range of  $-0.4$  to  $0.6\text{ V}$  at scan rates of  $0.01$ – $1\text{ V s}^{-1}$ . The measured voltammetry curves show a quite rectangular shape, attractive for capacitor applications. An average capacitance ( $120\text{ F g}^{-1}$ ) was obtained, which is considerably higher than those of vertically-aligned,<sup>[287]</sup> and nonaligned CNT electrodes.<sup>[271,310]</sup> It should be noted that the CVs are still rectangular in shape even at exceedingly high scan rates of  $\approx 0.8$  and  $1\text{ V s}^{-1}$ , indicating rapid charging and discharging with a low equivalent series resistance of the electrodes.<sup>[311]</sup> These results indicate the exciting potential for the use of this new class of hybrid carbon films in high performance supercapacitors.

On the other hand, recent theoretical studies<sup>[312–315]</sup> have indicated that 3D pillared architectures, consisting of parallel graphene layers supported by VA–CNTs in between, possess desirable out-of-plane transport and mechanical properties while maintaining the excellent properties of their building blocks. Of particular interest, computer modeling has predicted that such a 3D pillared VA–CNT–graphene structure can be used for efficient hydrogen storage after being doped

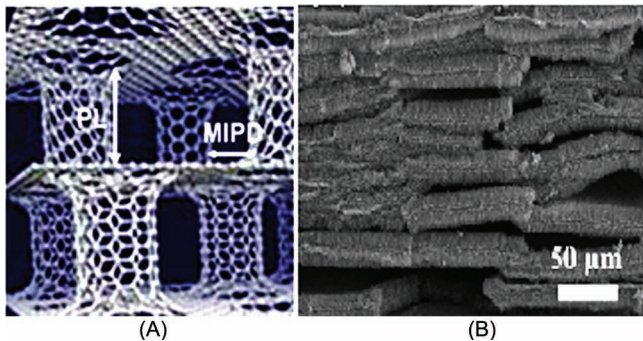


**Figure 21.** A) Schematic picture of a 3D pillared VA–CNT–graphene nanostructure. B) A typical SEM image of the 3D pillared VA–CNT–graphene architectures prepared by intercalated growth of VA–MWNTs into the thermally expanded HOPG. Reproduced with permission.<sup>[316]</sup> Copyright 2011, American Chemical Society.

with lithium cations.<sup>[313]</sup> Computer modeling studies carried out by Varshney and co-workers<sup>[312]</sup> indicate that thermal transport properties of the 3D pillared VA–CNT–graphene structure is governed by the minimum interpillar distance (MIPD) and the CNT pillar length (PL) (**Figure 21A**).

These inherently nanoporous 3D pillared VA–CNT–graphene architectures with large surface areas should allow for tunable thermal, mechanical, and electrical properties useful in many potential applications, including advanced supercapacitors. In this context, Du et al.<sup>[316]</sup> have developed a rational strategy for creating the 3D pillared VA–CNT–graphene architectures by intercalated growth of VA–CNTs into thermally expanded highly ordered pyrolytic graphite (HOPG) (Figure 21B). By controlling the fabrication process, the length of the VA–CNT pillars can be tuned. In conjunction with electrodeposition of nickel hydroxide to introduce the pseudo-capacitance, these 3D pillared VA–CNT–graphene architectures with a controllable nanotube length were demonstrated to show a high specific capacitance and remarkable rate capability, significantly outperformed many electrode materials currently used in the state-of-the-art supercapacitors.

In addition, CNTs have also been employed to fabricate composite electrodes with activated carbons, conjugated polymers, or metal oxides, to improve the performances (especially energy density) for CNT supercapacitors. Comparing to activated carbons, CNTs have a relatively lower specific surface area but with excellent conductive, charge transport, and electrolyte-accessible properties. It is then desirable to combine activated carbons with CNTs to fabricate composites having the combined advantages from these two components. In this context, Portet et al.<sup>[317]</sup> have blended activated carbons, double-walled CNTs (DWNTs), and a polymer binder to synthesize CNT/activated carbon composites. Improved capacitive behavior (lower ESR, lower capacitance loss at high frequencies, and faster charge/discharge process) has been demonstrated for supercapacitors fabricated from these composite electrodes over those from conventional activated carbon electrodes. In a separate study, Liu et al.<sup>[318]</sup> mixed SWNTs with a polyacrylonitrile (PAN) dimethylformamide

solution to synthesize a SWNT/PAN composite film, followed by CO<sub>2</sub> activation to convert this film into a SWNT/activated carbon composite electrode. Capacitance of the composite electrode was found to be significantly higher than that of a pure SWNT buckypaper electrode, which has been confirmed to be due to the higher specific surface area of the composite electrode. This led to the significantly improved power and energy densities for the SWNT/activated carbon composite electrode over those of the SWNT buckypaper electrode.

An appropriate balance between the surface area and the mesoporosity is believed to be the key to ensure the high performance of the composite electrodes. In this regard, Lu et al.<sup>[319]</sup> adopted and modified a conventional slurry procedure to combine high-surface-area activated carbons, commercially available CNTs, and ionic liquids to fabricate AC/CNT/IL nanocomposite electrodes. Unlike the aggregation of carbon black particles usually observed in a conventional activated carbon electrode, CNTs in the nanocomposite are well-distributed, providing a uniform conductive network for the electrode. Also, the combination of CNTs and activated carbons provided a good balance between the mesoporosity and the surface area, and hence an enhanced capacitive behavior for the composite electrode. Furthermore, introduction of ionic liquids in the nanocomposite helped unbundle the nanotube bundles (due to the reduced van der Waals forces between CNTs<sup>[320,321]</sup> and hence further enhanced the distribution of CNT conductive network for the composite. Consequently, in an ionic liquid electrolyte, the AC/CNT/IL nanocomposite electrode showed a significantly improved capacitance (188 F g<sup>-1</sup>) over a conventional activated carbon electrode (90 F g<sup>-1</sup>) and a pure CNT paper electrode (20 F g<sup>-1</sup>).<sup>[322]</sup> Based on these nanocomposite electrodes and an ionic liquid electrolyte, these authors have further developed prototype supercapacitors with a high cell voltage (4 V) as well as superior energy and power densities (50 Wh kg<sup>-1</sup> and 22 kW kg<sup>-1</sup> (in terms of the mass of the active electrode material), respectively. Combining the high capacitive behavior of this nanocomposite electrode with the large electrochemical window of an ionic liquid electrolyte, therefore, the resultant supercapacitors<sup>[319,322]</sup> showed the potential to significantly outperform the current supercapacitor technology.<sup>[274]</sup> Thus, these studies provide a new approach in fabricating advanced supercapacitors with a high performance, inherently safe operation, and long lifetime.<sup>[319,322]</sup>

Faradaic reactions within the bulk of the materials, such as conjugated polymers and transition metal oxides, provide additional charge storage (i.e., pseudocapacitance).<sup>[267]</sup> Recently, there is a research trend in combining the high energy-storage capability of the redox materials with the high-power-delivery capability of CNTs to fabricate composites with improved capacitance and rate capability. Conjugated polymers possess the advantages of low cost, light weight, and good processability over transition metal oxides, and high energy-storage capability over high-surface-area activated carbons. Therefore, conjugated polymers have been combined with CNTs to fabricate nanocomposites electrodes with improved capacitance and rate capability. CNT/polymer nanocomposites can be readily electrodeposited from a monomer-containing solution onto a CNT electrode or

from a CNT/monomer-containing solution onto a traditional conductive substrate. For instance, Jurewicz et al.<sup>[323]</sup> have electrochemically coated polypyrrole onto a MWNT bucky-paper and demonstrated substantially increased capacitance for the resultant CNT/polypyrrole composites over the pristine MWNT electrode ( $163 \text{ F g}^{-1}$  vs.  $50 \text{ F g}^{-1}$ ). Gao et al.<sup>[324]</sup> and Hughes et al.<sup>[325]</sup> have potentiostatically grown polypyrrole onto aligned MWNTs to fabricate the nanocomposites. In both cases, the resulting polypyrrole layer was uniformly coated on the aligned nanotubes. The MWNT/polypyrrole composite showed a much larger capacitance ( $2.55 \text{ F cm}^{-2}$  vs.  $0.62 \text{ F cm}^{-2}$ ) and higher knee frequency than a pure polypyrrole film electrode. Hughes et al.<sup>[326]</sup> have electrochemically polymerized pyrrole monomer in a suspension of acid-oxidized MWNTs. The negatively charged MWNTs acted both as a supporting electrolyte and as a dopant during the polymerization and deposition of polypyrrole on a graphite electrode. The resultant nanoporous 3D polypyrrole-coated MWNTs facilitated the electron and ion transfer relative to pure polypyrrole films, leading to a higher capacitance ( $192 \text{ F g}^{-1}$  or  $1.0 \text{ F cm}^{-2}$ ) and a higher knee frequency for the composites electrode. The CNT/polymer nanocomposites could also be prepared through a chemical oxidative polymerization. For instance, Frackowiak et al.<sup>[271]</sup> deposited polypyrrole on MWNTs using  $(\text{NH}_4)_2\text{S}_2\text{O}_8$  as oxidant and achieved a higher capacitance ( $170 \text{ F g}^{-1}$ ) for the resultant polypyrrole/MWNT composites over pure nanotubes (ca.  $80 \text{ F g}^{-1}$ ) or pure polypyrrole (ca.  $90 \text{ F g}^{-1}$ ). An et al.<sup>[327]</sup> used  $\text{FeCl}_3$  as oxidant to polymerize polypyrrole on SWNTs. Due to the uniform polypyrrole coating on the porous and conductive support of SWNTs, the SWNT/polypyrrole nanocomposite electrode showed a much higher capacitance ( $265 \text{ F g}^{-1}$ ) than either pure polypyrrole or pure SWNT electrodes.

Noble metal oxides, such as  $\text{RuO}_2$  and  $\text{IrO}_2$ , have been identified as the promising electrode materials for supercapacitors due to their remarkable specific capacitance, good electrical conductivity, and high chemical stability.<sup>[272]</sup> However, the high cost and scarce source of these materials retard their commercial acceptance. Recent researches have been focused on cheap transition metal oxides.<sup>[328]</sup> Among them, vanadium oxide ( $\text{V}_2\text{O}_5$ ) and manganese oxide ( $\text{MnO}_2$ ) are two important examples. Capacitive performance was demonstrated to be significantly improved by combining these metal oxides with CNTs as electrodes for supercapacitors.  $\text{V}_2\text{O}_5$  has the advantages of non-toxicity, low cost, and high theoretical capacity ( $590 \text{ mAh g}^{-1}$ ),<sup>[329]</sup> but its disadvantages include the low electronic conductivity ( $10^{-6}\text{--}10^{-7} \text{ S cm}^{-1}$ ),<sup>[330]</sup> and slow  $\text{Li}^+$  diffusion within the host matrix (diffusion coefficient:  $\approx 10^{-13} \text{ cm}^2 \text{ s}^{-1}$ ).<sup>[331]</sup> One effective approach to addressing these issues is to combine  $\text{V}_2\text{O}_5$  with CNTs to fabricate nanocomposites electrodes with a high-capacity and high-rate capability, which has been utilized for supercapacitor and Li-ion battery (vide infra) applications. In particular, Kim et al.<sup>[332]</sup> have electrochemically deposited  $\text{V}_2\text{O}_5$  thin film onto a preformed CNT film substrate to prepare the  $\text{V}_2\text{O}_5/\text{CNT}$  composite electrodes. With a thin  $\text{V}_2\text{O}_5$  film coating ( $\approx 6 \text{ nm}$ ), the  $\text{V}_2\text{O}_5/\text{CNT}$  electrode showed a very high capacity of  $680 \text{ mAh g}^{-1}$  (based on the mass of  $\text{V}_2\text{O}_5$ ) at a current density of  $5 \text{ A g}^{-1}$ , and retained 67% of this capacity

even at a current density of as high as  $100 \text{ A g}^{-1}$ . The porous and electrolyte accessible structures of  $\text{V}_2\text{O}_5$  on a CNT substrate, in contrast to the compact structures of a dense  $\text{V}_2\text{O}_5$  film on a conventional Pt electrode, are responsible for these improvements.  $\text{MnO}_2$  is also a nontoxic, low-cost, and high-capacity (theoretical:  $616 \text{ mAh g}^{-1}$ ) metal oxide. In order to improve its electrochemical utilization, capacity, and rate capability for energy storage applications,  $\text{MnO}_2$  has also been combined with CNTs to fabricate nanocomposites. Different approaches (e.g., electrochemical deposition,<sup>[333]</sup> thermal deposition,<sup>[334]</sup> and direct redox reaction deposition,<sup>[335]</sup>) have been investigated to synthesize the composites. For example, the resultant  $\text{MnO}_2$  can be in-situ coated on the CNTs through the direct redox reaction between the CNTs and permanganate ions ( $\text{MnO}_4^-$ ). Using this method, Ma et al.<sup>[335]</sup> have deposited birnessite-type  $\text{MnO}_2$  on CNTs. The resultant  $\text{MnO}_2/\text{CNT}$  nanocomposite showed a large capacitance of  $250 \text{ F g}^{-1}$  even at a large current density of  $1 \text{ A g}^{-1}$ , indicating the excellent electrochemical utilization of the  $\text{MnO}_2$  on the highly conductive and porous CNT support.

## 4.2. Lithium-Ion Batteries

Since their first commercialization by Sony Corporation in 1991,<sup>[336]</sup> lithium-ion (Li-ion) batteries have become the premier rechargeable battery.<sup>[337]</sup> Li-ion batteries offer significant benefits over conventional rechargeable batteries, including the reduced weight and higher energy storage capability. They have been displacing Nickel Metal Hydride (NiMH) batteries in the consumer electronics market and have begun to displace NiMH or Nickel–Cadmium (NiCd) batteries in the power tool market. In recent years, Li-ion batteries are actively being developed for advanced transportation technologies (e.g., electric vehicles, hybrid electric vehicles, and plug-in hybrids).<sup>[338]</sup> To satisfy the rapidly increasing performance demanded for these applications, however, the currently available Li-ion batteries need to be improved.

A Li-ion battery consists of three essential components, namely the  $\text{Li}^+$  intercalation anode and cathode as well as the electrolyte, in which  $\text{Li}^+$  ion move from the cathode to the anode during charging, and back when discharging (Figure 22).<sup>[339]</sup> Properties of the electrodes play an important role in determining not only the energy and power densities but also the safety and cycle life of the batteries.

### 4.2.1. Lithium-Ion Batteries with Graphite Electrodes

Graphite has been the preferred anode material for Li-ion batteries due to its relatively high capacity, good cyclability, and low redox potential versus lithium metal. Intercalation/deintercalation of  $\text{Li}^+$  in and out of the graphite upon charge/discharge forms the basis of graphite as the anode of the battery (Figure 22). The thermodynamic equilibrium saturation concentration of the graphite is  $\text{LiC}_6$ , corresponding to a theoretical capacity of  $372 \text{ mAh g}^{-1}$ . To achieve higher energy density for advanced Li-ion batteries, new anode materials with higher capacity is needed. In addition, the graphite anode limits the recharge rates of Li-ion batteries. At rates

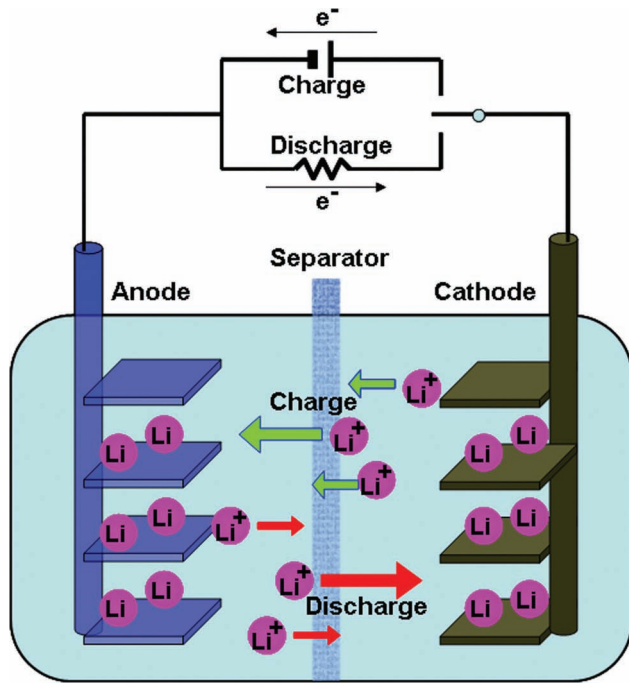


**Figure 22.** Schematic representation of the working principle a Li-ion battery.

higher than 1C, metallic lithium can be plated on the graphite causing a safety hazard. New anode materials that can be charged/discharged at higher rates are needed to solve this problem.<sup>[340]</sup> Besides, an optimal anode material for advanced Li-ion batteries should have a higher reversible capacity and higher charge/discharge rate than graphite.<sup>[285]</sup>

Transition metal oxides are commonly used cathode materials for Li-ion batteries.<sup>[341]</sup> Having a redox potential of about 4 V (vs. Li/Li<sup>+</sup>), these oxides are usually referred as 4 V cathode materials. Among them, lithium cobalt oxide (LiCoO<sub>2</sub>) has been the most frequently used cathode material in commercial Li-ion batteries.<sup>[342]</sup> However, cobalt-based materials are toxic and expensive. They are sensitive to temperature and present a potential fire hazard. Also, only 50% of the theoretical capacity of LiCoO<sub>2</sub> could be practically achieved (i.e., 140 mAh g<sup>-1</sup> vs. 274 mAh g<sup>-1</sup>). Research on nontoxic and low-cost cathode materials (e.g., manganese-, iron-, or vanadium-based) represents a trend in developing safe Li-ion batteries. Furthermore, to improve energy storage and delivery capabilities for advanced Li-ion batteries, new cathode materials having a higher specific capacity and higher rate capability are required.

#### 4.2.2. Lithium-Ion Batteries with Carbon Nanotube Electrodes

Having a large specific-surface-area and facilitated ion diffusion, nanostructured electrode materials have been extensively studied for Li-ion batteries.<sup>[331,343,344]</sup> Owning to their novel properties of high electrical conductivity, high charge transport capability, high specific surface area, high mesoporosity, and high electrolyte accessibility, CNTs are also attractive materials for Li-ion batteries.<sup>[285,345]</sup> For anode applications, CNTs have been studied as host materials and

as conductive additives. CNTs are attractive host anode materials for Li<sup>+</sup> intercalation. There have been several reports on successful intercalation of Li<sup>+</sup> into both SWNTs and MWNTs.<sup>[345–348]</sup>

It has been assumed that a large amount of Li<sup>+</sup> can be stored in the central core, the interlayer space (for MWNTs), or the empty space between the nanotubes when they are assembled in bundles.<sup>[349]</sup> Reversible Li<sup>+</sup> intercalation capacities of as high as 400 mAh g<sup>-1</sup> for MWNTs<sup>[350]</sup> and 500 mAh g<sup>-1</sup> for SWNTs<sup>[349]</sup> have been reported. Higher capacities of CNTs than that of graphite (372 mAh g<sup>-1</sup>) is believed to be due to the higher specific surface areas of CNTs. The capacity of CNTs can be further increased by opening or cutting the CNTs. Shimoda et al.<sup>[351]</sup> reported a reversible capacity of about 700 mAh g<sup>-1</sup> for SWNTs that were etched by strong acids to open the tubes and reduce their length, while Gao et al.<sup>[347]</sup> achieved a reversible capacity of 1000 mAh g<sup>-1</sup> for their SWNTs treated by ball milling. High rate characteristics have also been demonstrated for CNT electrodes. For example, 60% of the full capacity could be retained when the charge/discharge rate was increased from 50 mA g<sup>-1</sup> to 500 mA g<sup>-1</sup>.

#### 4.2.3. Lithium-Ion Batteries with Vertically Aligned Carbon Nanotube Electrodes

However, CNT anodes suffer from two major problems. One of them is the irreversible capacity associated with the formation of a passivating layer, the so-called solid electrolyte interphase (SEI) at the carbon surface, which is similar to the situation at a conventional graphite anode.<sup>[352]</sup> The other is the undesirable voltage hysteresis between charge and discharge that is mainly related to the kinetics of the Li<sup>+</sup> intercalation/deintercalation reactions at the CNT anode. Attempts have been made to try to solve these problems, for example, by cutting the nanotubes to short segments to improve the charge transfer capability of the electrode.<sup>[353]</sup> With their improved properties mentioned earlier, VA-CNTs are attracting more and more attention as the new anode materials for Li-ion batteries.<sup>[354]</sup>

Although CNTs and other negative electrode nanomaterials have been shown to exhibit similar or greater capacities compared to the graphite in commercial lithium-ion batteries (maximum theoretical capacity of 372 mAh g<sup>-1</sup>), they do not improve graphite's moderate rate capability.<sup>[355]</sup> Recent studies suggested that aligned CNTs could allow for better contact with the current collector and increased ion diffusivity to significantly improve bulk electron transport properties, thereby allowing for improved rate capabilities.<sup>[287,288,292,356]</sup> Recently, Chen et al.<sup>[357]</sup> Pushparaj et al.<sup>[358]</sup> and Masarapu et al.<sup>[359]</sup> have incorporated aligned CNTs into lithium-ion battery electrodes. However, relatively low capacities were obtained at low discharge rates due possibly to poor electron transport resulting from a poor contact between the CNTs and their current collectors. In this context, Welna et al.<sup>[69]</sup> investigated the electrochemical properties of VA-MWNTs produced by pyrolysis of FePc for lithium-ion battery negative electrodes. The VA-MWNTs are supported at their base by a thin nickel metal film, which acts as a support to the

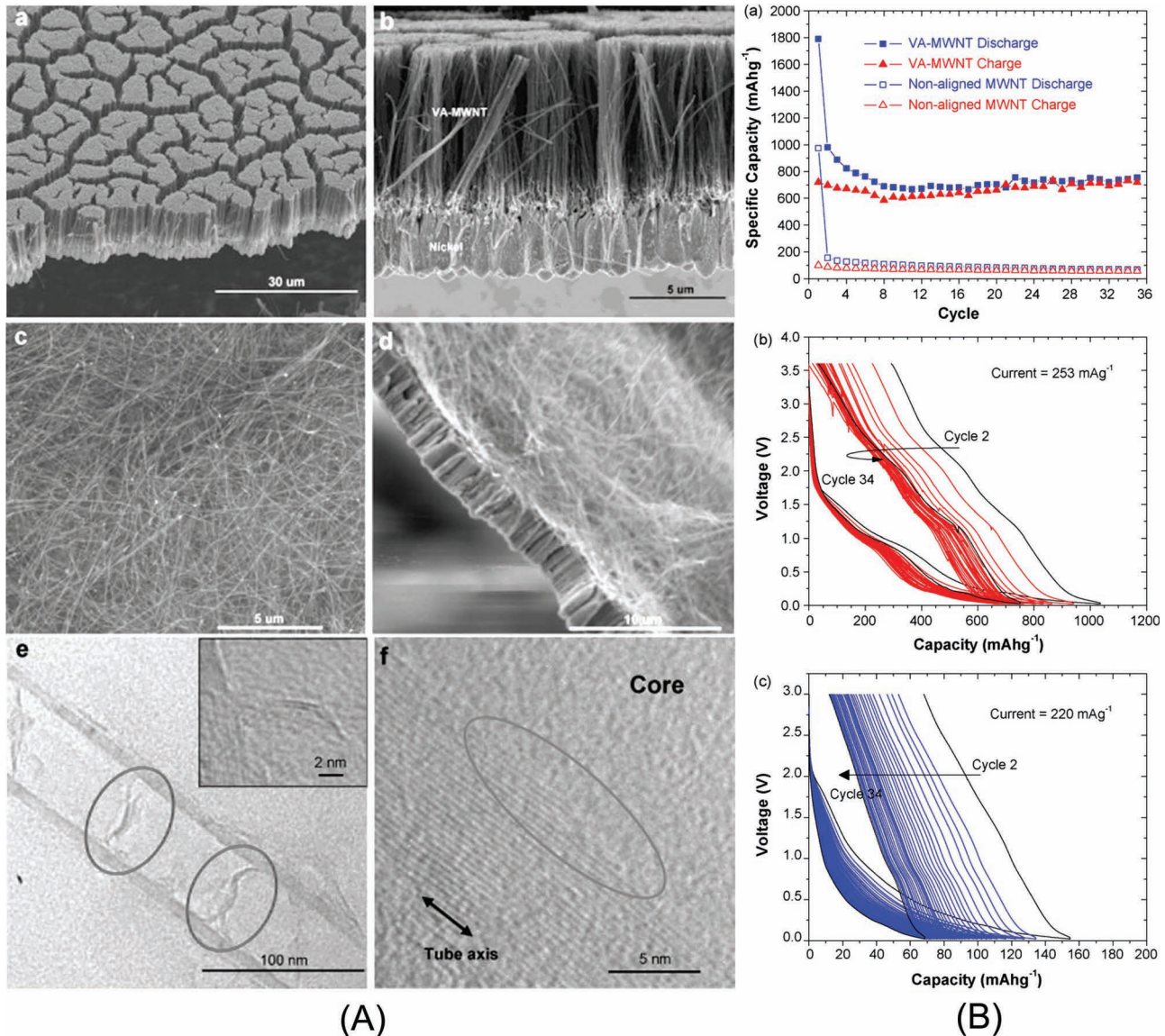


**Figure 23.** A) SEM images of a VA–MWNT (a,b) and an nonaligned MWNT (c,d) electrode. TEM images of a VA–MWNT electrode, showing the loose graphene layers (e) and the graphene nanotube edges (f) within the internal nanotube structure. The distance between the graphene nanotube layers is 0.335 nm. B) Specific capacity as a function of cycle for VA–MWNT and nonaligned MWNT electrodes at similar discharge rates (a). Voltage profile of cycles 2–34 for VA–MWNT (b) and nonaligned MWNT (c) electrodes. Reproduced with permission.<sup>[69]</sup> Copyright 2010, Elsevier.

nanotubes, helping to maintain their alignment (**Figure 23A**). The nickel film also acts as an excellent current collector due to the intimate contact with the VA–MWNTs. It was found that the alignment of the MWNTs in the direction of ion diffusion in a battery cell significantly increased the accessibility of the electrode interior to the electrolyte. The lithium-ion storage capacity and rate capability of the aligned nanotubes were shown to be significantly improved compared to graphite and their non-aligned counterparts. These authors reported a substantially greater rate capability than any value previously reported for CNT electrodes,<sup>[346,358,360–365]</sup> as exemplified by Figure 23B. The specific capacities of both the VA–MWNTs and the unaligned MWNTs as a function of cycle number are shown in Figure 23Ba, while the voltage profiles for these cycles are shown in Figure 23Bb,c. After the

irreversible capacity loss of the first cycle ( $Q_{\text{irr}}$ ), the reversible capacity ( $Q_{\text{rev}}$ ) of the VA–MWNTs decreased from 980 mAh g<sup>-1</sup> to a minimum near the tenth cycle, after which it increased slightly and stabilized near 750 mAh g<sup>-1</sup>. On the other hand,  $Q_{\text{rev}}$  for the unaligned MWNTs continuously decreased from 158 to 58 mAh g<sup>-1</sup> by cycling 35 times. The alignment of the nanotubes in the direction of ion diffusion could allow lithium-ions to more readily access the open nanotube ends and significantly increased the  $Q_{\text{rev}}$  of the VA–MWNTs compared to the nonaligned MWNTs.

The TEM images in Figure 23Ae,f show that the internal core of the nanotubes contains irregular structural features, such as loose graphene layers (circles) and graphene nanotube edges (oval). These structural features can significantly increase the effective surface area of the nanotubes and

provide more defect sites at which lithium-ions could be adsorbed to the surfaces of loosely bound graphene layers or to hydrogen-containing edge carbon sites.<sup>[347,366,367]</sup> In addition, the intimate contact between each of the vertically aligned nanotubes and the nickel metal current collector provides a low resistance pathway, allowing for effective connectivity throughout the electrode. The large specific capacity of the aligned CNTs and their ability to maintain moderate specific capacities at very high discharge rates make them attractive for high power lithium-ion batteries.

#### 4.2.4. Lithium-Ion Batteries with Carbon Nanotube and/or Graphene Hybrid Electrodes

CNTs have also been demonstrated to be excellent conductive additives for Li-ion batteries. With their unique properties as described above, addition of CNTs in the graphite anode can efficiently improve rate capability, cyclability, and safety of the resulting graphite/CNT composite electrodes. For example, the cyclic efficiency of a graphite anode was maintained at almost 100% up to 50 cycles by adding 10 wt% of MWNTs.<sup>[368]</sup> Indeed, CNTs have been used as anode additives in commercial Li-ion batteries. More than 50% of cell phones and notebooks are already using batteries that contain CNTs.

CNTs have also been explored as conductive additives for cathode applications, including in a large range of materials (e.g., LiCoO<sub>2</sub>,<sup>[369]</sup> LiFePO<sub>4</sub>,<sup>[370]</sup> MnO<sub>2</sub>,<sup>[371]</sup> V<sub>2</sub>O<sub>5</sub>,<sup>[372,373]</sup>). For example, introducing SWNTs as conductive additives into the V<sub>2</sub>O<sub>5</sub> aerogels,<sup>[372]</sup> the resulting V<sub>2</sub>O<sub>5</sub>/SWNT nanocomposite showed a high capacity with a high capacity retention. Moreover, CNTs have also been combined with acetylene blacks, the conductive additives of conventional Li-ion battery technology, to improve the performance for Li-ion battery cathode materials.<sup>[374]</sup>

V<sub>2</sub>O<sub>5</sub> has been investigated as a potential cathode material to replace LiCoO<sub>2</sub> for rechargeable Li-ion batteries due to its ability to insert large amounts of lithium.<sup>[375,376]</sup> V<sub>2</sub>O<sub>5</sub> has a reversible Li<sup>+</sup> intercalation/deintercalation with the moles of Li<sup>+</sup> intercalated into per mole of V<sub>2</sub>O<sub>5</sub> up to four,<sup>[329]</sup> corresponding to a very high theoretical capacity of 590 mAh g<sup>-1</sup>. As mentioned earlier, however, the major disadvantages of V<sub>2</sub>O<sub>5</sub> are its intrinsically low electronic conductivity ( $10^{-6}$ – $10^{-7}$  S cm<sup>-1</sup>)<sup>[329]</sup> and slow diffusion of Li<sup>+</sup> within the host matrix (diffusion coefficient:  $\approx 10^{-13}$  cm<sup>2</sup> s<sup>-1</sup>).<sup>[331]</sup> One effective approach to addressing these issues is to utilize V<sub>2</sub>O<sub>5</sub> as a thin film to improve its electrochemical utilization capability, and thus the enhanced capacity and rate capability for V<sub>2</sub>O<sub>5</sub>. Indeed, a capacity of up to 408 mAh g<sup>-1</sup> has been achieved for V<sub>2</sub>O<sub>5</sub> thin films produced by CVD method.<sup>[377]</sup> Indeed, V<sub>2</sub>O<sub>5</sub> thin films have been preferred as cathode for miniaturized high energy/power density batteries to power microsystems, such as microsensors, smart cards, implantable medical devices, and intelligent labels.<sup>[378]</sup> For large size applications (e.g., cell phones, laptops, and even transportation technologies), capacity of these thin film batteries need to be further improved, indicating the need for a large loading of V<sub>2</sub>O<sub>5</sub> on the cathode. However, the loading (or thickness) of V<sub>2</sub>O<sub>5</sub> on

a planar substrate electrode is limited by its intrinsically low electronic conductivity<sup>[330]</sup> and slow Li<sup>+</sup> diffusion.<sup>[331]</sup>

To exploit the high conductivity of the SWNTs for having them to provide electronic conduction without blocking electrolyte access to the V<sub>2</sub>O<sub>5</sub> active material, Sakamoto and Dunn<sup>[372]</sup> introduced SWNTs, having a similar morphological character and dimensional scale as the V<sub>2</sub>O<sub>5</sub> ribbons, as conductive additives into the V<sub>2</sub>O<sub>5</sub> aerogels to develop V<sub>2</sub>O<sub>5</sub>/SWNT nanocomposite cathodes. The resultant V<sub>2</sub>O<sub>5</sub>/SWNT composite possesses a high pore volume that ensures electrolyte access throughout the electrode, while multiple point contact was established between the two phases at the nanometer level along the V<sub>2</sub>O<sub>5</sub> ribbons. This nanocomposite electrode showed a high specific capacity of 452 mAh g<sup>-1</sup> and retained up to 65% of this capacity when the discharge rate is increased from 112 (0.2C) to 2800 mA g<sup>-1</sup> (5C). Electronically conducting network developed from the SWNTs within the V<sub>2</sub>O<sub>5</sub>/SWNT nanocomposite is believed to be responsible for the observed high performance.

Achieving both high energy and high power densities for a same energy storage device has attracted considerable attention in energy storage community.<sup>[379,380]</sup> Supercapacitors have a higher power density but a lower energy density than a battery. It is then desirable to combine the high-capacity-capability of batteries with the high-rate-capability of supercapacitors to obtain a high-energy and high-power energy storage device. Along with the use of VA-CNTs and metal-oxide hybrid electrodes in supercapacitors (Section 4.1.4), VA-CNTs have also been used in Li-ion batteries either directly as electrode materials (Li<sup>+</sup> intercalation anode),<sup>[69,354]</sup> or as conductive substrates for the deposition of electroactive materials (e.g., conducting polymers<sup>[326]</sup> and metal oxides<sup>[290]</sup>) to develop high-capacity and high-rate electrode materials.<sup>[380]</sup> Therefore, a variety of materials (e.g., conjugated polymers,<sup>[326]</sup> manganese oxide,<sup>[290]</sup> and vanadium oxide)<sup>[381]</sup> have been deposited onto VA-CNTs for cathode applications. Figure 24 illustrates the obvious advantages of VA-CNTs, in contrast to traditional activated carbons, for this application.

Using VA-CNTs sheathed with and without a coaxial layer of vanadium oxide (V<sub>2</sub>O<sub>5</sub>) as both cathode and anode, respectively, in conjugation with environmentally friendly ionic liquid electrolytes, Lu et al.<sup>[382]</sup> have recently developed high-performance Li-ion batteries with significantly improved energy density, power density, safety, and lifetime attractive for various applications. Figure 24A schematically shows that the VA-CNTs sheathed with and without a coaxial layer of vanadium oxide (V<sub>2</sub>O<sub>5</sub>) were used as the cathode and anode, respectively, in a Li-ion battery.

It was found that the VA-CNT anode and the V<sub>2</sub>O<sub>5</sub>-VA-CNT composite cathode showed a high capacity (600 and 368 mAh g<sup>-1</sup>, respectively) with a high rate capability in the ionic liquid electrolyte (i.e., *N*-Ethyl-*N,N*-dimethyl-2-methoxyethylammonium bis(trifluormethylsulfonyl)imide, [EDMMEA][TFSI]), and that the resultant battery test cells showed an excellent energy density (297 Wh kg<sup>-1</sup>) and power density (12 kW kg<sup>-1</sup>) (estimated from active-material-based performances) to significantly outperform the current state-of-the-art Li-ion battery technology (i.e., energy density:

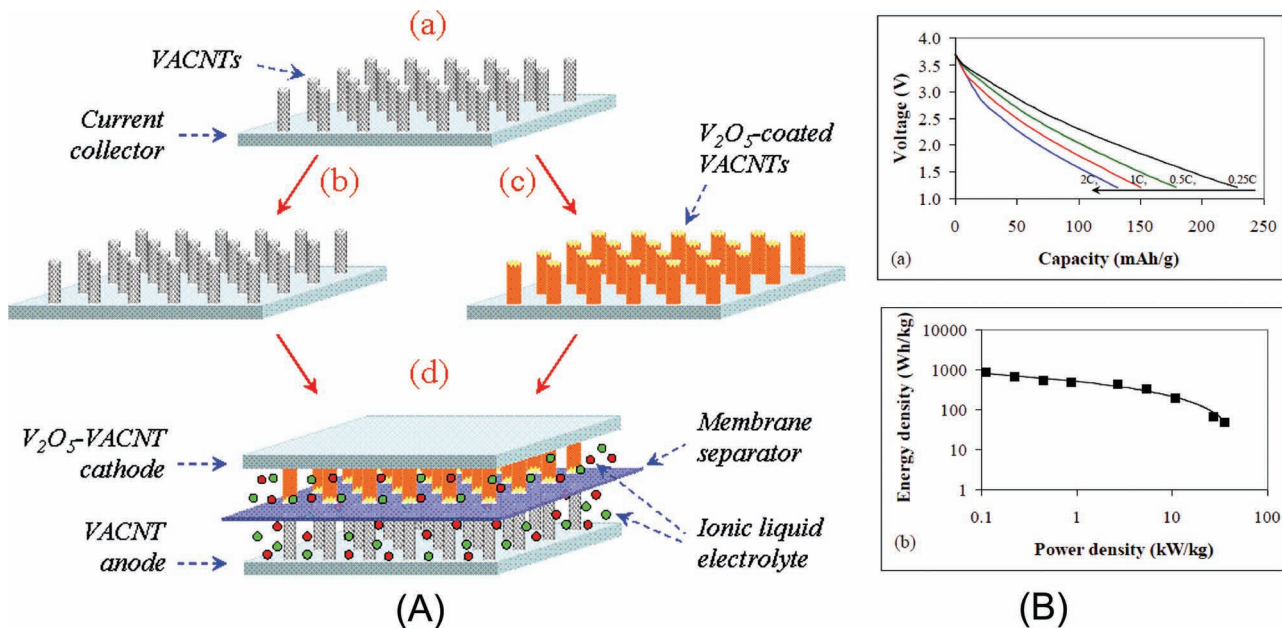


**Figure 24.** A) a) Growth of VA-CNTs on a conductive substrate (as current collector). b) Direct use of VA-CNTs as the anode. c) Deposition of V<sub>2</sub>O<sub>5</sub> on VA-CNTs to synthesize V<sub>2</sub>O<sub>5</sub>-VA-CNT composite cathode. d) Assembly of the VA-CNT anode, the V<sub>2</sub>O<sub>5</sub>-VA-CNT cathode, a membrane separator, and an ionic liquid electrolyte to fabricate the battery. High capacity and high rate capability of the VA-CNT anode and the V<sub>2</sub>O<sub>5</sub>-VA-CNT cathode ensure a high energy density and a high power density, while superior safety-related properties of ionic liquid electrolytes ensure high safety and long lifetime for the battery thus prepared. B) a) Discharge curves of a VA-CNT/V<sub>2</sub>O<sub>5</sub>-VA-CNT battery recorded at the rates increasing from 0.25C to 2C as indicated by the arrow. The capacity is defined by the total active-material-mass of the anode and the cathode. Cut-off voltage: 1.2–3.7 V. b) Ragone plot of the VA-CNT/V<sub>2</sub>O<sub>5</sub>-VA-CNT battery. Performance of the battery is defined by the total active-material-mass of the VA-CNT anode and the V<sub>2</sub>O<sub>5</sub>-VA-CNT cathode.<sup>[382]</sup>

$\approx 100\text{--}250 \text{ Wh kg}^{-1}$  and power density:  $\approx 0.3\text{--}1.5 \text{ kW kg}^{-1}$ , Figure 24B). Furthermore, the use of ionic liquid electrolytes with superior safety-related properties ensured a high safety and long lifetime for the newly-developed batteries based on the VA-CNT electrodes and ionic liquid electrolytes. By so doing, the multiple drawbacks (e.g., the energy storage, power delivery, safety, and lifetime) associated with the current Li-ion batteries were addressed and solved simultaneously in a single battery system, opening up a new approach in developing high-performance Li-ion batteries. However, further research is still needed to investigate the scaling-up feasibility and the electrolyte compatibility of these new electrode materials in order to fabricate high-energy and high-power energy storage devices with a high safety and long lifetime.

Graphene, as a 2D carbon-based material, has been considered as promising electrode materials for Li-ion batteries due to its high electrical conductivity, large surface area and a good electrochemical stability.<sup>[76,383–385]</sup> However, the specific capacity of graphene is relatively low because every six carbon atoms can hold only one lithium ion.<sup>[386]</sup> To overcome this major drawback, many other methods such as the formation of hybrid materials with metal oxide,<sup>[387–389]</sup> incorporation of chemical dopants,<sup>[390]</sup> and controlling the formation of layered structures,<sup>[77]</sup> have been developed. By the formation of hybrid materials with metal oxide and graphene, the reversible cycling performance is greatly enhanced in comparison with that of the bare metal oxide electrode. For examples, Paek et al.<sup>[391]</sup> has prepared graphene nanosheets

decorated with SnO<sub>2</sub> nanoparticles. The SnO<sub>2</sub>/graphene electrode exhibited a reversible capacity of 810 mAh g<sup>-1</sup> and good reversible cycling performance.

The main purpose of developing composites with graphene and metal oxide for anode materials is to utilize both advantages of graphene and metal oxide. Metal oxide anode has a main drawback, a huge volume changes during charge/discharge process resulting in the cracking of electrode and poor reversibility, although it can possess larger lithium ion storage capacities.<sup>[392]</sup> In composites, graphene can act as not only a mechanical support layer to relieve the cracking but also a good conductive layer for electron and ion.<sup>[393]</sup>

In addition to the formation of composite materials with metal oxide, the modification of carbon nanomaterials (e.g., graphene) with chemical dopants such as boron,<sup>[394]</sup> phosphorous,<sup>[395]</sup> and nitrogen,<sup>[396]</sup> has been investigated to improve the specific capacity of carbon materials. Recently, Leela et al.<sup>[390]</sup> reported that the N-doped graphene made by CVD method showed almost the double reversible discharge capacitance compared with that of pristine graphene. The large number of surface defects by N-doping and the introduction of pyridinic N atom<sup>[397]</sup> are supposed to be the main reason for this enhancement.

## 5. Concluding Remarks

The world energy consumption, along with CO<sub>2</sub> emission, has been increasing exponentially over the past 50 years or so.

As we become more aware of “greenhouse gases” and their detrimental effects on our planet, it has become more important than ever to develop clean and renewable energy systems (e.g., solar cells, fuel cells) and advanced energy storage devices (e.g., supercapacitors, batteries). Nanotechnology has opened up new frontiers in materials science and engineering to meet this challenge by offering unique enabling technology to create new materials/systems for energy generation and storage. Since the discovery of fullerene C<sub>60</sub> in 1985, various novel carbon nanomaterials and technologies have been developed that are deemed transformative to the future of energy. While carbon nanomaterials have been demonstrated to be useful for many general applications, they are particularly attractive for advanced energy conversion and storage.

Just like C<sub>60</sub> has been widely used as an electron acceptor in polymer solar cells, controlled growth and functionalization of CNTs have opened up new frontiers for energy-relevant research. Carbon nanotubes, stood vertically from an electrode, can be packed together very tightly, like stalks of corn in a cornfield. The exposed “tops” of these cylindrical nanotubes provide as much available surface area as traditional and nonaligned nanotubes (more overlapping and spaghetti-like). Separation between these tubes allows for even more surface space, including the unobstructed cylinders “sides”. In a solar cell, this novel arrangement can increase surface area as much as a thousand fold. Greater solar absorption and charge collection can arise from this increase in surface area and unique alignment, leading to significant improvements in efficiency and power. Advanced polymer and dye-sensitized solar cells can be created by coating individual nanotubes within a vertically aligned array with a photosensitive dye and titanium dioxide layer. Although CNTs and graphene with a higher electron mobility and lower percolation threshold have been studied as an alternative to fullerenes or charge-transport materials for polymer solar cells, the use of CNTs/graphene in organic solar cells is still in their initial research stage. Continued research efforts in this embryonic field could give birth to a flourishing area of photovoltaic technologies.

In addition to solar cells, nanotechnology has also made big impact on other energy conversion systems as exemplified by the recent work on nanotube/graphene-based fuel cells. Instead of burning fuel to create heat, fuel cells convert chemical energy directly into electricity, making them one of the most efficient and environmentally benign technologies to meet the demand for alternative energy sources. Fuel cells require a catalyst for the oxygen reduction reaction, the process that breaks the bonds of the oxygen molecules. Due to its efficiency in catalyzing this process, platinum is considered the state-of-the-art fuel cell catalyst. However, its properties degrade over time and it is expensive: a barrier to larger-scale production of fuel cells for commercial applications. Lowering precious-metal loading, enhancing catalyst activity, and prolonging catalyst durability remain the major challenges for fuel cells. Nitrogen-doped CNTs and graphene have been demonstrated to be promising materials to overcome these challenges. Comparing to traditional carbon black support materials, CNTs and graphene have a higher surface area, higher mesoporosity, higher electrical conductivity, stronger mechanical strength and higher

corrosion-resistance. These superb properties enable CNTs and graphene to be the catalyst support with an excellent activity and durability. Comparing to random CNTs, VA-CNTs ensured a better dispersion of catalysts with increased triple-phase boundaries and enhanced charge transport capability, further enhancing the catalytic activity of the catalysts. Comparing to pristine CNTs and graphene, nitrogen-doped CNTs and nitrogen-doped graphene improved the dispersion and strengthened the binding of catalysts on the CNT surface, further enhancing the catalytic activity and durability for the catalysts. Along with the intensive research efforts to find a replacement for platinum electrochemical catalysts, it has been further demonstrated that carbon nanomaterials (e.g., CNT, graphene, porous carbon), with and without N-doping, can act as effective metal-free ORR catalysts through the intramolecular and intermolecular charge-transfer, respectively. In addition, these new catalysts have been shown to be more electrochemically robust and mechanically stable than the platinum-based electrodes. This catalytic technology is having a large impact on the fuel-cell field and energy community, suggesting considerable room for cost-effective preparation of efficient metal-free catalysts for oxygen reduction in fuel cells, and even new catalytic materials for applications beyond fuel cells.

Improved energy density and power density have been in high demands for supercapacitors for a long time. High electrical conductivity, high charge transport capability, high mesoporosity, and high electrolyte accessibility are intrinsic properties of CNTs that make them attractive for supercapacitors. Having appropriately balanced surface area and mesoporosity, CNTs showed improved capacitance and rate capability over the conventional activated carbon electrodes. With the well-defined tube alignment, intertube spacing, and end-cap opening, VA-CNTs provide a more electrolyte-accessible surface, and thus improved capacitive behavior with respect to their random counterparts. Higher power densities have been demonstrated for CNT-based supercapacitors over the current supercapacitor technology. In order to further improve the energy density for CNT supercapacitors, CNTs have been combined with high-surface-area activated carbons, graphene nanosheets, conjugated polymers, or transition metal oxides to develop high-capacitance composite electrodes or with ionic liquid electrolytes to develop high-voltage capacitors.

On the other hand, carbon nanomaterials have also been explored for battery applications to decrease harmful emissions and reduce reliance on petroleum sources. Li-ion batteries represent the current state-of-the-art of rechargeable battery technologies. Nevertheless, the performances of the current Li-ion batteries still need to be improved. CNTs, graphene, and their derivatives have been studied as new electrode materials or electrode additives to address these issues. While CNTs are developed as new host anode materials, they are also employed as conductive additives combining with conventional graphite anode to improve rate performance, safety, and cyclability for Li-ion batteries. CNTs are also excellent conductive additives for cathode materials. Furthermore, combining CNTs with high-capacity metal oxides, the resultant cathode composites possess both a high capacity

and a high rate capability. Expanding this concept, there is a research trend in combining the high-capacity capability of batteries with the high-rate capability of supercapacitors to develop advanced high-energy and high-power energy-storage devices. With their unique properties, VA-CNTs have been demonstrated to be the ideal base materials to realize this novel hybrid energy storage technology.

As can be seen from the above discussions, the use of carbon nanomaterials for energy conversion and storage is an exciting research topic. Vast opportunities remain for developing novel carbon electrode nanomaterials for highly efficient energy-conversion and storage systems. Recent developments in the syntheses of carbon nanomaterials with controlled structures (e.g., VA-CNTs, 3D pillared CNT-graphene architectures) would speed up the applications of carbon nanomaterials for advanced energy conversion and storage. Further development in this exciting field will surely revolutionize the way in which future energy systems are developed.

## Acknowledgements

The authors thank our colleagues for their contributions to the work cited. Due to the huge amount of literature has been generated in this field, and the number of publications is still rapidly increasing every year, the examples presented in this paper may not exhaust all significant work reported in the literature in order to review a topic of such breadth in an article of a reasonable length. Therefore, we apologize to the authors of papers not cited here. We are also grateful for financial support from the NSF (CMMI-1000768, CMS-0609077, CMMI-1047655, IIP-0924197, DMR-1106160), AFOSR (FA9550-09-1-0331, FA9550-10-1-0546, FA8650-07-D-5800, FA2386-10-1-4071, TSI-2356-10-81529, AOARD-104055), DOD-AFOSR-MURI (FA9550-12-1-0037), AFRL/UTC (11-S587-1000-01-C1), AFRL/DAGSI (RX2-CWRU-10-1), DOD-Army (W911NF-11-1-0209), WCU Project through UNIST from the Ministry of Education, Science and Technology in Korea, and US-Korea NBIT and Basic Research Laboratory (BRL) programs through the National Research Foundation (NRF) of Korea and US Air Force Office of Scientific Research (AFOSR).

- [1] T. G. Doung, "2002 Annual Progress Report for Energy Storage Research and Development", Freedom Car & Vehicle Technologies Program, **2003**.
- [2] P. V. Kamat, G. C. Schatz, *J. Phys. Chem. C* **2009**, *113*, 15437.
- [3] U. Sahaym, N. M. Grant, *J. Mater. Sci.* **2008**, *43*, 5395.
- [4] P. V. Kamat, *J. Phys. Chem. Lett.* **2011**, *2*, 242.
- [5] P. J. F. Harris, *Carbon Nanotubes and Related Structures - New Materials for the Twenty-First Century*, Cambridge University Press, Cambridge **2001**.
- [6] *Carbon Nanotechnology: Recent Developments in Chemistry, Physics, Materials Science and Device Applications* (Ed: L. Dai), Elsevier Science, London **2006**.
- [7] X. Huang, Z. Yin, S. Wu, X. Qi, Q. He, Q. Zhang, Q. Yan, F. Boey, H. Zhang, *Small* **2011**, *7*, 1876.

- [8] A. Arico, *Nat. Mater.* **2005**, *4*, 366.
- [9] Y. G. Guo, J. S. Hu, L. J. Wan, *Adv. Mater.* **2008**, *20*, 2878.
- [10] D. R. Rolison, J. W. Long, J. C. Lytle, A. E. Fischer, C. P. Rhodes, T. M. McEvoy, M. E. Bourg, A. M. Lubers, *Chem. Soc. Rev.* **2009**, *38*, 226.
- [11] J. Liu, G. Cao, Z. Yang, D. Wang, D. Dubois, X. Zhou, G. L. Graff, L. R. Pederson, J. G. Zhang, *ChemSusChem* **2008**, *1*, 676.
- [12] H. Marsh, *Introduction to Carbon Science*, Butterworths, London **1989**.
- [13] H. W. Kroto, J. R. Heath, S. C. O'Brien, R. F. Curl, R. E. Smalley, *Nature* **1985**, *318*, 162.
- [14] A. Hirsch, *The Chemistry of the Fullerenes*, Thieme, Stuttgart **1994**.
- [15] R. Taylor, *The Chemistry of Fullerenes*, World Scientific, Singapore **1995**.
- [16] S. Iijima, *Nature* **1991**, *354*, 56.
- [17] M. S. Dresselhaus, G. Dresselhaus, P. Eklund, *Science of Fullerenes and Carbon Nanotubes*, Academic, San Diego **1996**.
- [18] K. Novoselov, A. Geim, S. Morozov, D. Jiang, Y. Zhang, S. Dubonos, I. Grigorieva, A. Firsov, *Science* **2004**, *306*, 666.
- [19] M. Z. Jacobson, *Energy Environ. Sci.* **2009**, *2*, 148.
- [20] R. M. Dell, D. A. J. Rand, *J. Power Sources* **2001**, *100*, 2.
- [21] G. S. Hammond, V. J. Kuck, *Fullerenes: Synthesis, Properties and Chemistry of Large Carbon Clusters*, American Chemical Society, Washington DC **1992**.
- [22] H. Kroto, A. Allaf, S. Balm, *Chem. Rev.* **1991**, *91*, 1213.
- [23] *Acc. Chem. Res.* **1992**, *25* (A Special Issue on C<sub>60</sub>).
- [24] W. Kratschmer, L. D. Lamb, K. Fostiropoulos, D. R. Huffman, *Nature* **1990**, *347*, 354.
- [25] A. Hebard, *Ann. Rev. Mater. Sci.* **1993**, *23*, 159.
- [26] C. N. R. Rao, R. Seshadri, A. Govindaraj, R. Sen, *Mater. Sci. Eng. Rep.* **1995**, *15*, 209.
- [27] R. Bakry, R. M. Vallant, M. Najam-Ul-Haq, M. Rainer, Z. Szabo, C. W. Huck, G. K. Bonn, *Int. J. Nanomedicine* **2007**, *2*, 639.
- [28] N. S. Sariciftci, L. Smilowitz, A. J. Heeger, F. Wudl, *Science* **1992**, *258*, 1474.
- [29] N. Sariciftci, D. Braun, C. Zhang, V. Srdanov, A. Heeger, G. Stucky, F. Wudl, *Appl. Phys. Lett.* **1993**, *62*, 585.
- [30] G. Yu, J. Gao, J. Hummelen, F. Wudl, A. Heeger, *Science* **1995**, *270*, 1789.
- [31] M. Dresselhaus, *Physics World* **1996**, *9*, 18.
- [32] A. Peigney, C. Laurent, E. Flahaut, R. R. Bacsa, A. Rousset, *Carbon* **2001**, *39*, 507.
- [33] H. Chen, A. Roy, J.-B. Baek, L. Zhu, J. Qu, L. Dai, *Mater. Sci. Eng. Rep.* **2010**, *70*, 63.
- [34] T. W. Ebbesen, P. M. Ajayan, *Nature* **1992**, *358*, 220.
- [35] C. Journet, W. K. Maser, P. Bernier, A. Loiseau, M. Lamy de la Chapelle, S. Lefrant, P. Deniard, R. Lee, J. E. Fischer, *Nature* **1997**, *388*, 756.
- [36] A. Thess, R. Lee, P. Nikolaev, H. Dai, P. Petit, J. Robert, C. Xu, Y. H. Lee, S. G. Kim, A. G. Rinzler, D. T. Colbert, G. E. Scuseria, D. Tománek, J. E. Fischer, R. E. Smalley, *Science* **1996**, *273*, 483.
- [37] B. Zheng, C. Lu, G. Gu, A. Makarovski, G. Finkelstein, J. Liu, *Nano Lett.* **2002**, *2*, 895.
- [38] L. Dai, A. Patil, X. Gong, Z. Guo, L. Liu, Y. Liu, D. Zhu, *ChemPhysChem* **2003**, *4*, 1150.
- [39] Y. Yan, M. B. Chan Park, Q. Zhang, *Small* **2007**, *3*, 24.
- [40] L. Qu, L. Dai, *J. Mater. Chem.* **2007**, *17*, 3401.
- [41] B. Wei, R. Vajtai, Y. Jung, J. Ward, R. Zhang, G. Ramanath, P. Ajayan, *Nature* **2002**, *416*, 495.
- [42] W. Li, S. Xie, L. X. Qian, B. Chang, B. Zou, W. Zhou, R. Zhao, G. Wang, *Science* **1996**, *274*, 1701.
- [43] L. Qu, Q. Peng, L. Dai, G. Spinks, G. Wallace, R. H. Baumann, *Mater. Res. Soc. Bull.* **2008**, *33*, 215.
- [44] S. Fan, M. G. Chapline, N. R. Franklin, T. W. Tombler, A. M. Cassell, H. Dai, *Science* **1999**, *283*, 512.

- [45] C. Rao, R. Sen, *Chem. Commun.* **1998**, 1525.
- [46] Z. Ren, Z. Huang, J. Xu, J. Wang, P. Bush, M. Siegal, P. Provencio, *Science* **1998**, 282, 1105.
- [47] S. Huang, L. Dai, A. W. H. Mau, *J. Phys. Chem. B* **1999**, 103, 4223.
- [48] Y. Yang, S. Huang, H. He, A. W. H. Mau, L. Dai, *J. Am. Chem. Soc.* **1999**, 121, 10832.
- [49] A. Patil, T. Ohashi, A. Buldum, L. Dai, *Appl. Phys. Lett.* **2006**, 89, 103103.
- [50] K. Hata, D. N. Futaba, K. Mizuno, T. Namai, M. Yumura, S. Iijima, *Science* **2004**, 306, 1362.
- [51] G. Zhang, D. Mann, L. Zhang, A. Javey, Y. Li, E. Yenilmez, Q. Wang, J. P. McVittie, Y. Nishi, J. Gibbons, *Proc. Natl. Acad. Sci. USA* **2005**, 102, 16141.
- [52] Y. Q. Xu, E. Flor, M. J. Kim, B. Hamadani, H. Schmidt, R. E. Smalley, R. H. Hauge, *J. Am. Chem. Soc.* **2006**, 128, 6560.
- [53] S. Chakrabarti, T. Nagasaka, Y. Yoshikawa, L. Pan, *Jpn. J. Appl. Phys.* **2006**, 45, L720.
- [54] G. F. Zhong, T. Iwasaki, K. Honda, Y. Furukawa, I. Ohdomari, H. Kawarada, *Jpn. J. Appl. Phys.* **2006**, 44, 1558.
- [55] J. Yang, L. Qu, Y. Zhao, Q. H. Zhang, L. Dai, J. W. Bauer, B. Maruyama, R. A. Via, E. Shin, P. T. Murray, H. X. Luo, Z. X. Guo, *J. Nanosci. Nanotechnol.* **2007**, 7, 1573.
- [56] L. Li, J. Yang, R. Vaia, L. Dai, *Synth. Met.* **2005**, 154, 225.
- [57] J. Yang, L. Dai, R. A. Vaia, *J. Phys. Chem. B* **2003**, 107, 12387.
- [58] L. Qu, R. A. Vaia, L. Dai, *ACS Nano* **2011**, 5, 994.
- [59] C. Niu, E. K. Sichel, R. Hoch, D. Moy, H. Tennent, *Appl. Phys. Lett.* **1997**, 70, 1480.
- [60] R. H. Baughman, A. A. Zakhidov, W. A. De Heer, *Science* **2002**, 297, 787.
- [61] P. G. Collins, P. Avouris, *Sci. Am.* **2000**, 283, 62.
- [62] L. Dai, P. Soundarajan, T. Kim, *Pure Appl. Chem.* **2002**, 74, 1753.
- [63] A. C. Dillon, K. M. Jones, T. A. Bekkedahl, C. H. Kiang, D. S. Bethune, M. J. Heben, *Nature* **1997**, 386, 377.
- [64] K. Loh, J. Kim, J. Lynch, in *Bridge Maintenance, Safety, Management, Health Monitoring and Informatics* (Eds: K. Loh, D. M. Fangopol), Taylor & Francis, London **2005**.
- [65] A. Kumar, S. Choudhury, S. Saha, S. Pahari, D. De, S. Bhattacharya, K. P. Ghatak, *Physica B: Condensed Matter* **2010**, 405, 472.
- [66] M. H.-C. Jin, L. Dai, in *Organic Photovoltaics*, (Eds: S. Sun, N.S. Cariciftci), CRC Press, Boca Raton **2005**.
- [67] Z. Liu, X. Lin, J. Y. Lee, W. Zhang, M. Han, L. M. Gan, *Langmuir* **2002**, 18, 4054.
- [68] D. Yu, E. Nagelli, F. Du, L. Dai, *J. Phys. Chem. Lett.* **2010**, 1, 2165.
- [69] D. T. Welna, L. Qu, B. E. Taylor, L. Dai, M. F. Durstock, *J. Power Sources* **2010**, 196, 1455.
- [70] W. Lu, L. Qu, K. Henry, L. Dai, *J. Power Sources* **2009**, 189, 1270.
- [71] K. Lee, L. Li, L. Dai, *J. Am. Chem. Soc.* **2005**, 127, 4122.
- [72] N. Chopra, M. Majumder, B. J. Hinds, *Adv. Funct. Mater.* **2005**, 15, 858.
- [73] Q. Chen, L. Dai, M. Gao, S. Huang, A. W. H. Mau, *J. Phys. Chem. B* **2001**, 105, 618.
- [74] T. Enoki, K. Takai, V. Osipov, M. Baidakova, A. Vul, *Chem. Asian J.* **2009**, 4, 796.
- [75] J. Liang, Y. Xu, Y. Huang, L. Zhang, Y. Wang, Y. Ma, F. Li, T. Guo, Y. Chen, *J. Phys. Chem. C* **2009**, 113, 9921.
- [76] X. Wang, L. Zhi, K. Mullen, *Nano Lett.* **2008**, 8, 323.
- [77] E. J. Yoo, J. Kim, E. Hosono, H. Zhou, T. Kudo, I. Honma, *Nano Lett.* **2008**, 8, 2277.
- [78] S. R. C. Vivekchand, C. S. Rout, K. S. Subrahmanyam, A. Ovindaraj, C. N. R. Rao, *J. Chem. Sci.* **2008**, 120, 9.
- [79] X. Wang, L. Zhi, N. Tsao, Tomovi, J. Li, K. Mullen, *Angew. Chem. Int. Ed.* **2008**, 47, 2990.
- [80] G. Eda, G. Fanchini, M. Chhowalla, *Nat. Nanotechnol.* **2008**, 3, 270.
- [81] W. Yang, K. R. Ratinac, S. P. Ringer, P. Thordarson, J. J. Gooding, F. Brat, *Angew. Chem. Int. Ed.* **2010**, 49, 2114.
- [82] O. C. Compton, S. T. Nguyen, *Small* **2010**, 6, 711.
- [83] P. Sutter, *Nat. Mater.* **2009**, 8, 171.
- [84] J. Kedzierski, P. L. Hsu, P. Healey, P. W. Wyatt, C. L. Keast, M. Sprinkle, C. Berger, W. A. de Heer, *IEEE Transactions on Electron Devices* **2008**, 55, 2078.
- [85] L. W. C. Ren, L. B. Gao, L. P. Ma, H. M. Cheng, *New Carbon Mater.* **2011**, 26, 71.
- [86] I. Pletikosic, M. Kralj, P. Pervan, R. Brako, J. Coraux, A. N'Diaye, C. Busse, T. Michely, *Phys. Rev. Lett.* **2009**, 102, 056808.
- [87] K. S. Kim, Y. Zhao, H. Jang, S. Y. Lee, J. M. Kim, J. H. Ahn, P. Kim, J. Y. Choi, B. H. Hong, *Nature* **2009**, 457, 706.
- [88] S. Bae, H. Kim, Y. Lee, X. Xu, J. S. Park, Y. Zheng, J. Balakrishnan, T. Lei, H. R. Kim, Y. I. Song, *Nat. Nanotechnol.* **2010**, 5, 574.
- [89] L. Qu, Y. Liu, J. B. Baek, L. Dai, *ACS Nano* **2010**, 4, 1321.
- [90] X. Li, W. Cai, J. An, S. Kim, J. Nah, D. Yang, R. Piner, A. Velamakanni, I. Jung, E. Tutuc, *Science* **2009**, 324, 1312.
- [91] D. R. Lenski, M. S. Fuhrer, *J. Appl. Phys.* **2010**, 110, 013720.
- [92] Z. Sun, Z. Yan, J. Yao, E. Beitler, Y. Zhu, J. M. Tour, *Nature* **2011**, 471, 124.
- [93] M. Choucair, P. Thordarson, J. A. Stride, *Nat. Nanotechnol.* **2008**, 4, 30.
- [94] W. S. Hummers, R. E. Offeman, *J. Am. Chem. Soc.* **1958**, 80, 1339.
- [95] J. Shen, Y. Hu, M. Shi, X. Lu, C. Qin, C. Li, M. Ye, *Chem. Mater.* **2009**, 21, 3514.
- [96] G. Brumfiel, *Nature* **2009**, 10, 1038.
- [97] D. V. Kosynkin, A. L. Higginbotham, A. Sinitskii, J. R. Lomeda, A. Dimiev, B. K. Price, J. M. Tour, *Nature* **2009**, 458, 872.
- [98] L. Jiao, L. Zhang, X. Wang, G. Diankov, H. Dai, *Nature* **2009**, 458, 877.
- [99] Y. Xu, H. Bai, G. Lu, C. Li, G. Shi, *J. Am. Chem. Soc.* **2008**, 130, 5856.
- [100] H. A. Becerril, J. Mao, Z. Liu, R. M. Stoltzenberg, Z. Bao, Y. Chen, *ACS Nano* **2008**, 2, 463.
- [101] Z. S. Wu, S. Pei, W. Ren, D. Tang, L. Gao, B. Liu, F. Li, C. Liu, H. M. Chen, *Adv. Mater.* **2009**, 21, 1756.
- [102] X. L. Li, G. Y. Zhang, X. D. Bai, X. M. Sun, X. R. Wang, E. Wang, H. Dai, *Nat. Nanotechnol.* **2008**, 3, 538.
- [103] D. S. Su, J. Zhang, B. Frank, A. Thomas, X. Wang, J. Paraknowitsch, R. Schlogl, *ChemSusChem* **2010**, 3, 169.
- [104] C. Ewels, M. Glerup, *J. Nanosci. Nanotechnol.* **2005**, 5, 1345.
- [105] Y. Shao, J. Sui, G. Yin, Y. Gao, *Appl. Catal. B: Environ.* **2008**, 79, 89.
- [106] E. G. Wang, *Adv. Mater.* **1999**, 11, 1129.
- [107] L. Jiang, L. Gao, *Carbon* **2003**, 41, 2923.
- [108] S. Roy, A. Harding, A. Russell, K. Thomas, *J. Electrochem. Soc.* **1997**, 144, 2323.
- [109] R. A. Sidik, A. B. Anderson, N. P. Subramanian, S. P. Kumaraguru, B. N. Popov, *J. Phys. Chem. B* **2006**, 110, 1787.
- [110] M. M. Titirici, A. Thomas, M. Antonietti, *J. Mater. Chem.* **2007**, 17, 3412.
- [111] M. Glerup, J. Steinmetz, D. Samaille, O. Stephan, S. Enouz, A. Loiseau, S. Roth, P. Bernier, *Chem. Phys. Lett.* **2004**, 387, 193.
- [112] J. C. Hummelen, B. Knight, J. Pavlovich, R. Gonzalez, F. Wudl, *Science* **1995**, 269, 1554.
- [113] L. Qu, F. Du, L. Dai, *Nano Lett.* **2008**, 8, 2682.
- [114] M. Terrones, H. Terrones, N. Grobert, W. K. Hsu, Y. Q. Zhu, J. P. Hare, H. W. Kroto, D. R. M. Walton, P. Kohler-Redlich, M. Ruuhle, *Appl. Phys. Lett.* **1999**, 75, 3932.
- [115] M. Trasobares, O. Stephan, C. Colliex, W. K. Hsu, H. W. Kroto, D. R. M. Walton, *J. Chem. Phys.* **2002**, 116, 8966.

- [116] A. Kudashov, A. Okotrub, L. Bulusheva, I. Asanov, Y. V. Shubin, N. Yudanov, L. Yudanova, V. Danilovich, O. Abrosimov, *J. Phys. Chem. B* **2004**, *108*, 9048.
- [117] P. X. Hou, H. Orikasa, T. Yamazaki, K. Matsuoka, A. Tomita, N. Setoyama, Y. Fukushima, T. Kyotani, *Chem. Mater.* **2005**, *17*, 5187.
- [118] T. Maiyalagan, B. Viswanathan, U. V. Varadaraju, *Electrochem. Commun.* **2005**, *7*, 905.
- [119] J. Jang, J. H. Oh, *Chem. Commun.* **2004**, 882.
- [120] C. Wang, M. Waje, X. Wang, J. M. Tang, R. C. Haddon, Y. Yan, *Nano Lett.* **2004**, *4*, 345.
- [121] K. Gong, F. Du, Z. Xia, M. Durstock, L. Dai, *Science* **2009**, *323*, 760.
- [122] A. Reina, X. Jia, J. Ho, D. Nezich, H. Son, V. Bulovic, M. S. Dresselhaus, J. Kong, *Nano Lett.* **2008**, *9*, 30.
- [123] D. Wei, Y. Liu, Y. Wang, H. Zhang, L. Huang, G. Yu, *Nano Lett.* **2009**, *9*, 1752.
- [124] E. K. Choi, I. Y. Jeon, S. Y. Bae, H. J. Lee, H. S. Shin, L. Dai, J.-B. Baek, *Chem. Commun.* **2010**, *46*, 6320.
- [125] I. Y. Jeon, S. Y. Bae, D. Yu, D. W. Chang, L. Dai, J.-B. Baek, *Chem. Mater.* **2011**, *23*, 3987.
- [126] H. He, J. Klinowski, M. Forster, A. Lerf, *Chem. Phys. Lett.* **1998**, *287*, 53.
- [127] A. Lerf, H. He, M. Forster, J. Klinowski, *J. Phys. Chem. B* **1998**, *102*, 4477.
- [128] A. Becquerel, *Comptes Rendus* **1839**, *9*, 561.
- [129] M. Grätzel, *Nature* **2001**, *414*, 338.
- [130] Q. L. Song, C. M. Li, M. B. Chan-Park, M. Lu, H. Yang, X. Y. Hou, *Phys. Rev. Lett.* **2007**, *98*, 176403.
- [131] M. Pagliaro, R. Ciriminna, G. Palmisano, *ChemSusChem* **2008**, *1*, 880.
- [132] D. M. Chapin, C. S. Fuller, G. L. Pearson, *J. Appl. Phys.* **1954**, *25*, 676.
- [133] M. A. Green, K. Emery, D. L. King, S. Igari, W. Warta, *Prog. Photovol: Res. Appl.* **2004**, *12*, 365.
- [134] R. M. Swanson, *Prog. Photovol: Res. Appl.* **2006**, *14*, 443.
- [135] S. E. Shaheen, D. S. Ginley, G. E. Jabbour, *MRS Bull* **2005**, *30*, 10.
- [136] J. Johnson, *Chem. Engin. News* **2004**, *82*, 13.
- [137] R. O. Loutfy, J. H. Sharp, *J. Chem. Phys.* **1979**, *71*, 1211.
- [138] B. J. Stanberry, M. Gouterman, R. M. Burges, *J. Phys. Chem.* **1985**, *89*, 4950.
- [139] K. Yamashita, Y. Hariyama, H. Iwashima, *J. Phys. Chem.* **1987**, *91*, 3055.
- [140] M. Hiramoto, H. Fujiwara, M. Yokoyama, *Appl. Phys. Lett.* **1991**, *58*, 1061.
- [141] C. Brabec, V. Dyakonov, J. Parisi, N. Sariciftci, *Organic Photovoltaics: Concepts and Realization*, Vol. 60 Springer, New York, USA **2003**
- [142] L. Dai, *Intelligent Macromolecules for Smart Devices: From Materials Synthesis to Device Applications*, Springer-Verlag, Berlin **2004**.
- [143] R. H. Bube, *Photoelectronic Properties of Semiconductors*, Cambridge University Press, Cambridge, UK **1992**.
- [144] C. Tang, *Appl. Phys. Lett.* **1986**, *48*, 183.
- [145] B. Kraable, J. C. Hummelen, D. Vacar, D. Moses, N. S. Sariciftci, A. J. Heeger, F. Wudl, *J. Chem. Phys.* **1996**, *104*, 4267.
- [146] N. S. Sariciftci, A. J. Heeger, *Int. J. Mod. Phys. B* **1994**, *8*, 237.
- [147] A. Zakhidov, K. Taka, K. Yoshino, *Synth. Met.* **1995**, *71*, 2113.
- [148] A. Zakhidov, K. Yoshino, *Synth. Met.* **1995**, *71*, 1875.
- [149] C. Lee, G. Yu, D. Moses, K. Pakbaz, C. Zhang, N. Sariciftci, A. Heeger, F. Wudl, *Phys. Rev. B: Condens. Matter Mater. Phys.* **1993**, *48*, 15425.
- [150] G. Yu, V. Pakbaz, A. J. Heeger, *Appl. Phys. Lett.* **1994**, *64*, 3422.
- [151] S. Morita, A. A. Zakhidov, K. Yoshino, *Jpn. J. Appl. Phys.* **1993**, *32*, L873.
- [152] A. Kohler, H. Wittmann, R. Friend, M. Khan, J. Lewis, *Synth. Met.* **1996**, *77*, 147.
- [153] P. V. Kamat, K. D. Asmus, *Electrochem. Soc. Interface* **1996**, *5*, 22.
- [154] G. Yu, A. J. Heeger, *J. Appl. Phys.* **1995**, *78*, 4510.
- [155] J. J. M. Halls, C. A. Walsh, N. C. Greenham, E. A. Marseglia, R. H. Friend, S. C. Moratti, A. B. Holmes, *Nature* **1995**, *376*, 498.
- [156] Y. Y. Liang, L. P. Yu, *Polym. Rev.* **2010**, *50*, 454.
- [157] J. Y. Kim, S. H. Kim, H. H. Lee, K. Lee, W. Ma, X. Gong, A. J. Heeger, *Adv. Mater.* **2006**, *18*, 572.
- [158] G. Li, V. Shrotriya, Y. Yao, Y. Yang, *J. Appl. Phys.* **2005**, *98*, 043704.
- [159] M. Reyes-Reyes, K. Kim, J. Dewald, R. L. Sandoval, A. Avadhanula, S. Curran, D. L. Carroll, *Org. Lett.* **2005**, *7*, 5749.
- [160] Y. He, Y. Li, *Phys. Chem. Chem. Phys.* **2011**, *13*, 1970.
- [161] T. Durkop, S. Getty, E. Cobas, M. Fuhrer, *Nano Lett.* **2004**, *4*, 35.
- [162] G. H. Bauer, P. Wurfel, *Quantum Solar Energy Conversion in Organic Solar Cells*, in *Organic Photovoltaics: Concepts and Realization*, (Eds: C. Brabec, V. Dyakonov, J. Parisi, N.S. Sariciftci), Springer, New York **2003**.
- [163] V. D. Mihailescu, J. K. J. Van Duren, P. W. M. Blom, J. C. Hummelen, R. A. J. Janssen, J. M. Kroon, M. T. Rispen, W. J. H. Verhees, M. M. Wienk, *Adv. Funct. Mater.* **2003**, *13*, 43.
- [164] N. S. Sariciftci, *Materials Today* **2004**, *7*, 36.
- [165] D. B. Romero, M. Carrard, W. De Heer, L. Zuppiroli, *Adv. Mater.* **1996**, *8*, 899.
- [166] S. A. Curran, P. M. Ajayan, W. J. Blau, D. L. Carroll, J. N. Coleman, A. B. Dalton, A. P. Davey, A. Drury, B. McCarthy, S. Maier, A. Strevens, *Adv. Mater.* **1998**, *10*, 1091.
- [167] J. N. Coleman, S. Curran, A. Dalton, A. Davey, B. McCarthy, W. Blau, R. Barklie, *Phys. Rev. B* **1998**, *58*, 7492.
- [168] W. Wu, J. Li, L. Liu, L. Yanga, Z. X. Guo, L. Dai, D. Zhu, *Chem. Phys. Lett.* **2002**, *364*, 196.
- [169] E. Kymakis, G. A. J. Amaral, *Appl. Phys. Lett.* **2002**, *80*, 112.
- [170] Q. Sun, K. Park, L. Dai, *J. Phys. Chem. C* **2009**, *113*, 7892.
- [171] Q. Sun, L. Dai, X. Zhou, L. Li, Q. Li, *Appl. Phys. Lett.* **2007**, *91*, 253505.
- [172] D. H. Wang, H. K. Lee, D. G. Choi, J. H. Park, O. O. Park, *Appl. Phys. Lett.* **2009**, *95*, 043505.
- [173] Y. Li, R. Mastria, A. Fiore, C. Nobile, L. Yin, M. Biasiucci, G. Cheng, A. M. Cuocolo, R. Cingolani, L. Manna, *Adv. Mater.* **2009**, *21*, 4461.
- [174] B. K. Kuila, K. Park, L. Dai, *Macromolecules* **2010**, *43*, 6699.
- [175] M. Reyes-Reyes, R. Lopez-Sandoval, J. Liu, D. Carroll, *Sol. Energy Mater. Sol. Cells* **2007**, *91*, 1478.
- [176] B. Pradhan, S. K. Batabyal, A. J. Pal, *Appl. Phys. Lett.* **2006**, *88*, 093106.
- [177] J. Arranz-Andres, W. J. Blau, *Carbon* **2008**, *46*, 2067.
- [178] P. R. Somani, S. P. Somani, E. Flahaut, M. Umeno, *Nanotechnology* **2007**, *18*, 185708.
- [179] C. Li, Y. Chen, Y. Wang, Z. Iqbal, M. Chhowalla, S. Mitra, *J. Mater. Chem.* **2007**, *17*, 2406.
- [180] B. Kannan, K. Castelino, A. Majumdar, *Nano Lett.* **2003**, *3*, 1729.
- [181] Q. Liu, Z. Liu, X. Zhang, L. Yang, N. Zhang, G. Pan, S. Yin, Y. Chen, J. Wei, *Adv. Funct. Mater.* **2009**, *19*, 894.
- [182] Z. Liu, Q. Liu, Y. Huang, Y. Ma, S. Yin, X. Zhang, W. Sun, Y. Chen, *Adv. Mater.* **2008**, *20*, 3924.
- [183] Y. H. Hu, H. Wang, B. Hu, *ChemSusChem* **2010**, *3*, 782.
- [184] D. Yu, Y. Yang, M. Durstock, J. B. Baek, L. Dai, *ACS Nano* **2010**, *4*, 5633.
- [185] N. Yang, J. Zhai, D. Wang, Y. Chen, L. Jiang, *ACS Nano* **2010**, *4*, 887.
- [186] D. Yu, K. Park, M. Durstock, L. Dai, *J. Phys. Chem. Lett.* **2011**, *2*, 1113.
- [187] O. M. Bakr, V. Amendola, C. M. Aikens, W. Wenseleers, R. Li, L. Dal Negro, G. C. Schatz, F. Stellacci, *Angew. Chem. Int. Ed.* **2009**, *121*, 6035.
- [188] P. V. Kamat, *J. Phys. Chem. C* **2008**, *112*, 18737.

- [189] S. S. Sun, N. S. Sariciftci, *Organic Photovoltaics: Mechanism, Materials, and Devices*, CRC, Boca Raton 2005.
- [190] B. Farrow, P. V. Kamat, *J. Am. Chem. Soc.* **2009**, *131*, 11124.
- [191] L. Hu, Y. L. Zhao, K. Ryu, C. Zhou, J. F. Stoddart, G. Gruner, *Adv. Mater.* **2008**, *20*, 939.
- [192] I. Robel, B. A. Bunker, P. V. Kamat, *Adv. Mater.* **2005**, *17*, 2458.
- [193] L. Sheeney-Haj-Ichia, B. Basnar, I. Willner, *Angew. Chem. Int. Ed.* **2005**, *44*, 78.
- [194] F. Farrow, P. V. Kamat, *J. Am. Chem. Soc.* **2008**, *130*, 8890.
- [195] D. M. Guldi, G. M. A. Rahman, V. Sgobba, N. A. Kotov, D. Bonifazi, M. Prato, *J. Am. Chem. Soc.* **2006**, *128*, 2315.
- [196] H. J. Snaith, L. Schmidt-Mende, *Adv. Mater.* **2007**, *19*, 3187.
- [197] H. B. Yang, Q. L. Song, C. M. Li, Z. S. Lu, *Energy Environ. Sci.* **2008**, *1*, 389.
- [198] C. X. Guo, H. B. Yang, Z. M. Sheng, Z. S. Lu, Q. L. Song, C. M. Li, *Angew. Chem. Int. Ed.* **2010**, *49*, 3014.
- [199] D. Li, M. B. Muller, S. Gilje, R. B. Kaner, G. G. Wallace, *Nat. Nanotechnol.* **2008**, *3*, 101.
- [200] Z. Pan, S. Xie, B. Chang, C. Wang, L. Lu, W. Liu, W. Zhou, W. Li, L. Qian, *Nature* **1998**, *394*, 631.
- [201] Y. Li, Y. Hu, Y. Zhao, G. Shi, L. Deng, Y. Hou, L. Qu, *Adv. Mater.* **2011**, *6*, 776.
- [202] B. O'regan, M. Gratzel, *Nature* **1991**, *353*, 737.
- [203] DSSCs, <http://www.chemphys.lu.se/research/projects/wholedsscsle> (last accessed August 2011).
- [204] A. Yella, H.-W. Lee, H. N. Tsao, C. Yi, A. K. Chandiran, M. K. Nazeeruddin, E. W.-G. Diau, C.-Y. Yeh, S. M. Zakeeruddin, M. Gratzel, *Science* **2011**, *334*, 629.
- [205] Y. Kim, J. Kim, M. S. Kang, M. Lee, J. Won, J. C. Lee, Y. Kang, *Adv. Mater.* **2004**, *16*, 1753.
- [206] G. K. Mor, K. Shankar, M. Paulose, O. K. Varghese, C. A. Grimes, *Appl. Phys. Lett.* **2007**, *91*, 152111.
- [207] M. K. Nazeeruddin, F. De Angelis, S. Fantacci, A. Selloni, G. Viscardi, P. Liska, S. Ito, B. Takeru, M. Gratzel, *J. Am. Chem. Soc.* **2005**, *127*, 16835.
- [208] Y. Chiba, A. Islam, Y. Watanabe, R. Komiya, N. Koide, L. Han, *Jpn. J. Appl. Phys.* **2006**, *45*, 638.
- [209] F. T. Kong, S. Y. Dai, *Prog. Chem.* **2006**, *18*, 1409.
- [210] C. Y. Chen, Y. K. Lin, S. H. Liao, C. C. Weng, C. C. Huang, Y. H. Hsiao, C. C. M. Ma, M. C. Chang, H. Shao, M. C. Tsai, *Nanotechnology* **2008**, *19*, 1.
- [211] S. Sun, L. Gao, Y. Liu, *Appl. Phys. Lett.* **2010**, *96*, 083113.
- [212] Y. Yang, L. Qu, L. Dai, T. S. Kang, M. Durstock, *Adv. Mater.* **2007**, *19*, 1239.
- [213] T. S. Kang, A. P. Smith, B. E. Taylor, M. F. Durstock, *Nano. Lett.* **2009**, *9*, 601.
- [214] W. Hong, Y. Xu, G. Lu, C. Li, G. Shi, *Electrochim. Commun.* **2008**, *10*, 1555.
- [215] T. Lin, F. Huang, J. Liang, Y. Wang, *Energy Environ. Sci.* **2011**, *4*, 862.
- [216] L. Kavan, J. H. Yum, M. Grätzel, *ACS Nano* **2011**, *3*, 165.
- [217] V. Ramani, *Electrochim. Soc. Interface* **2006**, Spring, 41.
- [218] Fuel Cells, <http://www.fuelcells.org/basics/how.html> (last accessed August 2011).
- [219] US Department of Energy, <http://americanhistory.si.edu/fuel-cells/pem/pemain.html> (last accessed August 2011).
- [220] E. J. Carson, P. Kopf, J. Sinha, S. Sriramulu, Y. Yang, *Cost Analysis of PEM Fuel Cell System for Transportation*, TIAX LLC Cambridge, Massachusetts, Sep 30 2005.
- [221] US Department of Energy, <http://www1.eere.energy.gov/hydrogenandfuelcells/mypp/> (last accessed August 2011).
- [222] H. Liu, C. Song, L. Zhang, J. Zhang, H. Wang, D. P. Wilkinson, *J. Power Sources* **2006**, *155*, 95.
- [223] A. S. Aricò, S. Srinivasan, V. Antonucci, *Fuel Cells* **2001**, *1*, 133.
- [224] M. Uchida, Y. Fukuoka, Y. Sugawara, H. Ohora, A. Ohta, *J. Electrochim. Soc.* **1998**, *145*, 3708.
- [225] K.-W. Park, B.-K. Kwon, J.-H. Choi, I.-S. Park, Y.-M. Kim, Y.-E. Sung, *J. Power Sources* **2002**, *109*, 439.
- [226] Z. X. Liang, T. S. Zhao, *J. Phys. Chem. C* **2007**, *111*, 8128.
- [227] W. Li, C. Liang, W. Zhou, J. Qiu, Z. Zhou, G. Sun, Q. Xin, *J. Phys. Chem. B* **2003**, *107*, 6292.
- [228] J. Xie, D. L. Wood III, D. M. Wayne, T. A. Zawodzinski, P. Atanassov, R. L. Borup, *J. Electrochim. Soc.* **2005**, *152*, A104.
- [229] K. H. Kangasniemi, D. A. Condit, T. D. Jarvi, *J. Electrochim. Soc.* **2004**, *151*, E125.
- [230] K. Lee, J. Zhang, H. Wang, D. P. Wilkinson, *J. Appl. Electrochem.* **2006**, *36*, 507.
- [231] T. Matsumoto, T. Komatsu, K. Arai, T. Yamazaki, M. Kijima, H. Shimizu, Y. Takasawa, J. Nakamura, *Chem. Commun.* **2004**, *10*, 840.
- [232] W. Li, C. Liang, J. Qiu, W. Zhou, H. Han, Z. Wei, G. Sun, Q. Xin, *Carbon* **2002**, *40*, 791.
- [233] G. Girishkumar, K. Vinodgopal, P. V. Kamat, *J. Phys. Chem. B* **2004**, *108*, 19960.
- [234] X. Wang, W. Li, Z. Chen, M. Waje, Y. Yan, *J. Power Sources* **2006**, *158*, 154.
- [235] H.-J. Ahn, W. J. Moon, T.-Y. Seong, D. Wang, *Electrochim. Commun.* **2009**, *11*, 635.
- [236] H. Tang, J. Chen, S. Yao, L. Nie, Y. Kuang, Z. Huang, D. Wang, Z. Ren, *Mater. Chem. Phys.* **2005**, *92*, 548.
- [237] B. Rajesh, K. Ravindranathan Thampi, J. M. Bonard, N. Xanthopoulos, H. J. Mathieu, B. Viswanathan, *J. Phys. Chem. B* **2003**, *107*, 2701.
- [238] W. Li, X. Wang, Z. Chen, M. Waje, Yan, *Langmuir* **2005**, *21*, 9386.
- [239] Y. Shao, G. Yin, J. Wang, Y. Gao, P. Shi, *J. Power Sources* **2006**, *161*, 47.
- [240] K. Prehn, R. Adelung, M. Heinen, S. P. Nunes, K. Schulte, *J. Membrane Sci.* **2008**, *321*, 123.
- [241] G. Vijayaraghavan, K. J. Stevenson, *Langmuir* **2007**, *23*, 5279.
- [242] B. Viswanathan, *Catal. Today* **2009**, *141*, 52.
- [243] B. J. Landi, S. K. Castro, H. J. Ruf, C. M. Evans, S. G. Bailey, R. P. Raffaelle, *Sol. Energy Mater. Sol. Cells* **2005**, *87*, 733.
- [244] S. Maldonado, K. J. Stevenson, *J. Phys. Chem. B* **2005**, *109*, 4707.
- [245] J. Yang, D.-J. Liu, N. N. Kariuki, L. X. Chen, *Chem. Commun.* **2008**, 329.
- [246] Z. Shi, J. Zhang, Z.-S. Liu, H. Wang, D. P. Wilkinson, *Electrochim. Act.* **2006**, *51*, 1905.
- [247] Z. Chen, M. Waje, W. Li, Y. Yan, *Angew. Chem. Int. Ed.* **2007**, *46*, 4060.
- [248] H. F. Cui, J. S. Ye, X. Liu, W. D. Zhang, F. S. Sheu, *Nanotechnology* **2006**, *17*, 2334.
- [249] E. H. Yu, K. Scott, *J. Power Sources* **2004**, *137*, 248.
- [250] V. C. Tung, M. J. Allen, Y. Yang, R. B. Kaner, *Nat. Nanotechnol.* **2009**, *4*, 25.
- [251] A. K. Geim, K. S. Novoselov, *Nat. Mater.* **2007**, *6*, 183.
- [252] A. Dato, V. Radmilovic, Z. Lee, J. Philips, M. Frenklach, *Nano Lett.* **2008**, *8*, 2012.
- [253] K. V. Emtsev, A. Bostwick, K. Horn, J. Jobst, G. L. Kellogg, L. Ley, J. L. McChesney, T. Ohta, S. A. Reshanov, J. Rohrl, E. Rotenberg, A. K. Schmid, D. Waldmann, H. B. Weber, T. Seyller, *Nat. Mater.* **2009**, *8*, 203.
- [254] R. Liu, D. Wu, X. Feng, K. Mullen, *Angew. Chem. Int. Ed.* **2010**, *122*, 2619.
- [255] C. Jin, T. C. Nagaiah, W. Xia, B. Spliethoff, S. Wang, M. Bron, W. Schuhmann, M. Muhler, *Nanoscale* **2010**, *2*, 981.
- [256] X. Wang, J. S. Lee, Q. Zhu, J. Liu, Y. Wang, S. Dai, *Chem. Mater.* **2010**, *22*, 2178.
- [257] W. Xiong, F. Du, Y. Liu, A. Perez Jr., M. Supp, T. S. Ramakrishnan, L. Dai, L. Jiang, *J. Am. Chem. Soc.* **2010**, *132*, 15839.
- [258] D. Yu, Q. Zhang, L. Dai, *J. Am. Chem. Soc.* **2010**, *132*, 15127.
- [259] S. Kundu, T. C. Nagaiah, W. Xia, Y. Wang, S. V. Dommele, J. H. Bitter, M. Santa, G. Grundmeier, M. Bron, W. Schuhmann, *J. Phys. Chem. C* **2009**, *113*, 14302.

- [260] J. Ozaki, S. Tanifuji, A. Furuichi, K. Yabutsuka, *Electrochim. Acta* **2010**, *55*, 1864.
- [261] M. Zhao, Y. Xia, J. P. Lewis, R. Zhang, *J. Appl. Phys.* **2003**, *94*, 2398.
- [262] Z. Chen, D. Higgins, H. Tao, R. S. Hsu, *J. Phys. Chem. C* **2009**, *113*, 21008.
- [263] S. Wang, D. Yu, L. Dai, *J. Am. Chem. Soc.* **2011**, *133*, 5182.
- [264] S. Wang, D. Yu, L. Dai, D. W. Chang, J.-B. Baek, *ACS Nano* **2011**, *5*, 6202.
- [265] R. Kannan, B. A. Kakade, V. K. Pillai, *Angew. Chem. Int. Ed.* **2008**, *47*, 2653.
- [266] R. Kannan, M. Parthasarathy, S. U. Maraveedu, S. Kurungot, V. K. Pillai, *Langmuir* **2009**, *25*, 8299.
- [267] A. Burke, *J. Power Sources* **2000**, *91*, 37.
- [268] B. E. Conway, *Electrochemical Supercapacitors: Scientific Fundamentals and Technological Applications*, Kluwer Academic/Plenum, New York **1999**.
- [269] R. Kötz, M. Carlen, *Electrochim. Acta* **2000**, *45*, 2483.
- [270] M. Ehsani, Y. Gao, S. E. Gay, A. Emadi, *Modern Electric, Hybrid Electric, and Fuel Cell Vehicles—Fundamentals, Theory and Design*, CRC Press, Boca Raton **2005**.
- [271] E. Frackowiak, F. Beguin, *Carbon* **2001**, *39*, 937.
- [272] J. P. Zheng, P. J. Cygan, T. R. Jow, *J. Electrochem. Soc.* **1995**, *142*, 2699.
- [273] A. Rudge, J. Davey, I. Raistrick, S. Gottesfeld, J. P. Ferraris, *J. Power Sources* **1994**, *47*, 89.
- [274] A. Burke, M. Arulepp, *Electrochim. Soc. Proc.* **2001**, *21*, 576.
- [275] K. H. An, W. S. Kim, Y. S. Park, J. M. Moon, D. J. Bae, S. C. Lim, Y. S. Lee, Y. H. Lee, *Adv. Funct. Mater.* **2001**, *11*, 387.
- [276] B. Kastening, S. Spinzig, *J. Electroanal. Soc.* **1986**, *214*, 295.
- [277] S. T. Mayer, R. W. Pekala, J. L. Kaschmitter, *J. Electrochem. Soc.* **1993**, *140*, 446.
- [278] I. Tanahashi, A. Yoshida, A. Nishino, *J. Electrochem. Soc.* **1990**, *137*, 3052.
- [279] J. Chmiola, G. Yushin, Y. Gogotsi, C. Portet, P. Simon, P. L. Taberna, *Science* **2006**, *313*, 1760.
- [280] J. Huang, B. G. Sumpter, V. Meunier, *Angew. Chem. Int. Ed.* **2008**, *47*, 520.
- [281] E. Raymundo-Piñero, K. Kierzek, J. Machnikowski, F. Béguin, *Carbon* **2006**, *44*, 2498.
- [282] T. E. Rufford, D. Hulicova-Jurcakova, Z. Zhu, G. Q. Lu, *J. Phys. Chem. C* **2009**, *113*, 19335.
- [283] D. Zilli, P. R. Bonelli, A. L. Cukierman, *Nanotechnology* **2006**, *17*, 5126.
- [284] S. Huang, L. Dai, *J. Phys. Chem. B* **2002**, *106*, 3543.
- [285] E. Frackowiak, F. Béguin, *Carbon* **2002**, *40*, 1775.
- [286] C. Du, J. Yeh, N. Pan, *Nanotechnology* **2005**, *16*, 350.
- [287] D. N. Futaba, K. Hata, T. Yamada, T. Hiraoka, Y. Hayamizu, Y. Kakudate, O. Tanaike, H. Hatori, M. Yumura, S. Iijima, *Nat. Mater.* **2006**, *5*, 987.
- [288] Y. Honda, T. Haramoto, M. Takeshige, H. Shiozaki, T. Kitamura, M. Ishikawa, *Electrochim. Solid-State Lett.* **2007**, *10*, A106.
- [289] H. Zhang, G. Gao, Y. Yang, *Nanotechnology* **2007**, *18*, 195607.
- [290] H. Zhang, G. Cao, Z. Wang, Y. Yang, Z. Shi, Z. Gu, *Nano Lett.* **2008**, *8*, 2664.
- [291] Q. L. Chen, K. H. Xue, W. Shen, F. F. Tao, S. Y. Yin, W. Xu, *Electrochim. Acta* **2004**, *49*, 4157.
- [292] H. Zhang, G. Cao, Y. Yang, Z. Gu, *J. Electrochem. Soc.* **2008**, *155*, K19.
- [293] W. Lu, L. Qu, L. Dai, K. Henry, *ECS Trans.* **2007**, *6*, 257.
- [294] C. Liu, M. Liu, F. Li, H. Cheng, *Appl. Phys. Lett.* **2008**, *92*, 143108.
- [295] S. Yongchao, T. S. Edward, *Chem. Mater.* **2008**, *20*, 6792.
- [296] C. Liu, Z. Yu, D. Neff, A. Zhamu, B. Z. Jang, *Nano Lett.* **2010**, *10*, 3598.
- [297] J. Xia, F. Chen, J. Li, N. Tao, *Nat. Nanotechnol.* **2009**, *4*, 505.
- [298] M. D. Stoller, S. Park, Y. Zhu, J. An, R. S. Ruoff, *Nano Lett.* **2008**, *8*, 3498.
- [299] Y. Zhu, S. Murali, M. D. Stoller, A. Velamakanni, R. D. Piner, R. S. Ruoff, *Carbon* **2010**, *48*, 2118.
- [300] Y. Zhu, M. D. Stoller, W. Cai, A. Velamakanni, R. D. Piner, D. Chen, R. S. Ruoff, *ACS Nano* **2010**, *4*, 1227.
- [301] S. Chen, J. Zhu, X. Wu, Q. Han, X. Wang, *ACS Nano* **2010**, *4*, 2822.
- [302] D. Yu, L. Dai, *J. Phys. Chem. Lett.* **2010**, *1*, 467.
- [303] J. Yan, T. Wei, B. Shao, F. Ma, Z. Fan, M. Zhang, C. Zheng, Y. Shang, W. Qian, F. Wei, *Carbon* **2010**, *48*, 1731.
- [304] D. W. Wang, F. Li, J. Zhao, W. Ren, Z. G. Chen, J. Tan, Z. S. Wu, I. Gentle, G. Q. Lu, H. M. Cheng, *ACS Nano* **2010**, *3*, 1745.
- [305] J. Yan, Z. Fan, T. Wei, W. Qian, M. Zhang, F. Wei, *Carbon* **2009**, *47*, 3371.
- [306] J. Yan, T. Wei, B. Shao, Z. Fan, W. Qian, M. Zhang, F. Wei, *Carbon* **2010**, *48*, 487.
- [307] D. Cai, M. Song, C. Xu, *Adv. Mater.* **2008**, *20*, 1706.
- [308] B. Kim, H. Park, W. M. Sigmund, *Langmuir* **2003**, *19*, 2525.
- [309] J. Kim, S. W. Lee, P. T. Hammond, Y. Shao-Horn, *Chem. Mater.* **2009**, *21*, 2993.
- [310] Y. T. Kim, T. Mitani, *J. Power Sources* **2006**, *158*, 1517.
- [311] C. Du, J. Yeh, N. Pan, *Nanotechnology* **2005**, *16*, 350.
- [312] V. Varshney, S. S. Patnaik, A. K. Roy, G. Froudakis, B. L. Farmer, *ACS Nano* **2010**, *4*, 1153.
- [313] G. K. Dimitrakakis, E. Tylianakis, G. E. Foudakis, *Nano Lett.* **2008**, *8*, 3166.
- [314] Y. L. Mao, J. X. Zhong, *New J. Phys.* **2009**, *11*, 093002.
- [315] E. F. Sheka, L. A. Chernozatonskii, *J. Comput. Theor. Nanos.* **2009**, *7*, 1814.
- [316] F. Du, D. Yu, L. Dai, S. Ganguli, V. Varshney, A. K. Roy, *Chem. Mater.* **2011**, *23*, 4810.
- [317] C. Portet, P. Taberna, P. Simon, E. Flahaut, *J. Power Sources* **2005**, *139*, 371.
- [318] T. Liu, T. V. Sreekumar, S. Kumar, R. H. Hauge, R. E. Smalley, *Carbon* **2003**, *41*, 2440.
- [319] W. Lu, R. Hartman, L. Qu, L. Dai, K. Kulkarni, D. Carnahan, *ECS Trans.* **2008**, *16*, 69.
- [320] T. Fukushima, A. Kosaka, Y. Ishimura, T. Yamamoto, T. Takigawa, N. Ishii, T. Aida, *Science* **2003**, *300*, 2072.
- [321] P. Du, S. Liu, P. Wu, C. Cai, *Electrochim. Acta* **2007**, *52*, 6534.
- [322] W. Lu, R. Hartman, L. Qu, L. Dai, *J. Phys. Chem. Lett.* **2011**, *2*, 655.
- [323] K. Jurewicz, S. Delpeux, V. Bertagna, F. Béguin, E. Frackowiak, *Chem. Phys. Lett.* **2001**, *347*, 36.
- [324] M. Cao, S. Huang, L. Dai, G. Wallace, R. Cao, Z. Wang, *Angew. Chem. Int. Ed.* **2000**, *39*, 3664.
- [325] M. Hughes, M. S. P. Shaffer, A. C. Renouf, C. Singh, G. Z. Chen, D. J. Fray, A. H. Windle, *Adv. Mater.* **2002**, *14*, 382.
- [326] M. Hughes, G. Z. Chen, M. S. P. Shaffer, D. J. Fray, A. H. Windle, *Chem. Mater.* **2002**, *14*, 1610.
- [327] K. H. An, K. K. Jeon, J. K. Heo, S. C. Lim, D. J. Bae, Y. H. Lee, *J. Electrochim. Soc.* **2002**, *149*, A1058.
- [328] J. Y. Lee, K. Liang, K. H. An, Y. H. Lee, *Synth. Met.* **2005**, *150*, 153.
- [329] D. B. Le, S. Passerini, J. Guo, J. Ressler, B. B. Owens, W. H. Smyrl, *J. Electrochim. Soc.* **1996**, *143*, 2099.
- [330] M. Benmoussa, E. Ibnouelghazi, A. Bennouna, E. L. Ameziane, *Thin Solid Films* **1995**, *265*, 22.
- [331] S. Passerini, J. J. Ressler, D. B. Le, B. B. Owens, W. H. Smyrl, *Electrochim. Act.* **1999**, *44*, 2209.
- [332] I. H. Kim, J. H. Kim, B. W. Cho, Y. H. Lee, K. B. Kim, *J. Electrochim. Soc.* **2006**, *153*, A989.
- [333] C. Y. Lee, H. M. Tsai, H. J. Chuang, S. Y. Li, P. Lin, T. Y. Tseng, *J. Electrochim. Soc.* **2005**, *152*, A716.
- [334] Z. Fan, J. Chen, M. Wang, K. Cui, H. Zhou, Y. Kuang, *Diam. Relat. Mater.* **2006**, *15*, 1478.
- [335] S. B. Ma, K. W. Nam, W. S. Yoon, X. Q. Yang, K. Y. Ahn, K. H. Oh, K. B. Kim, *J. Power Sources* **2008**, *178*, 483.
- [336] T. Nagaura, T. Tozawa, *Prog. Batt. Sol. Cell* **1991**, *10*, 218.

- [337] R. J. Brodd, K. R. Bullock, R. A. Leising, R. L. Middaugh, J. R. Miller, E. Takeuchi, *J. Electrochem. Soc.* **2004**, *151*, K1.
- [338] US Department of Energy, [http://www1.eere.energy.gov/vehiclesandfuel/technologies/energy\\_storage/index.html](http://www1.eere.energy.gov/vehiclesandfuel/technologies/energy_storage/index.html) (last accessed August 2011).
- [339] Lithium batteries, <http://auto.howstuffworks.com/fuel-efficiency/vehicles/lithium-ion-battery-car1.htm> (last accessed August 2011).
- [340] R. S. Morris, B. G. B. Dixon, T. Gennett, J. Blackburn, M. J. Heben, presented at 211th Electrochem. Soc. Meeting, Chicago, Illinois, May **2007**.
- [341] M. M. Thackeray, T. Ohzuku, in *Handbook of Battery Materials* (Ed: J.O. Besenhard), Wiley-WCH, New York **1999**.
- [342] Z. Chen, W. Q. Lu, J. Liu, K. Amine, *Electrochim. Acta* **2006**, *51*, 3322.
- [343] P. Poizot, S. Laruelle, S. Gruegeon, L. Dupont, J. M. Tarascon, *Nature* **2000**, *407*, 496.
- [344] K. Bullis, "Higher-Capacity Lithium-Ion Batteries, Nanostructured electrodes and active materials could shrink batteries for portable electronics and electric vehicles" in *Technology*, MIT Review, Cambridge, MA **2006**.
- [345] G. Che, B. B. Laurelle, S. Gruegeon, L. Dupont, J. M. Tarascon, *Nature* **2000**, *407*, 496.
- [346] E. Frackowiak, S. Gautier, H. Gaucher, S. Bonnamm, F. Beguin, *Carbon* **1999**, *37*, 61.
- [347] B. Cao, A. Kleinhammes, X. P. Tang, C. Bower, L. Fleming, Y. Wu, O. Zhou, *Chem. Phys. Lett.* **1999**, *307*, 153.
- [348] A. S. Claye, J. E. Fischer, C. B. Huffman, A. G. Rinzler, R. E. Smalley, *J. Electrochem. Soc.* **2000**, *147*, 2845.
- [349] G. Maurin, F. Henn, in *Encyclopedia of Nanoscience and Nanotechnology* (Ed: H.S. Nalwa) American Scientific Publisher, California **2003**, p. X/1.
- [350] F. Leroux, K. Méténier, S. Gautier, E. Frackowiak, S. Bonnamm, F. Béguin, *J. Power Sources* **1999**, *81–82*, 317.
- [351] H. Shimoda, B. Gao, X. P. Tang, A. Kleinhammes, L. Fleming, Y. Wu, O. Zhou, *Phys. Rev. Lett.* **2002**, *88*, 155021.
- [352] D. Aurbach, in *Advances in Lithium-ion Batteries* (Ed: W. V. Schalkwijk, B. Scrosati) Kluwer Academic/Plenum Publishers, New York **2002**.
- [353] P. Ajayan, O. Zhou, in *Carbon Nanotubes* (Eds: M. Dresselhaus, G. Dresselhaus, P. Avouris) Springer, Berlin **2001**, p. 391.
- [354] G. Wang, J. Yao, H. Liu, S. Dou, J. Ahn, *Met. Mater. Int.* **2006**, *12*, 413.
- [355] H. Buqa, D. Goers, M. Holzapfel, M. E. Spahr, P. Novak, *J. Electrochem. Soc.* **2005**, *152*, A474.
- [356] J. Zhao, Q. Gao, C. Gu, Y. Yang, *Chem. Phys. Lett.* **2002**, *358*, 77.
- [357] J. Chen, Y. Liu, A. I. Minett, C. Lynam, J. Wang, G. G. Wallace, *Chem. Mater.* **2007**, *19*, 3595.
- [358] V. L. Pushparaj, M. M. Shaijumon, A. Kumar, S. Murugesan, L. Ci, R. Vajtai, R. J. Linhardt, O. Nalamasu, P. M. Ajayan, *Proc. Natl. Acad. Sci USA* **2007**, *104*, 13574.
- [359] C. Masarapu, V. Subramanian, H. Zhu, B. Wei, *Adv. Funct. Mater.* **2009**, *19*, 1008.
- [360] G. Wang, J. Ahn, J. Yao, M. Lindsay, H. Liu, S. Dou, *J. Power Sources* **2003**, *119*, 16.
- [361] X. X. Wang, J. N. Wang, H. Chang, Y. F. Zhang, *Adv. Funct. Mater.* **2007**, *17*, 3613.
- [362] Q. Wang, L. Chen, X. Huang, *Electrochem. Solid-State Lett.* **2002**, *5*, A188.
- [363] G. Maurin, C. Bousquet, F. Henn, P. Bernier, R. Almairac, B. Simon, *Chem. Phys. Lett.* **1999**, *312*, 14.
- [364] G. Wu, C. Wang, X. Zhang, H. Yang, Z. Qi, P. He, W. Li, *J. Electrochem. Soc.* **1999**, *146*, 1696.
- [365] Z. Yang, Y. Feng, Z. Li, S. Sang, Y. Zhou, L. Zeng, *J. Electro. Chem.* **2005**, *580*, 340.
- [366] J. Dahn, T. Zheng, Y. Liu, J. Xue, *Science* **1995**, *270*, 590.
- [367] Z. Yang, H. Wu, *Mater. Chem. Phys.* **2001**, *71*, 7.
- [368] M. Endo, T. Hayashi, Y. A. Kim, *Pure Appl. Chem.* **2006**, *78*, 1703.
- [369] K. Sheem, Y. H. Lee, H. S. Lim, *J. Power Source* **2006**, *158*, 1425.
- [370] L. Wang, Y. Huang, R. Jiang, D. Jia, *J. Electrochem. Soc.* **2007**, *154*, A1015.
- [371] G. X. Wang, B. L. Zhang, Z. L. Yu, M. Z. Qu, *Solid State Ionics* **2005**, *176*, 1169.
- [372] J. S. Sakamoto, B. Dunn, *J. Electrochem. Soc.* **2002**, *149*, A26.
- [373] F. F. C. Bazito, R. M. Torresi, *J. Braz. Chem. Soc.* **2006**, *17*, 627.
- [374] C. Sotowa, G. Origgi, M. Takeuchi, Y. Nishimura, K. Takeuchi, I. Y. Jang, Y. J. Kim, T. Hayashi, Y. A. Kim, M. Endo, M. S. Dresselhaus, *ChemSusChem* **2008**, *1*, 911.
- [375] D. B. Le, S. Passerini, A. L. Tipton, B. B. Owens, W. H. Smyrl, *J. Electrochem. Soc.* **1995**, *142*, L102.
- [376] K. Salloux, F. Chaput, H. P. Wong, B. Dunn, M. W. Breiter, *J. Electrochem. Soc.* **1995**, *142*, L191.
- [377] J. G. Zhang, P. Liu, J. A. Turner, C. E. Tracy, D. K. Benson, *J. Electrochem. Soc.* **1998**, *145*, 1889.
- [378] C. Julien, in *Lithium Batteries, New Materials, Developments and Perspectives* (Ed: G. Pistoia) Elsevier, Amsterdam **1994**.
- [379] K. Kang, Y. S. Meng, J. Bréger, C. P. Grey, G. Ceder, *Science* **2006**, *311*, 977.
- [380] P. L. Taberna, S. Mitra, P. Poizot, P. Simon, J. M. Tarascon, *Nat. Mater.* **2006**, *5*, 567.
- [381] W.-C. Fang, *J. Phys. Chem. C* **2008**, *112*, 11552.
- [382] W. Lu, A. Goering, L. Qu, L. Dai, unpublished.
- [383] X. Li, X. Wang, L. Zhang, S. Lee, H. Dai, *Science* **2008**, *319*, 1229.
- [384] J. C. Meyer, A. Geim, M. Katsnelson, K. Novoselov, T. Booth, S. Roth, *Nature* **2007**, *446*, 60.
- [385] S. Gilje, S. Han, M. Wang, K. L. Wang, R. B. Kaner, *Nano Lett.* **2007**, *7*, 3394.
- [386] M. Liang, L. Zhi, *J. Mater. Chem.* **2009**, *19*, 5871.
- [387] D. Wang, D. Choi, J. Li, Z. Yang, Z. Nie, R. Kou, D. Hu, C. Wang, L. V. Saraf, J. Zhang, *ACS Nano* **2009**, *3*, 907.
- [388] D. Wang, R. Kou, D. Choi, Z. Yang, Z. Nie, J. Li, L. V. Saraf, D. Hu, J. Zhang, G. L. Graff, *ACS Nano* **2010**, *4*, 1587.
- [389] H. Wang, L. F. Cui, Y. Yang, H. S. Casalongue, J. T. Robinson, Y. Liang, Y. Cui, H. Dai, *J. Am. Chem. Soc.* **2010**, *132*, 13978.
- [390] A. Leela, M. Reddy, A. Srivastave, S. R. Gowda, H. Gullapalli, M. Dubey, P. M. Ajayan, *ACS Nano* **2010**, *4*, 6337.
- [391] S. M. Paek, E. J. Yoo, I. Honma, *Nano Lett.* **2008**, *9*, 72.
- [392] P. Poizot, S. Laruelle, S. Gruegeon, L. Dupont, J. Tarascon, *J. Power Sources* **2001**, *97*, 235.
- [393] O. Mao, J. R. Dahn, *J. Electrochem. Soc.* **1999**, *146*, 423.
- [394] S. Flandrois, B. Ottaviani, A. Derre, *J. Phys. Chem. Solids* **1996**, *57*, 741.
- [395] Y. Wu, S. Fang, Y. Jiang, *J. Mater. Chem.* **1998**, *8*, 2223.
- [396] W. J. Weydanz, B. M. Way, T. Buuren, J. R. Dahn, *J. Electrochem. Soc.* **1994**, *141*, 900.
- [397] Y. Wang, Y. Shao, D. W. Matson, J. Li, Y. Lin, *ACS Nano* **2010**, *4*, 1790.

Received: August 6, 2011

Revised: November 3, 2011

Published online: March 2, 2012